Tijana Jokic, M.Sc.

New pH and CO_2 sensitive materials based on BF2-chelated azadipyrromethenes

DISSERTATION

Zur Erlangung des akademischen Grades

eingereicht an der

Technischen Universität Graz

Betreuer

Univ. Prof. Dipl.-Chem. Dr.rer.nat. Ingo Klimant

Institut für Analytische Chemie und Lebensmittelchemie

Graz, 2015.

EIDESSTATTLICHE ERKLÄRUNG

Ich erkläre an Eides statt, dass ich die vorliegende Arbeit selbstständig verfasst, andere als die angegebenen Quellen/Hilfsmittel nicht benutzt, und die den benutzten Quellen wörtlich und inhaltlich entnommenen Stellen als solche kenntlich gemacht habe. Das in TUGRAZonline hochgeladene Textdokument ist mit der vorliegenden Dissertation identisch.

_____ _____

Datum Unterschrift

Danksagung

Ich möchte an erster Stelle Prof. Ingo Klimant danken, dass er mir eine wunderbare Möglichkeit gegeben hat auf einem interessanten Thema zu arbeiten und für seine Ünterstutzung und Geduld während dieser Arbeit.

Dr. Sergey Borisov möchte ich für sein Interesse an meiner Arbeit danken, der immer Zeit für meine vielen Fragen zur Synthese und optischen Sensorik hatte und mir dabei gern geholfen hat Lösungen für wissenschaftliche Probleme zu finden.

Ein besonderes Dankeschön geht an Dr. Ruslan Dmitriev, der mir die Grundlagen der Zell-biologie und Fluoreszenzmikroskopie erklärte und seine Einführung in die wunderbare irische Kultur.

Weiterhin ich möchte mich bei den Mitgliedern unserer Gruppe für eine schöne gemeinsame Zeit und die alltägliche Unterstützung bedanken.

Den sehr gute Freunden aus dem CHEBANA-Netzwerk möchte ich für eine schöne Zeit auf internationalen Meilensteinsitzungen und den wissenschaftlichen und nichtwissenschaftlichen Diskussionen danken.

Der Europäischen Kommission danke ich für die finanzielle Unterstützung dieser Arbeit.

Schließlich möchte ich meiner Familie danken, dass sie immer an mich geglaubt haben und für ihre vorbehaltlose Untersützung.

TABLE OF CONTENTS

CHAPTER 1

1.1 Motivation……...…1

1.2 State of the Art – pH Sensors ……..…2

1.3 State of the Art – CO_2 Sensors…….4

1.4 Read-out Schemes……....…6

1.5 Near-infrared Fluorescent Dyes……..…….9

1.6 Aza-BODIPY dyes – synthesis and properties…….……14

1.7 References……..…22

CHAPTER 2

Highly Photostable Near-Infrared Fluorescent pH Indicators and Sensors based on BF_2-Chelated Tetraarylazadipyrromethene Dyes……...27

2.1 Introduction……...28

2.2 Experimental……..……29

2.3 Results and Discussion……..…32

2.4 Conclusion…….43

2.5 References……..…..….44

2.6 Supporting Information…….....47

CHAPTER 3

NIR optical carbon dioxide sensors based on highly photostable dihydroxy-aza-BODIPY Dyes…….78

3.1 Introduction…….....78

3.2 Experimental……..…….....80

3.3 Results and Discussion……....….87

3.4 Conclusion…….....97

3.5 References…….....98

3.6 Supporting Information…….....101

CHAPTER 4

pH-sensitive aza-BODIPY probe for fluorescence lifetime imaging in MEF cells……..113

4.1 Introduction……...…113
4.2 Experimental……...114
4.3 Results and Discussion……...…116
4.4 Conclusion……..122
4.5 References…….……122

CHAPTER 5

CO_2 sensor based on rigid aza-BODIPY probe……..…..124

5.1 Introduction……..…...124
5.2 Experimental……..…..124
5.3 Results and Discussion……127
5.4 Conclusion……..…….135
5.5 References……..…….136
5.6 Spectra……..…...137

Chapter 1

1.1 Motivation

Optical pH and CO_2 sensing has new possibilities in many applications where electrochemical sensors fail. Optical sensors aren't prone to electrical interferences, they are noninvasive and enable remote measurements. They are also capable for continuous measurements and require low energy consumption. Most optical pH sensors are utilizing colorimetric or fluorescent indicator dyes. Although many pH indicators are currently available, only a few fulfill the requirements for use in pH sensors.

Therefore, the focus of this work was to synthesize and characterize new fluorescent probes suitable for preparation of pH and CO_2 sensors for various ranges of pH and pCO_2.

Several criteria dictated the choice of the indicator. BF_2-chelated-azadipyrromethenes were chosen due to their near-infrared emission, possibility of tuning the pK_a, straightforward synthesis and high photostability. For optimization of sensor properties different polymer supports were used onto which the indicators were immobilized. Performance of the sensors was also evaluated in different sensor formats – planar, nanoparticles formulation and microsensors.

Lifetime-based sensors (FLIM and DLR) are prepared due to particular advantages they have over intensity-based sensors like negligible signal drift arising from leaching and bleaching, or fluctuations arising from the light-source intensity and photodetector sensitivity.

Sensors are of interest in biotechnology, marine biology and clinical research.

1.2 State of the Art – pH Sensors

There has been an increased interest in the development and application of optical sensors in the last three decades. They have found application in areas such as process analytical technology, environmental monitoring, biotechnology and medical diagnostics. Optical chemical sensor is based on the use of indicator dyes, which are entrapped in a polymer matrix. This material is then deposited on a planar substrate[1] or on the tip of an optical fiber.[2] In the 1970s the first type of a pH sensor became available as a test stripe based on a pH indicator covalently linked to the cellulose matrix. In 1980 Peterson[3] developed the first optical pH sensor. The sensor contained phenol red as an indicator immobilized into polystyrene microbeads and was applied for physiological pH measurement. In 1982[4] first fluorescence-based pH sensor was reported based on covalently immobilized fluoresceinamin on cellulose.

Most frequently used pH indicators are fluorescein and its derivatives, seminaphthorhodafluor, 8-hydroxypyrene-1,3,6-trisulfonic acid sodium salt, and hydroxycoumarins[5-7]. The requirements for an optimal pH indicator are: excitation/emission spectra in the visible/near infrared wavelength range, high molar absorption coefficients and high fluorescence quantum yields, large Stokes shifts, pK_a value close to the measured pH, high photostability and no-cross-sensitivity to ionic strength. However, currently available indicators don't satisfy all of these requirements; for example, fluoresceins have limited photostability and small Stokes' shifts, the pK_a value of HPTS is strongly influenced by the ionic strength and most coumarins have low excitation wavelength.

After designing the pH indicator the next step in sensor development is the immobilization of the indicator in a polymer support. Indicator can be immobilized in a polymer matrix by different methods: adsorption, entrapment or covalent binding. Adsorption is the least reliable, due to possibility of dye leaching. Physical entrapment is straightforward and rapid way of immobilization. This method can show stability problems due to probe leaching causing reduced lifetime and sensor reproducibility. However, it is often used for the preparation of sensing material. Problems can be avoided by introduction of lipophilic alkyl chains or in case of negatively charged pH indicators by using quaternary ammonium salts. Covalent binding is the most reliable method, as the effects of aggregation, migration and leaching are eliminated.

Indicators can be covalently immobilized either by co-polymerization of functionalized dye-monomer and the corresponding co-monomer[8] or by linking the dyes to the polymer using suitable functional groups.[9] However, optical[10] and acid-base properties[11,12] can change after immobilization. Electrostatic immobilization[13] is possible onto materials with ion-exchange properties and with indicators that are charged in both the acid and base form. Hence, the sensors show fast response and leaching is not observed. However, the shortcoming of this approach is susceptibility to ionic strength. To minimize the effect of ionic strength on the pK_a value of the indicator Wolfbeis and Offenbacher[14] demonstrated a system in which a dual sensor arrangement can measure ionic strength and pH and simultaneously correct the pH measurement for variations in ionic strength.

The properties of sensing material depend greatly on the properties of the polymer matrix used for indicator immobilization. Many different materials are used for this purpose. These are mostly cellulose derivatives and polyurethane [15,16] or pHEMA hydrogels[17] which show good mechanical properties, temperature stability and high water uptake. Less hydrophilic materials, such as sol-gels and xerogels are also used, or hydrophobic materials such as poly(vinyl chloride)[18], where proton transport is achieved by use of proton carriers such as tetraphenylborate and similar lipophilic anions.

1.3 State of the Art - CO_2 Sensors

The monitoring of CO_2 has found application in environmental, health, food and beverage industries. Analysis of dissolved carbon dioxide has been performed with Severinghaus electrode, which is a pH electrode in contact with water solution of sodium bicarbonate, behind a membrane which is permeable to gases, but impermeable to ions. Change in the pH caused by the dissolved CO_2 is measured with the pH electrode. When carbon dioxide dissolves in water, it is in equilibrium with carbonic acid:

$$CO_2\,(g) \rightleftharpoons CO_2\,(aq) \qquad 1.1$$

$$CO_2\,(aq) + H_2O \rightleftharpoons H_2CO_3 \qquad 1.2$$

$$H_2CO_3 \rightleftharpoons H^+ + HCO_3^- \qquad 1.3$$

$$HCO_3^- \rightleftharpoons H^+ + CO_3^{2-} \qquad 1.4$$

The Severinghaus electrode is indirectly measuring the partial pressure of CO_2 through the pH change it is inducing. However, it has many drawbacks – expensive production, dimensional limitations and susceptiblity to electrical and chemical interferences. Therefore, there has been a consistent effort in the development of CO_2 optical sensors in the last two decades.

Wet Sensors

Severinghaus-type sensor has also been used for development of optical sensors for carbon dioxide with pH indicators instead of pH electrode for determination of pH changes. Sensors for carbon dioxide used suspended aqueous buffer solution (containing a pH indicator of pKa 7.5-9), in the form of aqueous droplets, in a hydrophobic polymer which is CO_2-permeable and proton-impermeable in order to avoid interferences by pH and prevent leaching of the indicator when measurements are done in water. The sensitivity of the sensor dependes on the sensitivity of the indicator to pH variations (e.g. on the pK_a of the indicator).[19] Therefore, sensor with optimal sensitivity in certain range can be designed using indicators with suitable pK_a value. This scheme has certain drawbacks, like changes of osmolarity and ionic strength of the water-buffer system (due to sensitivity of indicators to IS in terms of pK_a values). Additionally, sensor performance

can be affected by dehydration or hydration and therefore sensors should be stored under defined conditions.

Solid Sensors

In 1992 Mills et al.[20] made major progress in development of solid optical carbon dioxide sensors. They used a lipophilic base (instead of an aqueous buffer) which facilitated the dissolution of the pH indicator in a hydrophobic polymer, such as ethyl cellulose. pH indicator is forming an ion-pair with quaternary ammonium base, like tetraoctylammonium hydroxide (TOA^+OH^-), (17, 25-27) which acts as an internal buffer. The mechanism is presented by eq. 1.5.

$$\{TOA^+D^- \cdot x\ H_2O\} + CO_2 \rightarrow \{TOA^+HCO_3^- \cdot (x\text{-}1)\ H_2O \cdot HD\} \qquad 1.5$$

These sensors can be used for measurement of carbon dioxide concentrations in gas phase of different humidity or in water solutions of different osmotic pressure. They perform well in dry environment because the water molecules are tightly bound to the ion-pair.

The sensors can be poisoned with acidic gasses because of limited buffer capacity, which can be improved with addition of quaternary hydroxide[21]. The excess base acts as a bicarbonate buffer system and is present in the form of $TOA^+HCO_3^- \cdot XH_2O$. Another problem with solid-state sensors is to find a suitable polymer matrix. The sensor matrix can be ethyl cellulose, poly (vinyl alcohol), poly (vinyl chloride), etc. These polymers are proton permeable and therefore additional gas-permeable and proton-impermeable protection layer made from poly (tetrafluoroethylene), silicone or polystyrene is necessary. However, during formation of the protection layer air bubbles can be trapped what causes prolonged response time and problems with adhesion. This can be avoided by emulsification of the sensing material into a proton-impermeable, hydrophobic polymer, such as silicone matrix. This polymer has excellent permeability for gases[22].

1.4 Read-out Schemes

Referencing via Ratiometric Measurements

Ratiometric measurements overcome many problems associated with intensity-based measurements, since these measurements aren't influenced by variations of the light source intensity, dye degradation or detector accuracy.

If protonated and deprotonated form of a pH indicator are fluorescent, the ratio of their fluorescence intensities can be used as a referenced parameter. There are three different methods for ratiometric measurements:

a) Single emission and dual excitation wavelength;
b) Single excitation and dual emission wavelength;
c) Dual excitation and dual emission wavelength.

In case protonated or deprotonated form of a pH indicator isn't fluorescent, pH insensitive fluorophore can be added for ratiometric measurements. Two dyes should have overlapping emission spectra, but separate excitation bands or overlapping excitation bands and separate emission bands.

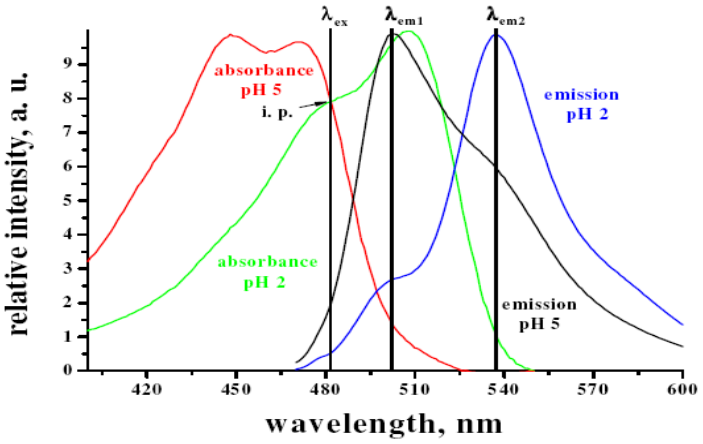

Figure 1. Example of ratiometric measurement when excitation is done at isobestic point and emission is recorded at two wavelengths.[23]

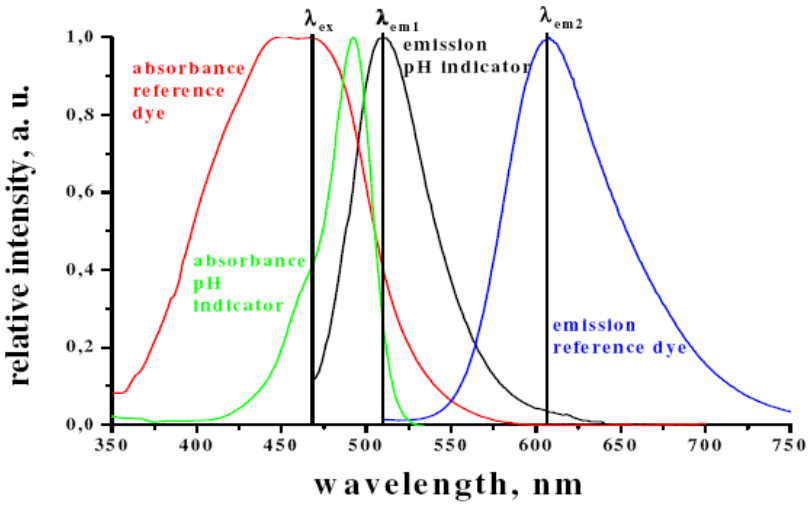

Figure 2. Example of a ratiometric measurement when excitation of indicator/reference fluorophore is done at one wavelength and both emissions are recorded at two wavelengths.[23]

Dual Lifetime Referencing (DLR)

Frequency domain method is a method for precise determination of fluorescence decay times. In Dual lifetime referencing (DLR) method[24,25] the intensity ratio of two fluorophores is transformed into a phase shift which is determined by the difference of the decay times of the indicator and the reference. The absorption and emission spectra of two fluorophores must overlap so one excitation wavelength can be used and monitoring of emission can be achieved. The modulation frequency of the excitation light is set according to the lifetime of the long-lived reference, and therefore the fluorescence of the indicator has no phase delay, while the reference fluorescence has a phase-shift and at the same time its emission amplitude is decreasing[26,27].

The overall phase shift Φ_m is determined only by ratio of the intensities of the two fluorophores. The fluorescence intensity of the reference dye is constant and the intensity of the indicator depends on the analyte concentration. This leads to high amplitude in unquenched state and low amplitude when fluorescence is quenched in the presence of the analyte. Therefore, phase shift is determined by the intensity of the indicator and therefore, the analyte concentration.

The following equations are obtained:[25]

$$A_m \cdot \cos \Phi_m = A_{ref} \cdot \cos \Phi_{ref} + A_{flu} \cdot \cos \Phi_{flu} \quad (1.6)$$

$$A_m \cdot \sin \Phi_m = A_{ref} \cdot \sin \Phi_{ref} + A_{flu} \cdot \sin \Phi_{flu} \quad (1.7)$$

Where A_m is the fluorescence signal intensity and Φ_m the phase shift. A_{flu} and A_{ref} are the amplitudes of the indicator and the reference dye, and Φ_{flu} and Φ_{ref} are their phase shifts. At low modulation frequencies, the indicator isn't causing phase shift (Φ_{flu}=0) and therefore following equations can be derived:

$$A_m \cdot \cos \Phi_m = A_{ref} \cdot \cos \Phi_{ref} + A_{flu} \quad (1.8)$$

$$A_m \cdot \sin \Phi_m = A_{ref} \cdot \sin \Phi_{ref} \quad (1.9)$$

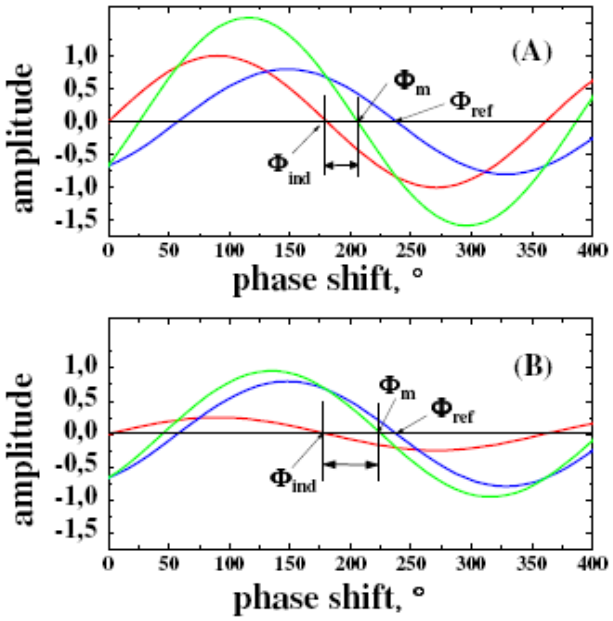

Figure 3.[23] The DLR scheme. Phase shift of the overall luminescence (Φ_m), the reference (Φ_{ref}), and the indicator (Φ_{ind}). (A) fluorescence of indicator in its unquenched state, (B) fluorescence of the indicator in the quenched state.

By dividing eq.1.8 by 1.9 the following relation is obtained:

$$(A_m \cdot \cos \Phi_m) / (A_m \cdot \sin \Phi_m) = \cot \Phi_m = \cot \Phi_{ref} + 1 / (\sin \Phi_{ref}) \cdot A_{flu} / A_{ref} \quad 1.10$$

Therefore, $\cot \Phi_m$ represents the referenced intensity of the indicator.

1.4 Near-infrared Fluorescent Dyes

Near-infrared emission fluorophores found application in optical engineering, analytical chemistry, biotechnology and medicine as new tools for noninvasive sensing. The advantages of near-infrared region are minimal background signal from autofluorescence of biomolecules, low-light scattering, deep light penetration and the use of inexpensive excitation light sources. In order to be used for real-world applications NIR dyes must fulfill a set of requirements regarding their optical, chemical and biological properties. They should possess high brightness, large Stokes shift, high chemo- and photostability and have low photo(toxicity).

Therefore, development of fluorophores for a particular application is not an easy task, as integration of all required properties in one molecular platform is quite challenging. In order to design fluorophores it is important to have an insight into structure-property relationship so their photophysical properties could be optimized. On the other hand, fluorophores often have limitations in respect to their optical properties, such as low quantum yield and photostability. For these reasons, intensive research effort has been made to find fluorophores with improved optical properties and stability.

Thanks to the extensive research that was done on NIR dyes, many have been used as platforms for the development of fluorescent probes for various analytes based on photo-induced electron transfer (PET), intramolecular charge transfer (ICT) and Förster resonance energy transfer (FRET) mechanism.

In PET-based fluorescent probes, fluorophore and receptor are connected with an aliphatic spacer, which electronically disconnects the π-electron system of the fluorophore and the receptor.[28] The fluorophore can act as an electron donor or acceptor. In the reductive PET, the fluorophore is reduced while the receptor is oxidized. However, in the oxidative PET, the fluorophore acts as an electron donor, which is an oxidant in the process.

When the fluorophore possesses an electron-donating group, intramolecular charge transfer (ICT) can take place from a donor to an acceptor (electron-withdrawing group) upon photo-excitation. Due to electron transfer in excited state, the increase in dipole moment is considerable, which is inducing the red shift in the fluorescence spectra when increasing solvent polarity.[29] The main difference between PET and ICT probes is in the different fluorescence response towards analyte detection. PET probes show fluorescence enhancement or quenching without spectral shifts, what rules out possibility of ratiometric measurements, while ICT probes show fluorescence band shifts after analyte binding, enabling ratiometric measurements.

FRET is the interaction between two chromophores, of which one is necessary fluorescent. The energy is transferred from a donor fluorophore which emits at a shorter wavelength to an acceptor chromophore which emits it at a longer wavelength. In order for FRET to take place, emission spectra of the donor and the absorption spectra of the acceptor should overlap and the chromophores should be at a molecular distance in the range of 10-80 Å.[30]

The need for noninvasive measurement technologies for pH monitoring has driven the development of pH probes based on NIR fluorescent dyes. pH probes based on NIR dyes that have been reported are BODIPY and azaBODIPY dyes,[31-33] cyanine-based probes,[34] diketo-pyrrolo-pyrrole pigments,[35] phenoxiazines and an aminoperylene compound.[36]

Cyanine-based pH indicators have attracted considerable attention due to their unique NIR emission. There are two types of cyanine-based pH indicators:

First type are cyanine dyes with a non-N-alkylated indolium moiety[37]. These type of pH sensitive cyanine dyes is using the advantage of the pH-dependent optical properties of non-N-alkylated cyanines. The dye is pH-sensitive when one or both of the indole nitrogen atoms are not alkylated. Probes aren't fluorescent when nitrogen atom is deprotonated, but they are highly fluorescent upon protonation. Synthetic modifications can tune the pK_a value of these probes, therefore probes for various pH ranges have been developed.

The second type of pH - sensitive cyanine dyes is based on PET sensing mechanism.[38] These contain a fluorophore and a nitrogen-containing electron-donor. Supression or enhancement of PET process is achieved by protonation/deprotonation of the electron donor. The pH changes

don’t have the effect on the shift of the fluorescence emission maxima, but the absorption maximum is red-shifted with the increase of pH.

BODIPY dyes are attractive due to many excellent features like intense absorption, high fluorescence quantum yield, narrow absorption and emission bands, insensitivity to polarity, good chemo- and photostability and ease of tuning of their photophysical properties by structural modifications. Due to their potential for fluorescence sensing applications, many strategies have been developed to push their absorption and emission to the NIR region (650-900 nm). Many derivatives such as styryl-substituted BODIPYs, aromatic units-fused BODIPYs, conformationally constrained BODIPYs and aza-BODIPYs have been synthesized.[39]

BODIPY pH probes based on the PET mechanism mostly have the proton receptor on the meso-position to disconnect with the fluorophore since the substituent at this position is usually orthogonal to the BODIPY core. Daub and coworkers constructed a styryl-substituted BODIPY probe for pH sensing with a dimethyl-aminophenyl - receptor on the meso-position.[40] The quenching of the fluorescence occurs in polar solvents owing to the PET process. Upon protonation, 2000- fold fluorescence enhancement was observed due to the supression of the PET process. With the similar approach Overkleeft and colleagues created a series of fluorescent pH probes with pK_a values ranging from 2.08 to 5.81.[41] The emission was shifted to the longer wavelength by condensation with various aldehydes at the 3,5-positions and the pK_a value was tuned by modifying the dialkylamine moiety at the meso-position.

O’Shea and colleagues developed two aza-BODIPY fluorescent pH probes based on a PET mechanism.[42] The probes contained incorporated diethylamine and morpholine receptors which enabled pH sensing. The diethylamine receptor analogue showed a significant enhancement of fluorescence intensity in acidic conditions, but for the morpholine receptor analogue only a moderate increase was observed. Apparent pK_a values of 6.9 and 4.8 were calculated, respectively. Application of diethylamine analogue for in vitro imaging was demonstrated.

Chen and coworkers investigated similar probes for intracellular pH sensing.[43] They synthesized and characterized the pH-sensitive NIR aza-BODIPY dye, which was highly fluorescent only under acidic conditions, due to the suppression of PET process. However, after incorporation of

the probe with micelles, liposomes and proteins, it was also fluorescent at neutral and basic pH, indicating that the pH-sensing properties were affected by cellular environment. Live-cell imaging also showed that the fluorescence was activated by intracellular components rather than pH. However, probes showed to be a good choice for cell-imaging although not pH indicators.

Instead of alkylated amines, hydroxyphenol can also serve as a pH-sensitive unit. O'Shea and colleagues[44] reported azide conjugatable pH sensitive fluorescence imaging probe. Probes were conjugated by an alkyne-azide cycloaddition containing amino, carboxy, and carbohydrate substituents. UV-VIS and fluorescence spectra for all three derivatives were 687/716 nm in methanol. pH sensing properties of the galactose conjugated derivative was investigated and pK_a of 6.9 was calculated. In vitro pH response was demonstrated by staining MDA-MB-231 cells with galactose conjugated derivative. Imaging with confocal laser scanning microscopy showed intense emission localized at the cytosol. After treating the cells with aqueous buffers almost complete quenching was observed at pH 8.0 and intense emission was restored at pH 6.6. The increase in fluorescence intensity from off to on-state was 6-fold.

If proton receptors are conjugated to the BODIPY core, the ICT mechanism is operative. Akkaya and colleagues constructed pH probes with proton receptors at 3,5-positions.[31] The probe with two 4-(dimethylamino)-phenylethynyl groups as proton receptors featured an absorption maximum at 700 nm and a weak fluorescence at around 750 nm in chloroform. Protonation caused a blue shift in absorption and emission and an increase in quantum yield due to the supression of the ICT process. However, probe with p-pyridinestyryl groups as the pH receptors exhibited a red shift in absorption and emission upon protonation, as the pyridyl substituents operate as the ICT acceptor instead of donor.

McDonnell and O'Shea also developed ICT-operative aza-BODIPY probe.[45] Aza-BODIPY dye contained two amine substituents as a pH-responsive unit. pH-dependent absorption and fluorescence response as well as visible color changes were observed for the non-, mono- and di-protonated form of the indicator. The triple emission sensor is advantageous for ratiometric sensing applications.

Liu et al. reported on NIR pH sensitive benzo[*a*]phenoxazines.[46] Derivatives with an electron-withdrawing aromatic group attached to nitrogen of the imino group exhibited pH-dependent absorption and emission properties under near-neutral and subacid conditions. Three water-soluble probes with different pyridinium structures are designed and synthesized. Their emission maxima are located at 688, 694 and 697 nm with the full emission ranging from 625 to 850 nm and the pK_a values were 2.7, 5.8 and 7.1, respectively. A composite probe containing the three benzo[*a*]phenoxazines showed a linear pH-emission relationship in the range of pH 1.9-8.0.

Schutting et al.[35] developed pH sensitive indicators for CO_2 sensors based on diketo-pyrrolo-pyrrole (DPP) pigments Irgazin Ruby and Irgazin Scarlet. After modification with bis(2-ethylhexyl) sulfonamide groups, the pigments were soluble in organic solvents and polymers and showed pH sensitivity. Optical carbon dioxide sensors were prepared by dissolving the indicators with a quaternary ammonium base in ethyl cellulose. Bathochromic shift of the absorption and emission spectra is observed and therefore the indicator can be used as colorimetric and fluorescent ratiometric probe.

Aigner et al.[36] developed the first NIR emissive pH indicators based on perylene bisimides. Cyclic secondary amine is introduced into the perylene core by substitution of chlorine what caused a bathochromic shift of 100-140 nm. The indicator was pH sensitive due to photoinduced electron transfer from non-protonated amine to the perylene chromophore. pH sensor with covalently linked indicator was prepared by co-polymerisation of the dye modified with methacrylate groups and acryloylmorpholine monomer and resulting in a cross-linked polymer covalently attached to a glass substrate.

1.5 Azabodipy dyes - Synthesis and Properties

During the past decade, various studies have been done on aza-BODIPYs owing to their efficient fluorescence in the far-red and near-IR regions of the spectrum. The nitrogen lone pair at the 8-position appears to contribute to the orbital levels of the actual cyanine framework, reducing the HOMO-LUMO energy gap relative to bodipy dyes bearing similar substituents. Electrochemical measurements and molecular-orbital calculations could confirm this effect, which is responsible for the red-shifted absorption and emission maxima. Fully conjugated aza-BODIPY core is suitable for attachment of different substituents and therefore tuning of the fluorescence properties. Azadipyrromethenes were first discovered by Rogers in the 1940s,[47] but the first borondifluoride azadipyrromethene was then synthesized by Boyer et al.[48] in 1993. The necessary research to obtain symmetric and asymmetric azabodipy dyes was conducted primarily by the groups of O'Shea and Carreira, motivated by the potential applications as biological labels, as sensitizers for photodynamic therapy[49] and as luminescent proton sensors.[50]

The simplest of the azaBODIPY family is difluoro-bora-1,3,5,7-tetraphenyl azadipyrromethene. The standard numbering systems of the BODIPY and azaBODIPY core are depicted in Fig. 4.

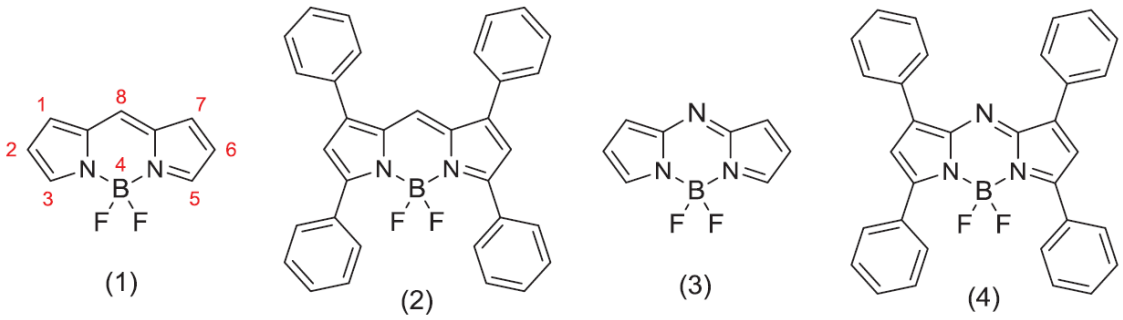

Figure 4. 1) BODIPY core, 2) tetraphenyldipyrromethene boron difluoride, 3) aza-BODIPY core, 4) tetraphenylazadipyrromethene boron difluoride.

Synthesis of Aza-BODIPYs

Synthesis of azadipyrromethenes

The first reported azadipyrromethene was tetraarylazadipyrromethene. Two methods for preparation of these dyes are known. In first, Michael addition products from chalcones and nitromethane are reacted with formamid or ammonium formate to give the azadipyrromethene (Scheme 1a). O'Shea and coworkers later made synthetic efforts to optimize the reaction conditions. They used ammonium acetate as ammonium source and alcohols instead of solvent-free approach. Scheme 1b illustrates the second method, where 2,4-diarylpyrroles are transformed into their 5-nitroso derivatives, and reacted with another pyrrole molecule. The restricted aza-BODIPY dyes are synthesized according to scheme 1c.

To gain insight into the mechanism of the synthesis of tetraphenylazadipyrromethenes, O'Shea and coworkers[51] synthesized ^{15}N-labeled potential intermediate 3,5-diphenyl-1H-pyrrol-2-amine. Investigation of its dimerization pathway showed that nitrogen rearrangement involving an exchange of a pyrrole nitrogen with an exocyclic nitrogen takes place in the final stage of the pathway. It is shown that 2,4-diphenylpyrrole, which is present in the reaction mixture as impurity, also reacts with 3,5-diphenyl-2H-pyrrol-2-imine (from oxidation of 3,5-diphenyl-1H-pyrrol-2-amine) to produce tetraphenylazadipyrromethene. Both pathways are ongoing concurrently under the reaction conditions that convert 4-nitro-1,3-diphenylbutan-1-one into tetraphenylazadipyrromethene.

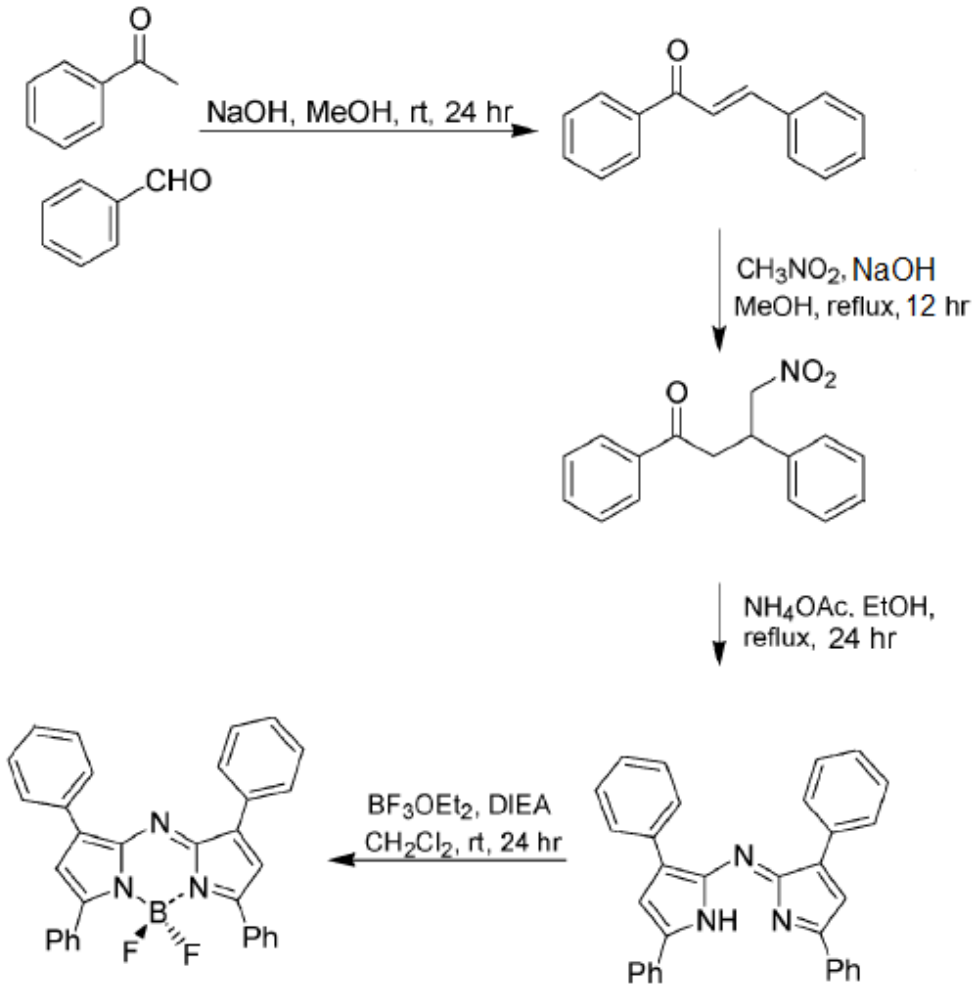

Scheme 1a. Formation of aza-BODIPYs from chalcones and nitromethane.

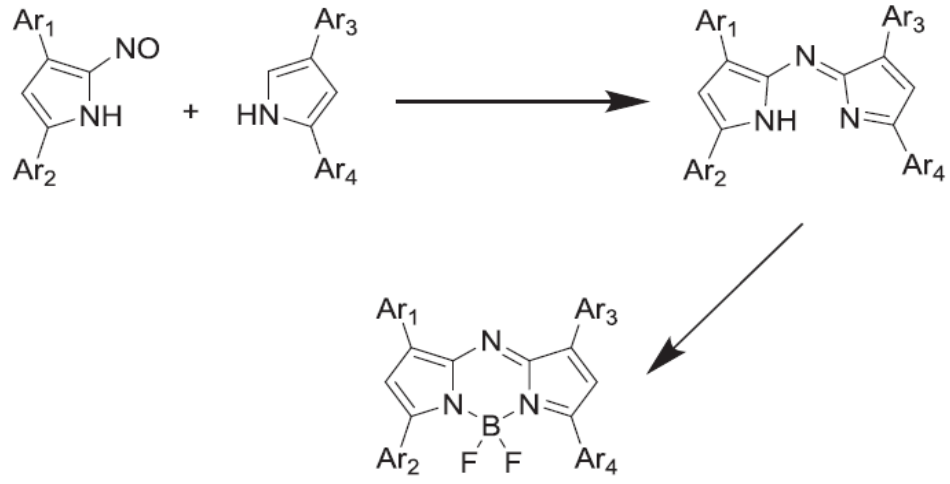

Scheme 1b. Formation of aza-BODIPYs from pyrrole and nitroso pyrrole.

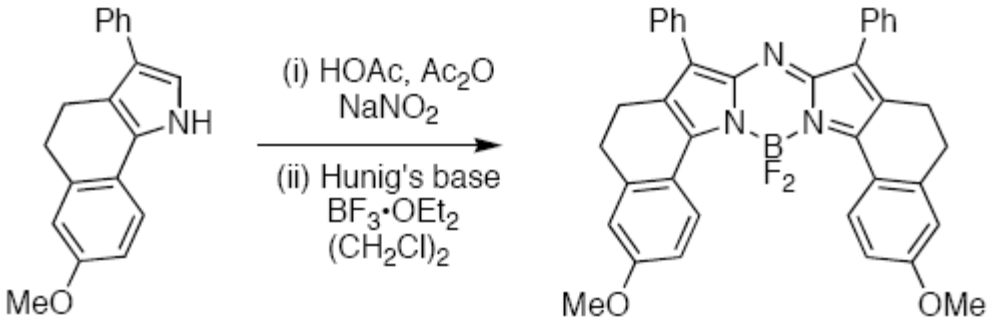

Scheme 1c. Formation of conformationally restricted aza-BODIPYs.

Absorption and Emission Properties of Aza-BODIPYs

As described in the research of O'Shea and colleagues[52] the absorption properties of aza-BODIPYs are strongly influenced by the substituents of the aryl groups. Introduction of the electron-donating groups on 5-aryl-substituents causes a red shift in the absorption maxima and increase in the molar absorption coefficients (**5** vs **1**). Electron-donating groups at the 3-aryl position have less effect, but still cause a bathochromic shift (**2** vs **3**).

The absorption spectral properties of the aza-BODIPY dyes are relatively independent of solvent polarity; only small blue-shifts are observed (6-9 nm) when changing solvents from toluene to ethanol. The molar absorption coefficients range from 75000 to 85000 $M^{-1}cm^{-1}$ and they also show large quantum yields.[53] Intense absorbance enables efficient production of singlet-oxygen and therefore these molecules found application in photodynamic therapy.[49]

Emission spectra of the aza-BODIPYs are also independent of the solvent polarity. Dyes **1** and **2** to **4** show high fluorescence quantum yields. In the case of **4**, bromine atoms are introduced on the 1- and 7-aryl groups, but no significant change in the quantum yield is detected.[52] However, if the bromine atom is attached to the aza-BODIPY core (compounds **6** to **8**) quantum yield is substantially decreased, demonstrating the heavy-atom effect. Most of the literature published on aza-BODIPY dyes is focused on their application in photodynamic therapy, but chemosensors based on these dyes have also been reported. Dye **9** has high selectivity for mercuric ion that is chelated between two 2-pyridyl groups at the 1 and 7 positions.[54] Upon complexation with Hg^{2+}, bathochromic shift and a 90-fold change in the emission are observed.

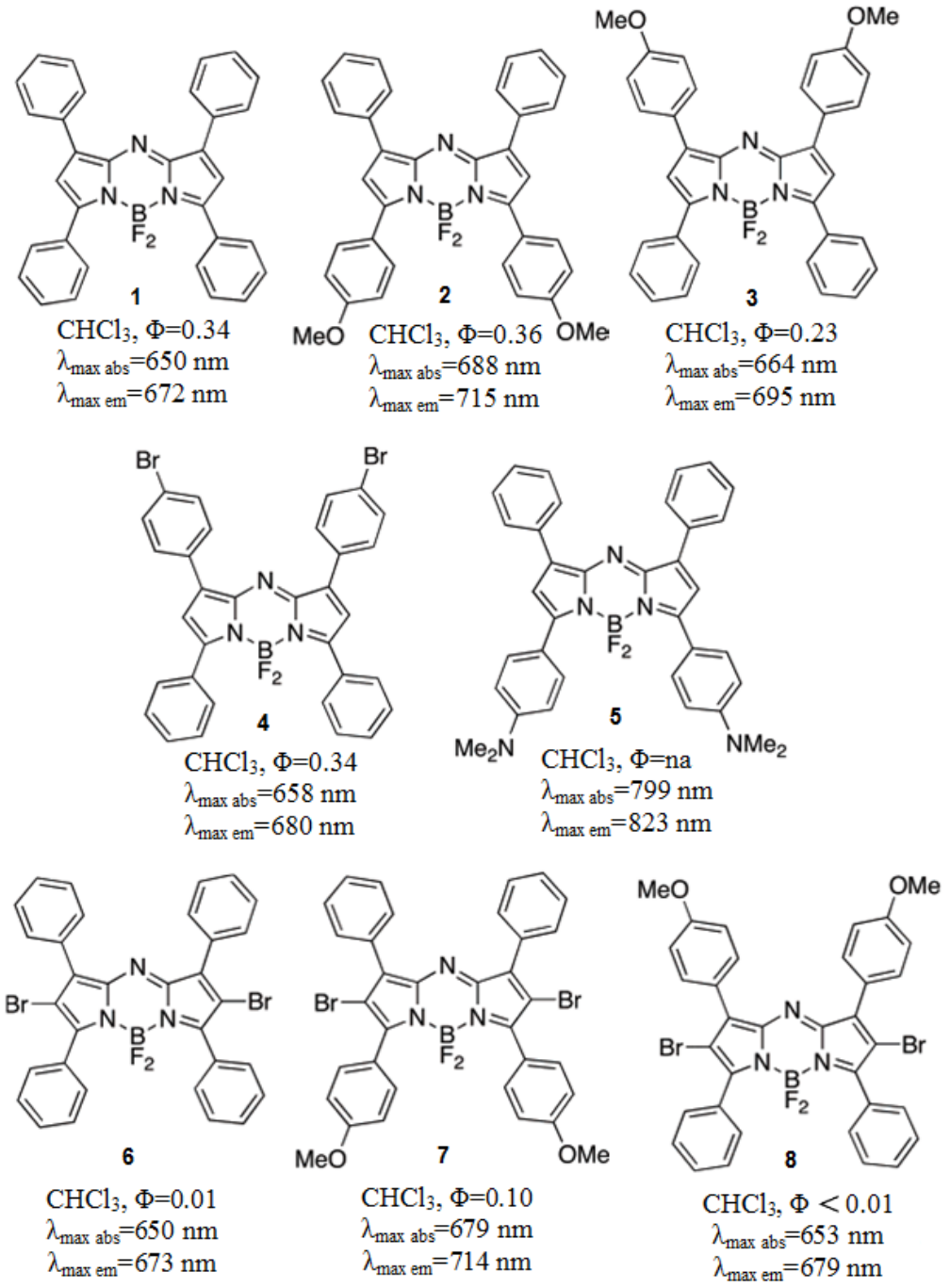

Figure 5. Aza-BODIPYs with different substituents.

Shen et al. developed selective colorimetric and fluorometric aza-BODIPY probe **10** containing two pyrazine rings.[55] The probe displayed absorption and emission maxima at 685 and 718 nm. The addition of NH_4^+ caused hypsochromic shift, decrease of the molar absorption coefficient and quenching of the fluorescence.

Dye **11** is a PET-based probe with incorporated crown ether and it is used as indicator for the shellfish toxin saxitoxin.[56] In the absence of saxitoxin, fluorescence is quenched due to PET from the crown ether to the fluorophore. After complexation with the toxin, PET is inhibited and fluorescence is recovered. Probe **11** and saxitoxin formed a complex with a binding constant $6.2x10^5\ M^{-1}$, what is the highest reported for any indicator of saxitoxin.

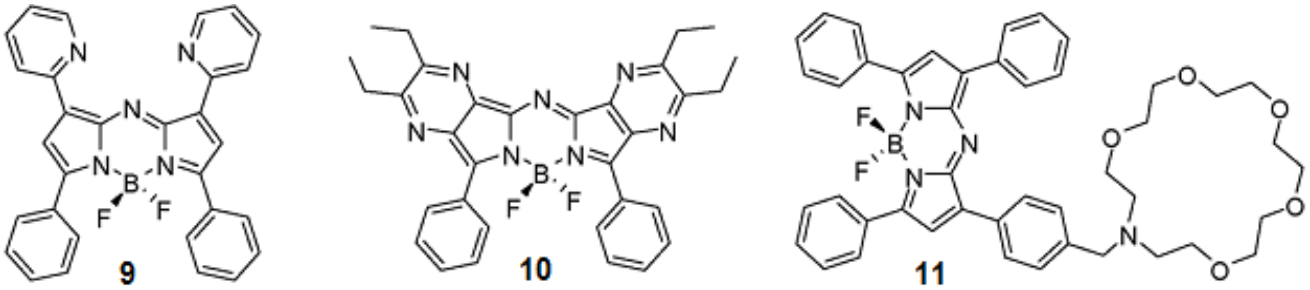

Figure 6. Chemosensors based on aza-BODIPY probe.

Recently, several research groups developed reaction-based aza-BODIPY indicators. Tang and coworkers designed a reaction-based probe **12** for fluorine ions (Fig. 64).[57] Due to PET the fluorescence of the probe is quenched. However, F^- - induced cleavage of the Si-B bond yielded the probe **13** with significant fluorescence enhancement. The probe exhibited high sensitivity to F- and was applied for fluorescence imaging of F^- in Hep G2 cells.

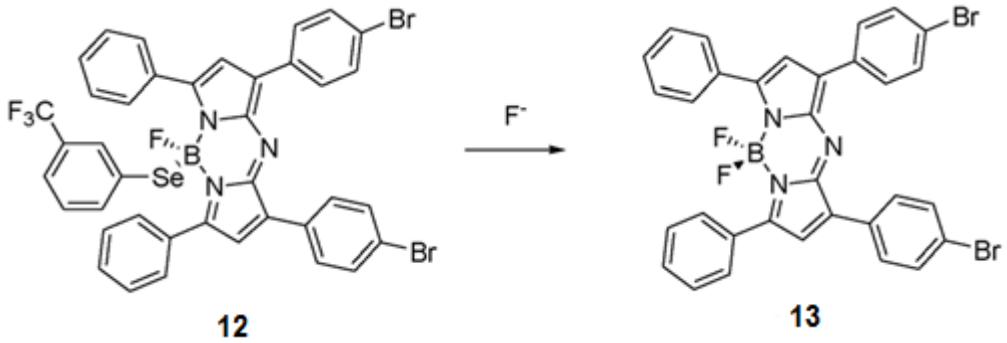

Figure 7. Detection of F^- based on aza-BODIPY probe.

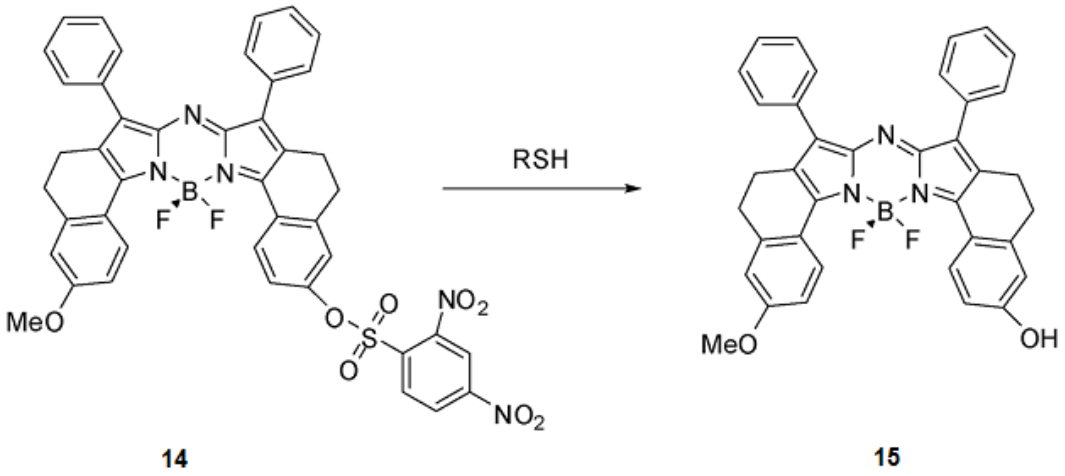

Figure 8. Detection of thiols based on aza-BODIPY probe.

Jiang et al constructed reaction-based fluorescent probe **14** for thiols (Fig. 65).[58] Due to PET the probe exhibited weak fluorescence with an emission maximum at 734 nm. After addition of thiols fluorescence enhancement was observed and bathochromic shift due to the cleavage of 2,4-dinitrobenzenesulfonyl (DNBS) moiety and formation of probe **15**. Probe **14** showed high selectivity for thiols and a detection limit of $5x10^{-7}$ M^{-1} was determined.

Extended Aza-BODIPY Dyes

Bathochromic shift of the emission of aza-BODIPY dyes has been achieved by introduction of electron-donating groups, structural rigidification and extension of the conjugation of the aza-BODIPY dye. Restricted aza-BODIPY dyes (Figure 9) have sharp, intense absorption bands at wavelengths above 650 nm. Incorporation of the electron-donating groups at the 3-position of the aza-BODIPY core results in a slightly higher fluorescence quantum yield and small blue shift, while the molar absorption coefficient is not affected (**16** vs **17**). Comparing the absorption spectra of these compounds with the non-restricted aza-BODIPY dyes, there is about a 50 nm bathochromic shift in the absorption.[59]

Aza-BODIPY containing two or one side carbocyclic rings have showed good photostability and intense fluorescence emission independent of solvent polarity.[60] The dye with incorporated sulfur (**18**) exhibited shorter absorption maximum, lower molar absorption coefficient and lower

quantum yield. Dehydrogenation of the carbocyclic ring in dye **19** decreases the quantum yield in comparison to **16**. Dyes with one restricted side have significantly lower molar absorption coefficients (**20**-**24** vs **16**) and their quantum yields are highly influenced by the substitution on the phenyl ring. Electron donating groups in para-positions results in higher quantum yield (**20** and **21**) with shorter absorption maxima.

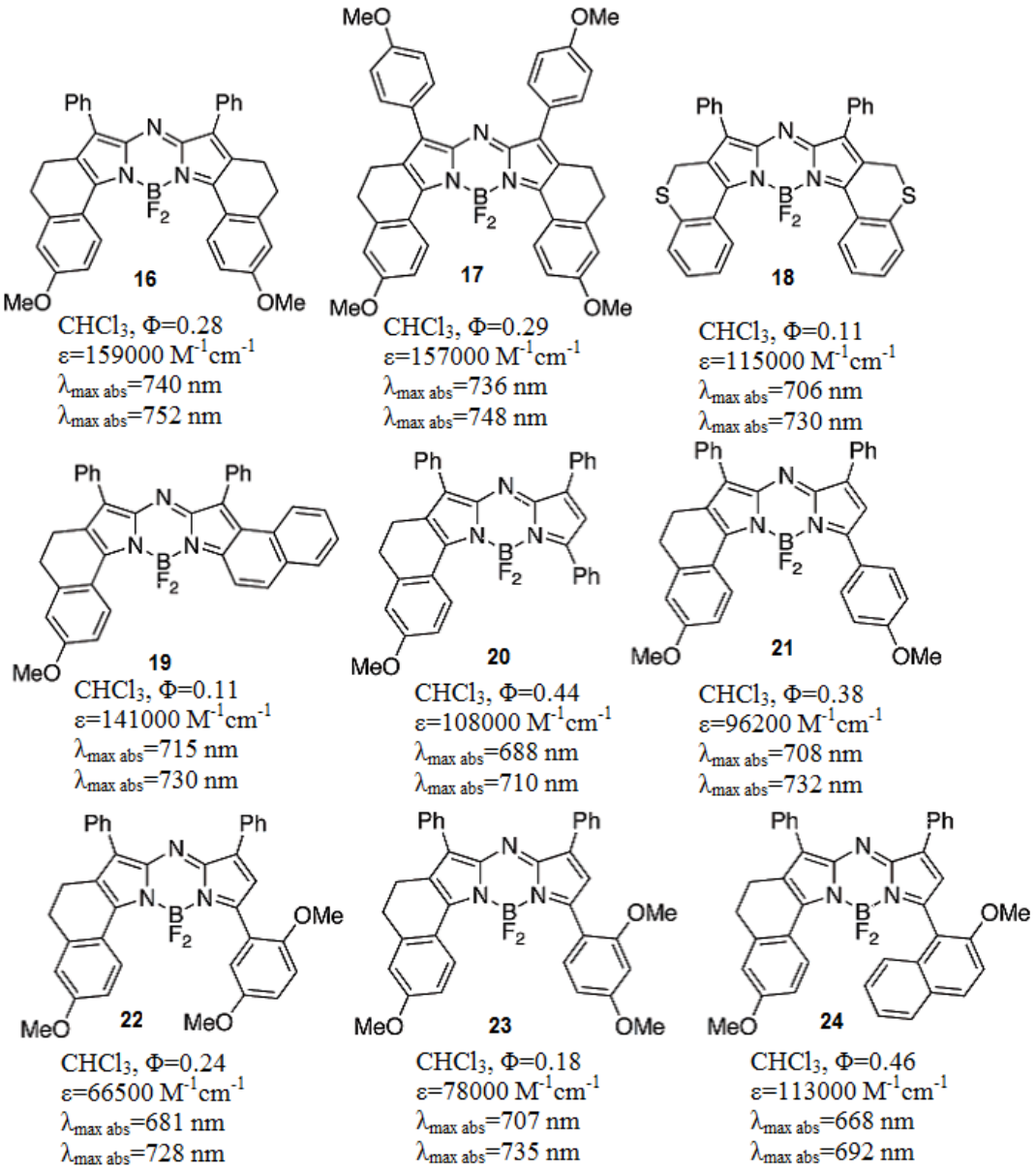

Figure 9. Conformationally restricted aza-BODIPY probes.

Electron donating groups in ortho-positions (**22** and **23**) cause shorter absorption maximum and lower molar absorption coefficient. In the case of **24** absorption and high quantum yields are obtained where 2-methoxy-1-naphthyl is substituent.

Another way to red-shift the emission can be achieved introducing ortho-hydroxy groups to chelate the boron atom, as in dye **25**.[61] Rigidification caused by the B-O coordination causes bathochromic shifts and a 7-fold increase in the quantum yield. Spectral properties can also be altered by benzannulation of the 1,7-aryl rings, as in dye **26**.[62]

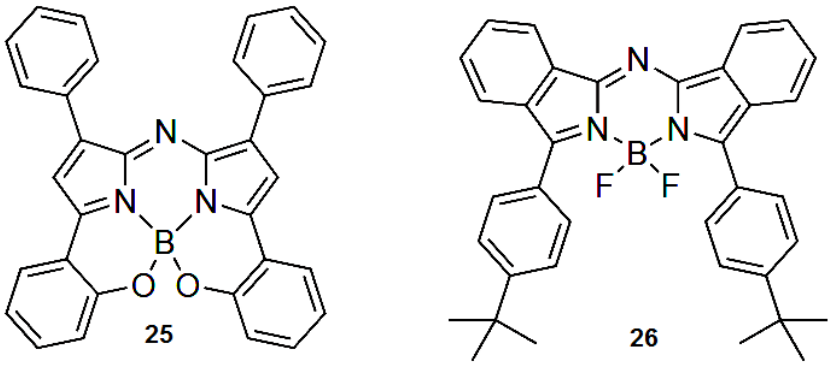

Figure 10. Aza-BODIPY probes for applications in bio-imaging (**25**) and photodynamic therapy (**26**).

1.7. References

1. Vasylevska, A. S., Karasyov, A. A., Borisov, S. M., Krause C., *Anal. Bioanal. Chem*. **2007**, 387, 2131-2141.

2. Carter J. C., Alvis R. M., Brown S. B., Langry K. C., Wilson T. S., McBride M. T., Myrick M. L., Cox W. R., Grove M. E., Colston B. W., *Biosens. Bioelectronics* **2006**, 21, 1359-1364.

3. Goldstein S. R., Peterson J. P., Fitzgerald R. V., *J. Biomech. Eng*. **1980**, 102, 141-146.

4. Saari L. A., Seitz W. R., *Anal. Chem*. **1982**, 54, 821-823.

5. Wolfbeis, O. S., Fürlinger E., Kroneis H., Marsoner H., *Fresenius Anal. Chem*. **1983**, 314, 119-124.

6. Whitaker, J. E., Haugland R. P., Prendergast F. G., *Anal. Biochem*. **1991**, 194, 330-344.

7. Offenbacher H., Wolfbeis O. S., Fürlinger E., *Sens. Actuators B* **1986**, 9, 73-84.

8. Bojinov, V., Grabchev, I., *Dyes and Pigments* **2003**, 59, 277-283.

9. Dawson, D. J., Otteson, K. M., Wang, P. C., Wingard, R. E., *Jr. Macromolecules* **1978**, 11, 320-324.

10. W. A. Wyatt, G. E. Poirier, F. V. Bright and G. M. Hieftje, *Anal. Chem.* **1987**, 59, 572-576.

11. Z. Zhujun and W.R. Seitz, *Anal. Chim. Acta* **1984**, 160, 47-55.

12. R. Narayanaswamy and F. Sevilla, *Anal. Chim. Acta* **1986**, 189, 3656-3669.

13. Leiner, M. J. P., Hartmann, P., *Sensors and Actuators B* **1993**, 11, 281-289.

14. Wolfbeis O. S., Offenbacher H., *Sens. Actuators* **1986**, 9, 85-91.

15. Werner T., Huber C., Heinl S., Kollmannsberger M., Daub J., Wolfbeis O. S., *Fresenius' J. Ana. Chem.* **1997**, 359, 150-154.

16. Draxber S., Lipittsch M. E., *Proc. SPIE* **1995**, 2388, 363-368.

17. Parker J. W., Laksin O., Yu C., Lau M. L., Klima S., Fisher R., Scott I., Atwater B. W., *Anal. Chem.* **1993**, 65, 2329-2334.

18. Papkovsky D. B., Ponomarev G. V., Wolfbeis O. S., *J. Photochem. Photobiol. A* **1997**, 104, 151-158.

19. Wolfbeis, O. S., E. Fürlinger, E., Kroneis, H., Marsoner, H., *Fresenius J. Anal. Chem*. **1983**, 314, 119-124.

20. Mills, A., Chang, Q., McMurray, N., *Anal. Chem*. **1992**, 64, 1383-1389.

21. Mills, A. Lepre, L. Wild, *Sensors Actuat. Part B* **1997**, B39, 419-425.

22. Wolfbeis, O. S., Weis, L., Leiner, M. J. P., Ziegler, W. E., *Anal. Chem*. **1988**, 60, 2028-2030.

23. Vasylevska, A. New pH sensitive sensor materials. Luminescent fiber-optic dual sensors for non-invasive and simultaneous measurement of pH and pO_2 (dissolved oxygen) in biological systems. PhD thesis, University of Regensburg, Regensburg, 2007, p 9.

24. Klimant, I., Ger. Pat. Appl. 1997, DE 198 29 657.

25. Klimant, I., Huber, C., Liebsch, G., Neurauter, G., Stanglmayer, A., Wolfbeis, O. S., Dual lifetime referencing (DLR) – a new scheme for converting fluorescence intensity into a frequency-domain or time-domain information. In New Trends in Fluorescence Spectroscopy, Springer Series on Fluorescence, **2001**, 257-274.

26. Huber, C., Klimant, I., Krause, C., Wolfbeis, O. S., *Anal. Chem*. **2001**, 73, 2097-2103.

27. Lakowitz, J. R., Castellano, F. N., Dattelbaum, J. D., Tolosa, L., Rao, G., Gryczynski, I., *Anal. Chem*. **1998**, 70, 5115-5121.

28. R. A. Marcus, *Angew. Chem., Int. Ed*. **1993**, 32, 111-1121.

29. Shao, J., Guo, H., Ji, S., Zhao, J., *Biosens. Bioelectron*. **2011**, 26, 3012-3017.

30. Förster, T., *Ann. Phys*. **1948**, 437, 55-75.

31. Deniz, E., Isbasar, G. C., Bozdemir, O. A., Yildirim, L. T., Siemiarczuk, A., Akkaya, E. U., *Org. Lett*. **2008**, 10, 3401-3403.

32. McDonnell, S. O., O'Shea, D. F., *Org. Lett*. **2006**, 8, 3493-3496.

33. Hall, M. J., Allen, L. T., O'Shea, D. F., *Org. Biomol. Chem*. **2006**, 4, 776-780.

34. Fan, L., Fu, Y. J., Liu, Q. L., Lu, D. T., Dong, C., Shuang, S. M., *Chem. Commun*. **2012**, 48, 11202-11204.

35. Schutting, S., Borisov, S. M., Klimant, I. *Anal. Chem*. **2013**, 85, 3271-3279.

36. Aigner, D., Borisov, S. M., Petritsch, P., Klimant, I. *Chem. Commun***. 2013**, 49, 2139-2141.

37. Lee, H., Akers, W., Bhushan, K., Bloch, S., Sudlow, G., Tang, R., Achilefu, S., *Bioconjugate Chem*. **2011**, 22, 777-784.

38. Myochin, T., Hanaoka, K., Kojima, H., Terai, T., Nagano, T., *J. Am. Chem. Soc*. **2011**, 133, 3401-3409.

39. Ni, Y., Wu, J., *Org. Biomol. Chem*. **2014**, 12, 3774-3791.

40. Rurack, K., Kollmannsberger, M., Daub, J., *New J. Chem*. **2001**, 25, 289-292.

41. Hoogendoorn, S., Blom, A. E. M., Willems, L. I., van der Marel, G. A., Overkleeft, H. S., *Org. Lett.*, **2011**, 13, 5656-5659.

42. Hall, M. J., Allen, L. T., O'Shea, D. F., *Org. Biomol. Chem*. **2006**, 4, 776-780.

43. Zhang, X., Wang, Z., Yue, X., Ma, Y., Kiesewetter, D. O., Chen, X., *Mol. Pharmaceutics* **2013**, 10, 1910-1917.

44. Murtagh, J., Frimannsson, D. O., O'Shea, D. F., *Org. Lett*. **2009**, 11, 5386-5389.

45. McDonnell, S. O., O'Shea, D. F., *Org. Lett*., **2006**, 8, 3493-3496.

46. Liu, W., Sun, R., Ge, J-F., Xu, Y-J., Xu, Y., Lu, J.M., Itoh, I., Ihara, M., *Anal. Chem*. **2013**, 85, 7419-7425.

47. Loudet, A.; Burgess, K. *Chem. Rev*. **2007**, 107, 4891-4932.

48. Sathyamoorthi, G., Soong, M. L., Ross, T. W., Boyer, J. H., *Heteroat. Chem***. 1993**, 4, 603-608.

49. Gallagher, W.M., Allen, L.T., O'Shea, C., Kenna, T., Hall, M., Gorman, A., Killoran, J., O'Shea, D.F., *Br. J. Cancer* **2005**, 92, 1702-1710.

50. Killoran, J., McDonnell, S. O., Gallagher, J. F., O'Shea, F., *New J. Chem***. 2008**, 32, 483-489.

51. Grossi, M., Palma, A., McDonnell, S. O., Hall, M. J., Dilip K. R., Muldoon, J., O'Shea, D. F., *J Org. Chem***. 2012**, 77, 9304-9312.

52. Gorman, A., Killoran, J., O'Shea, C., Kenna, T., Gallagher, W. M., O'Shea, D. F., *J. Am. Chem. Soc*. **2004**, 126, 10619-1631.

53. Flavin, K., Bartelmess, J., Tasior, M., Navio, C., Bittencourt, C., O'Shea, D. F., Guldi, D. M., Giordani, S., *ACS Nano* **2011**, 5, 1198-1206.

54. Coskun, A., Yilmaz, M. D., Akkaya, E. U., *Org. Lett.* **2007**, *9*, 607-609.

55. Liu, H., Mack, J., Guo, Q., Lu, H., Kobayashi, N., Shen, Z., *Chem. Commun.* **2011**, 47, 12092-12094.

56. Gawley, R. E., Mao, H., Haque, M. M., Thorne, J. B., Pharr, J. S., *J. Org. Chem*. **2007**, 72, 2187-2191.

57. Gong, W., Su, R. X., Li, L., Xu, K. H., Tang, B., *Chin. Sci. Bull*. **2011**, 56, 3260-3265.

58. Jiang, X.-D., Zhang, J., Shao, X., Zhao, W., *Org. Biomol. Chem*. **2012**, 10, 1966-1968.

59. Zhao, W., Carreira, E. M., *Angew. Chem., Int. Ed*. **2005**, 44, 1677-1679.

60. Loudet, A., Burgess K., *Chem. Rev*. **2007,** 107, 4891-4932.

61. A. Loudet, R. Bandichhor, K. Burgess, A. Palma, S. O. McDonnell, M. J. Hall, D. F. O'Shea, *Org. Lett*. **2008**, 10, 4771-4774.

62. V. F. Donyagina, S. Shimizu, N. Kobayashi, E. A. Lukyanets, *Tetrahedron Lett*. **2008**, 49, 6152-6154.

Chapter 2

Highly Photostable Near-Infrared Fluorescent pH Indicators and Sensors based on BF_2-Chelated Tetraarylazadipyrromethene Dyes

Tijana Jokic,[†] Sergey M. Borisov,[†*] Robert Saf,[‡] Daniel A. Nielsen,[§] Michael Kühl,[§⊥∥] and Ingo Klimant[†]

[†]Institute of Analytical Chemistry and Food Chemistry, Graz University of Technology, Stremayrgasse 9, 8010, Graz, Austria

[‡]Institute of Chemistry and Technology of Materials, Graz University of Technology, Stremayrgasse 9, 8010, Graz, Austria

[‡]Plant Functional Biology and Climate Change Cluster, Department of Environmental Science, University of Technology, Sydney, PO Box 123, Broadway NSW, Australia

[⊥]Singapore Centre on Environmental Life Sciences Engineering, School of Biological Sciences, Nanyang Technological University, Singapore

[∥]Marine Biology Section, Department of Biology, University of Copenhagen, Strandpromenaden 5, DK-3000 Helsingør, Denmark

Abstract

In this study a series of new BF_2-chelated tetraarylazadipyrromethane dyes are synthesized and are shown to be suitable for the preparation of on/off photoinduced electron transfer modulated fluorescent sensors. The new indicators are noncovalently entrapped in polyurethane hydrogel D4 and feature absorption maxima in the range 660-710 nm and fluorescence emission maxima at 680-740 nm. Indicators have high molar absorption coefficients of ~ 80000 $M^{-1}cm^{-1}$, good quantum yields (up to 20%), excellent photostability and low cross-sensitivity to the ionic strength. pK_a values of indicators are determined from absorbance and fluorescence measurements and range from 7 to 11, depending on the substitution pattern of electron-donating and -withdrawing functionalities. Therefore, the new indicators are suitable for exploitation and adaptation in a diverse range of analytical applications. Apparent pK_a values in sensor films

derived from fluorescence data show 0.5−1 pH units lower values in comparison with those derived from the absorption data due to Förster resonance energy transfer from protonated to deprotonated form. A dual-lifetime referenced sensor is prepared, and application for monitoring of pH in corals is demonstrated.

2.1 Introduction

Design, synthesis, and spectroscopic/photophysical characterization of novel fluorescent chemosensors remains a central research field in analytical chemistry.[1] The measurement of pH by fluorescence-based techniques is well established for both imaging and sensing applications[2,3] in various fields of experimental science, such as biomedical research,[4−10] marine biology,[11,12] and biotechnology.[13,14] The most frequently used fluorescent pH indicators are 8-hydroxypyrene-1,3,6-trisulfonic acid (HPTS), carboxyfluorescein derivatives, seminaphthorhodafluors (SNARFs), and hydroxycoumarins.[15−19] However, these indicators suffer from several drawbacks. For example, carboxyfluorescein has only moderate photostability, and the photostability of 2′,7′-dihexylfluorescein (suitable for measurements in seawater) is very poor;[20] the pK_a value of HPTS is highly dependent on ionic strength of solution; and most coumarins are excitable only by high-energy radiation in the range from 350 to 450 nm. In biological applications, it is desirable to use fluorophores with absorption/emission profiles in the red or near-infrared (NIR) spectral regions because they have many advantages: significant reduction of the background signal due to the low absorption and autofluorescence of biomolecules in the NIR region, low light scattering and deep penetration of the NIR light, and the possibility to use low-cost excitation light sources. Despite the optical benefits, there is a surprising scarcity of pH indicators that have such desired absorption and emission properties. Although the water-soluble SNARF indicators and their lipophilic derivatives do absorb at ∼630 nm, they possess only moderate brightness and photostability.[21] The same holds for the cyanine dyes, which are well-known NIR chromophores that have only scarcely been proposed as pH indicators.[22,23]

In contrast, BF_2-chelated tetraarylazadipyrromethane dyes (aza-BODIPYs) represent an interesting class of NIR chromophores that are amenable to structural modification and exhibit excellent photophysical properties.[24] Several fluorescent pH indicators based on aza-BODIPY

dyes bearing amino- or hydroxy-functionalized substituents were reported by O'Shea and co-workers.[25−27] These on/off pH indicators show photoinduced electron transfer from an amino group or a twisted phenolate to the aza-BODIPY subunit, causing fluorescence quenching in the deprotonated state. However, these probes cover only acidic and near-neutral range. A systematic study of the properties of these pH indicators and possible synthetic modifications with respect to tuning the pK_a values has not previously been reported in the literature.

In the present study, we investigated the synthesis and characterization of aza-BODIPY fluorophores that can probe pH changes by large associated changes in their emission intensity around 700 nm and possess pK_a values in the physiological and alkaline pH range. Eight 4,4-difluoro-4-bora-3*a*,4*a*-triaza-*s*-indacene dyes that can detect pH through a photoinduced electron transfer process were synthesized and characterized. We show that the pK_a values of the new indicators can be tuned over a wide range, and simple prediction rules can be derived. This enables a variety of potential applications for sensors and imaging. As an example, an application of the new sensing materials for fiber-optic pH measurements in marine biology is demonstrated.

2.2 Experimental

Materials

3′-Chloro-4′-hydroxyacetophenone, 1,3-diphenyl-2-propenone, tera-*tert*-butyl-29*H*,31*H*-phtalocyanine, *N*,*N*-diisopropylethylamine, ammonium acetate, benzaldehyde, seminaphthorhodafluor decyl ester (SNARF-DE, chromoionophore XIII), boron trifluoride diethyl etherate, MOPS buffer salt, and anhydrous sodium sulfate were purchased from Sigma Aldrich (www.sigmaaldrich.com). 3′-Hydroxyacetophenone, 4-hydroxychalcone, 4′-hydroxychalcone, 4′-methoxychalcone, 4,4′-dimethoxychalcone, and nitromethane were obtained from ABCR (www.abcr.com). 4′-Hydroxy-3′-methylacetophenone was obtained from TCI Europe (www.tcieurope.de). Deuterated dimethyl sulfoxide was obtained from Euriso-top (www.eurisotop.com). All other solvents (synthesis grade) as well as sodium chloride and the buffer salts CHES, MES, and CAPS were supplied by Carl Roth (www.roth.de). Silica-gel (0.04–0.063 mm) was from Acros (www.fishersci.com). Polyurethane hydrogel (Hydromed D4) was purchased from AdvanSource biomaterials (www.advbiomaterials.com). Poly(ethylene

glycol terephthalate) support (Mylar) was obtained from Goodfellow (www.goodfellow.com). Microcrystalline powder of phosphor chromium(III)-activated gadolinium aluminum borate ($Gd_3Al_{4.75}Cr_{0.25}O_{12}$, Cr-GAB) was prepared as described previously.[28]

Synthesis

The synthetic concept is exemplified by the following synthesis of **1**. The other dyes were obtained in a similar way, and their preparation is described in detail in the Supporting Information.

BF_2 Chelate of [5-(4-Hydroxyphenyl)-3-phenyl-1*H*-pyrrol-2-yl]-[5-phenyl-3-phenylpyrrol-2-ylidene]amine (1) 1-(4-Hydroxyphenyl)-4-nitro-3-phenylbutan-1-one (**1a**). A solution of 1-(4-hydroxyphenyl)-3-phenylpropenone (1 equiv, 2 g, 8.9 mmol), nitromethane (20 equiv, 9.63 mL, 178 mmol), and KOH (1.2 equiv, 0.6 g, 10.68 mmol) in EtOH (10 mL) was heated at 60 °C under reflux for 12 h. After cooling to room temperature, the solvent was removed in vacuo, and the oily residue obtained was acidified with 4 M HCl and partitioned between EtOAc (50 mL) and H_2O (50 mL). The organic layer was separated, dried over sodium sulfate, and evaporated under reduced pressure. The obtained product was used for further synthesis without purification (2.06 g, 80%).

1,3-Diphenyl-4-nitro-butan-1-on (**1b**). A solution of 1,3-diphenyl-2-propenone (1 equiv, 2 g, 9.6 mmol), nitromethane (20 equiv, 10.37 mL, 192 mmol) and KOH (0.2 equiv, 0.106 g, 1.9 mmol) in EtOH (10 mL) was heated at 60 °C under reflux for 12 h. After cooling to room temperature, the solvent was removed in vacuo, and the oily residue obtained was partitioned between EtOAc (50 mL) and H_2O (50 mL). The organic layer was separated, dried over sodium sulfate, and evaporated under reduced pressure. The obtained product was used for further synthesis without purification (1.52 g, 80%).

[5-(4-Hydroxyphenyl)-3-phenyl-1*H*-pyrrol-2-yl]-[5-phenyl-3-phenylpyrrol-2-ylidene]amine (**1c**). Compound **1a** (1 equiv, 1.0 g, 4.4 mmol), compound **1b** (1 equiv, 0.93 g, 4.4 mmol), and ammonium acetate (35 equiv, 8.06 g, 245 mmol) in butanol (50 mL) were heated under reflux for 24 h. The reaction was cooled to room temperature, and the crude product was purified by column chromatography on silica-gel eluting with dichloromethane (after eluting symmetric byproduct with hexane/dichloromethane 3:1 v/v) to yield **1c** as a blue-black solid. The product

was recrystallized from hexane/tetrahydrofuran mixture to give green metallic crystals (0.42 g, 25%). For the calculation, the theoretical yield of the asymmetrical product is set as 100%).[1]H NMR (300 MHz, DMSO-d_6) δ: 8.13–8.08 (m, 6H), 7.94 (s, 2H), 7.92 (s, 1 H), 7.80 (s, 1H), 7.63–7.58 (m, 1H), 7.5–7.33 (m, 8H), 7.02 (d, J = 8.8 Hz, 2H). Electron impact direct insertion time-of-flight (EI-DI-TOF) m/z [MH^+] found 465.1822, calc 465.1841.

BF_2 chelate of 1c

Compound **1c** (0.34 g, 0.73 mmol) was dissolved in dry CH_2Cl_2 (50 mL), treated with diisopropylethylamine (10 equiv, 0.54 mL, 3.11 mmol) and BF_3 diethyletherate (15 equiv, 0.55 mL, 4.35 mmol),. and stirred under argon for 24 h. Purification by column chromatography on silica gel eluting with CH_2Cl_2 and recrystallization from hexane/tetrahydrofurane gave the final product **1** as a red metallic solid (0.201 g, 43%). [1]H NMR (300 MHz, DMSO-d_6) δ: 10.72 (s, 1H), 8.23–7.99 (m, 8H), 7.77 (s, 1H), 7.61–7.36 (m, 10H), 6.95 (d, J = 8.8 Hz, 2H). Electron impact direct insertion time-of-flight (EI-DI-TOF) m/z[MH^+] found 512.186, calc 512.186.

Preparation of Sensor Foils and Fiber-Optic Microsensors A "cocktail" containing an indicator dye (0.25 mg), hydrogel D4 (100 mg) in 700 μL EtOH/H_2O (9:1 v/v), and tetrahydrofurane (300 μL) was knife-coated on a dust-free Mylar support to obtain a ∼2.5 μm thick sensing layer after solvent evaporation.

The "cocktail" for the dual-lifetime referenced sensor was prepared similarly from 0.1 mg of indicator dye **1**with addition of 200 mg of Cr-GAB particles. Subsequently, it was coated on the tip of an optical fiber (Ø 400 μm) from Specialty Photonics (www.specialtyphotonics.com). The sensors were allowed to dry 30 min in the ambient to ensure complete evaporation of the solvent. Between measurements, the sensors were stored in darkness at room temperature.

Methods

Absorption measurements were performed on a Cary 50 UV–vis spectrophotometer from Varian (www.varianinc.com). The molar absorption coefficients were determined as an average of three independent measurements for the concentrations of the dyes 2.5–3.4 × 10^{-6} M. Fluorescence spectra were recorded on a Hitachi F-7000 spectrofluorometer (www.hitachi.com). Relative fluorescence quantum yields were determined according to Demas and Crosby[29] using tera-*tert*-butyl-29*H*,31*H*-phtalocyanine (Fluka,www.sigmaaldrich.com) as a standard (quantum yield = 0.44).[30] Two independent measurements were performed to obtain the average value. The

concentration of the indicators was kept below 1.5×10^{-6} M to avoid dye aggregation and reabsorption of the fluorescence. NMR spectra were recorded on a 300 MHz instrument (Bruker) in DMSO-d_6 or $CDCl_3$ with TMS as a standard. Electron impact (EI, 70 eV) mass spectra were recorded on a Waters GCT Premier equipped with direct insertion (DI). The pH of the buffer solutions (CHES, MES, and CAPS) was controlled by a digital pH meter (InoLab pH/ion, WTW GmbH & Co. KG, www.wtw.com) calibrated at 25 °C with standard buffers of pH 7.0 and pH 4.0 (WTW GmbH & Co. KG, www.wtw.com). The buffers were adjusted to constant ionic strength (IS = 0.02 or 0.15 M) using sodium chloride as the background electrolyte. Dual-lifetime referenced measurements were performed with a fiber-optic Firesting fluorometer from Pyroscience (www.pyro-science.com) with a modulation frequency of 4 kHz.

Photobleaching experiments in solutions were performed by irradiating the samples with light from a 642-nm high-power 10 W LED array (www.led-tech.de) focused through a lens purchased from Edmund optics (www.edmundoptics.de). The photodegradation profiles were obtained by monitoring the absorption spectra. For the leaching test, sensor foil (D4) was placed in a flow-through cell, and the absorption of the films was monitored while aqueous buffer (IS = 0.02 M) was passed through it. A detailed description of the pH measurements in the gastric cavity of a symbiont bearing coral (*Goniopora* sp.) is contained in the Supporting Information.

2.3 Results and discussion

Synthesis. Two general methods to prepare azadipyrromethene chromophore are known. In the first method, 2,4-diarylpyrroles act as precursors, and are converted into their 5-nitroso derivatives, which are then condensed with a second molecule of pyrrole to yield unsymmetric derivatives.[31] In the second method, nitromethane adducts of chalcones are reacted with ammonium salts at elevated temperatures to give symmetric azadipyrromethenes.[32] Conversion of the diarylnitroketones into pyrroles and 5-nitrosopyrroles and the isolation of these products is not required in this method.

Unsymmetrical derivatives of the aza-BODIPYs bearing only one pH-sensitive group were strongly preferable to the symmetrical ones for several reasons: (i) a simple acid–base equilibrium including only two forms of the indicator; (ii) significantly higher hydrophobic character of the monosubstituted derivatives compared to the symmetrical ones, which prevents

the dye from leaching into an aqueous environment, particularly in case of the deprotonated form; (iii) a low charge of the deprotonated form (1−), which is expected to minimize the effect of the ionic strength on the sensing properties.

Keeping practical applications in mind (in which accessibility of the indicators is very important) we decided to employ the second method for preparation of the unsymmetrical dyes. In this approach, condensation of two different nitrochalcones results in a mixture of the aimed unsymmetrical aza-BODIPY and two symmetrical derivatives (Scheme 1), which are easily separated via chromatography on silica gel. The starting compounds for the synthesis were the diaryl α,β-unsaturated ketones (chalcones) that are either commercially available (for the synthesis of **1**, **5**, **7**, and **8**) or prepared by Claisen–Schmidt condensation (for the synthesis of **2**–**4**, **6**). These were synthesized from the corresponding aldehyde and acetophenone with KOH as a base in all cases, except for **6**, for which NaH was used. The Michael addition of nitromethane to the chalcones, with KOH as base,[33] yields the 1,3-diaryl-4-nitrobutan-1-ones in essentially quantitative yields after aqueous workup, which were then used without further purification. Condensation with ammonium acetate in refluxing butanol gave the azadipyrromethenes via a cascade of events (in situ formation of the pyrrole and corresponding nitrosopyrrole and subsequent condensation of those two entities). The obtained mixture was purified by chromatography with hexane/dichloromethane in the case of **1**–**6** or toluene/dichloromethane in case of **7** and **8**. Finally, complexation of the azadipyrromethenes with boron trifluoride gave the aza-BODIPYs in good yields.

Photophysical properties. The new aza-BODIPY compounds were dissolved in an EtOH/aqueous buffer mixture (1:1), and their spectroscopic properties were investigated (Figure S1 of the Supporting Information, Table 1). The absorption of the probes bearing a hydroxyl group in the p-position (R_1) of Ar^4 is rather similar (668–677 nm). The shortest wavelengths of the absorption maxima are observed for **5** and **6** (656 and 650 nm, respectively. These data indicate pronounced conjugation of the Ar^3 and Ar^4 rings with the aza-BODIPY chromophore and the absence of such conjugation for the Ar^1 and Ar^2 rings. This conjugation can be caused by a hydrogen bond between the fluorine atom and the hydrogen atom located in the o-positon of Ar^3 and Ar^4rings. Evidently, the electron-donating substituents (−OH or O–CH_3) in the p-position of the Ar^3 and Ar^4rings result in the bathochromic shift of the absorption spectrum but

have no effect on the spectral properties if located in the Ar^1 and Ar^2 rings. As expected, the hydroxyl group in the m-position of the Ar^4 has virtually no effect on the spectral properties. The molar absorption coefficients for all aza-BODIPY derivatives are in the 70 000–90 000 M^{-1} cm^{-1} range. It should be mentioned that precision of determination of molar absorptivities as well as fluorescence quantum yields can be affected by inpurities of the probes. Although all the indicators were obtained as single crystals, several indicators show solvent impurities in the ^1H NMR spectrum. As revealed by crystallographic study of **8** (Figure S2 of the Supporting Information), this is explained by incorporation of solvent molecules (tetrahydrofurane and hexane) into the crystal structure. Evidently, this slightly affects the calculated molar absorption coefficients. For instance, the crystals of **8** contain one molecule of tetrahydrofurane per each molecule of the dye, and this results in the reduction of molar absorption coefficients by about 8.8%.

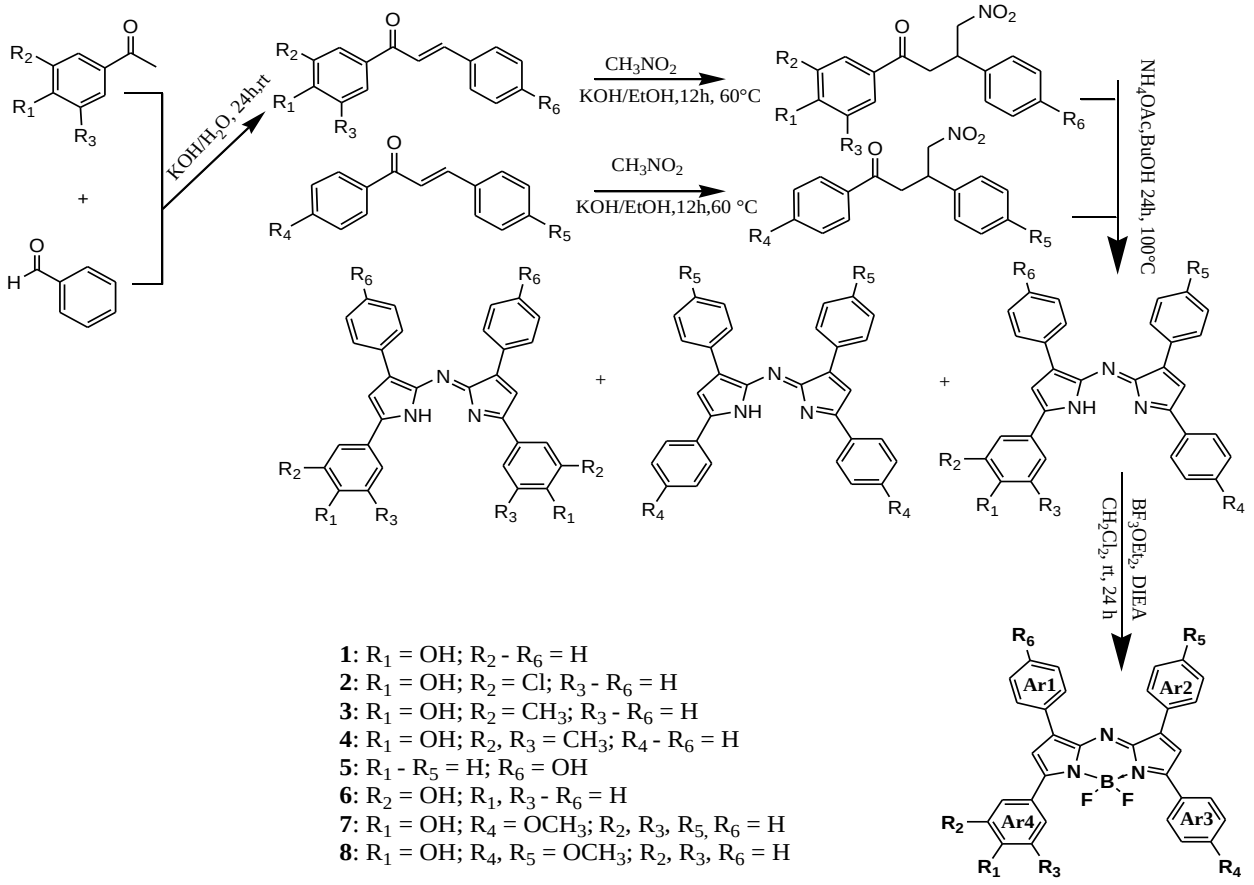

1: R_1 = OH; R_2 - R_6 = H
2: R_1 = OH; R_2 = Cl; R_3 - R_6 = H
3: R_1 = OH; R_2 = CH_3; R_3 - R_6 = H
4: R_1 = OH; R_2, R_3 = CH_3; R_4 - R_6 = H
5: R_1 - R_5 = H; R_6 = OH
6: R_2 = OH; R_1, R_3 - R_6 = H
7: R_1 = OH; R_4 = OCH_3; R_2, R_3, R_5, R_6 = H
8: R_1 = OH; R_4, R_5 = OCH_3; R_2, R_3, R_6 = H

Scheme 1. Synthesis of aza-BODIPY probes.

Table 1. Photophysical properties of the aza-BODIPY Probes: Absorbance Maxima for the acidic ($\lambda_{abs\text{-}acid}$) and the Basic Forms ($\lambda_{abs\text{-}base}$), Emission Maxima for the Acidic Form ($\lambda_{em\text{-}acid}$), Molar Absorption Coefficients (ε), and Luminescence Quantum Yields (QY)

dye	$\lambda_{abs\text{-}acid}$/ $\lambda_{abs\text{-}base}$ (EtOH/H_2O-1:1) (nm)	$\lambda_{em\text{-}acid}$ (EtOH/H_2O-1:1) (nm)	$\lambda_{abs\text{-}acid}$/ $\lambda_{abs\text{-}base}$ (hydrogel D4) (nm)	$\lambda_{em\text{-}acid}$ (hydrogel D4) (nm)	ε ($M^{-1}cm^{-1}$) (THF)	QY (THF) (%)*	QY (EtOH/buffer-1:1) (%)*
1	670/726	702	687/742	718	84000	14.5±1.1	11.1±2.7
2	668/734	699	683/754	730	80600	16.4±3.2	8.2±2.3
3	675/735	709	692/750	720	86200	17.6±4.1	8.4±0.9
4	677/741	714	694/752	722	89700	16.1±4	4.6±1.4
5	656/782,605	691	672/859,615	702	69500	7.3±1.8	2.9±0.8
6	650/656	676	660/663	686	71100	10.1±0.6	1.5±0.1
7	687/743	722	707/760	736	80100	17.4±1	13.5±1.3
8	690/750	721	708/768	736	74000	16.2±1.3	10.9±1.9

*for protonated form

The trend observed in absorption maxima was the same for fluorescence emission maxima (Table 1). The emission maxima of the probes bearing a hydroxyl group in the p-position (R_1) of Ar^4 were located between 699 and 714 nm. The compounds **5** and **6** clearly showed a hypsochromic shift (676 and 691 nm, respectively), and the emission of **7** and **8** was shifted bathochromically (721 and 722 nm, respectively) as compared with the parent compound **1**. The trends in the absorption and fluorescence maxima of indicators in hydrogel D4 mirrored those in solution with an additional bathochromic shift of ∼15 nm (Table 1). The fluorescence quantum yields (QYs) of most indicators were very similar (0.14–0.17 in tetrahydrofurane, Table 1). Again, the dyes **5** and **6** represent a notable exception as they exhibited significantly lower quantum yields. As can be seen, all the values are lower in EtOH/aqueous buffer. Although very low concentrations of the dyes were used ($<1.5 \times 10^{-6}$ M), some aggregation of the dyes in EtOH/water mixture cannot be excluded. On the other hand, lower quantum yields in this media can be explained by more efficient radiationless deactivation involving O–H vibrations. It should be mentioned that the QYs of most reported NIR-emitting dyes are generally lower than for those emitting in the visible part of the spectrum. In summary, the photophysical properties of

the new aza-BODIPY derivatives retain most of the advantages of the aza-BODIPY fluorophores (except for **5** and **6**), including narrow bandwidth, high molar absorption coefficient, and acceptable fluorescence quantum yields.

pH-sensing properties. pK_a values of the new probes were determined both in ethanol/aqueous buffered solution (1:1) and in a hydrogel D4 film from the absorption measurements. As can be seen, the absorption spectra shift bathochromically upon deprotonation of the hydroxyl group in all cases except for **6** as a result of the absence of conjugation with the aza-BODIPY core (Figure 1, Table 1). Notably, the absorption spectrum of deprotonated **5** is rather unusual and shows two peaks (Figure 1b). The pK_a values determined at two ionic strengths of the solution (0.02 and 0.15 M) were very similar (Table 2). Such low cross-sensitivity to the ionic strength is explained by the low charge of the indicator molecule (0 and −1 for the protonated and deprotonated forms, respectively). The pK_a of the aza-BODIPY derivatives can be tuned over a wide range by introducing electron-withdrawing/donating (remote) neighboring functionalities or changing the position of the hydroxyl group. If probe **1** (with pK_a of 8.38) is substituted at the m-position with a chlorine atom, the pK_a drops to 7.01 (**2**). When (inductively) electron-donating methyl groups are introduced in the m-positions, the pK_a is 8.47 for one methyl group (**3**) and 8.05 for two methyl groups (**4**). The increased acidity of a dimethyl-substituted derivative is surprising, but can be explained by the difficulties of formation of the solvent adduct due to steric hindrances. If a hydroxyl group is introduced in the p-position of the Ar^1 aryl ring instead of the Ar^4aryl ring, the pK_a increases to 9.68 (**5**). This is very close to the pK_a value of phenol (pK_a = 10),[34] which indicates the absence of the conjugation with the aza-BODIPY core. This observation is in good agreement with the trends obtained from the absorption spectra. A drastically high pK_a of **6** (10.88) compared with the pK_a of parent compound **1** (8.38) was attributed to the formation of an intramolecular hydrogen bond between the hydroxyl group and the neighboring fluorine atom. Introduction of a remote electron-donating substituent (methoxy group) in the p-position of the Ar^3 ring (**7**) slightly increases the pK_a value (by about 0.3 units), relative to the parent compound **1**. Evidently, the second methoxy group in the p-position on the Ar^2 aryl ring (**8**) has less effect on the pK_a value. Effects observed in this study are in line with the electron-withdrawing (or -donating) power of the neighboring (remote) substituents. In summary, pH indicators with tailored pK_a values can be realized, and the indicators can be easily adapted to

particular applications. The pK_a values determined in this study differ significantly from the reported pK_a of 6.9 of a phenolic derivative with a hydroxyl group in the p-position of the Ar[4] ring (similar to the compound **1** in our study),[26] possibly because of different media used by Murtagh et al. for the calibration of the pH indicator (nonionic surfactant) and higher concentration of the dye in these micelles. As will be demonstrated in the following, the concentration of the indicators is rather critical for determination of apparent pK_a values via fluorescence measurements.

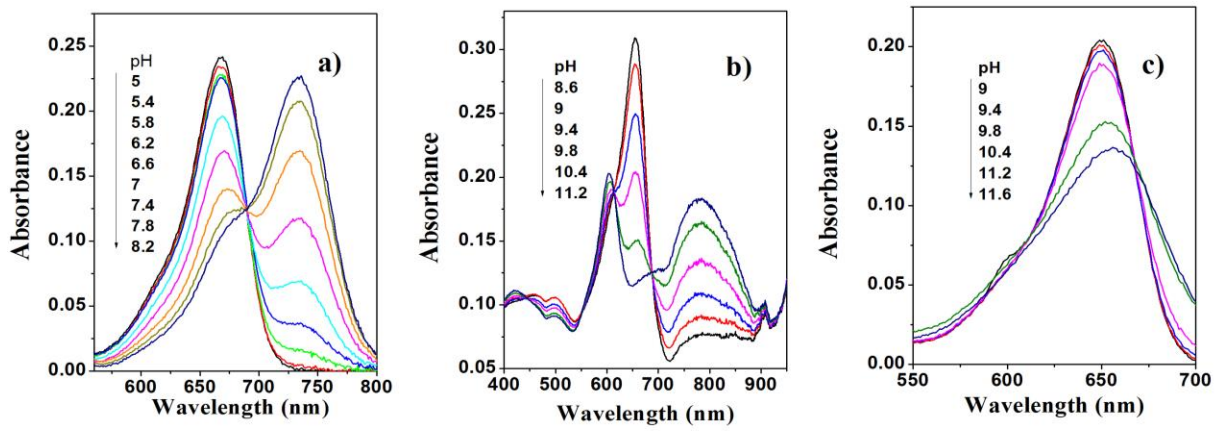

Figure 1. pH dependence of absorbance for **2** (a – 3.10×10^{-6} M), **5** (b – 3.32×10^{-6} M) and **6** (c – 3.01×10^{-6} M) in ethanol/aqueous buffer solution (1:1, IS 0.02 M).

Table 2. pK_a values of fluorescent aza-BODIPY probes

dye no.	pK_{abs} (IS=0.02M) (EtOH/H_2O-1:1)	pK_{em} (IS=0.02M) (EtOH/H_2O-1:1)	pK_{abs} (IS=0.15M) (EtOH/H_2O-1:1)	pK'_{em} (IS=0.15M) (EtOH/H_2O-1:1)	pK_{abs} (IS=0.02M) (hydrogel D4)	pK'_{em} (IS=0.02M) (hydrogel D4)
1	8.35	8.38	8.36	8.41	8.47	8.09
2	7.00	7.01	6.92	6.98	6.73	6.08
3	8.36	8.47	8.42	8.45	8.49	7.82
4	8.06	8.05	8.11	8.15	7.94	7.19
5	9.69	9.68	9.69	10.88	9.84	9.67
6	11.05	10.88	11.02	9.69	12.35	11.4
7	8.71	8.65	8.76	8.74	8.81	8.23
8	8.92	8.89	8.90	8.94	9.11	8.56

The fluorescence of the indicators is quenched upon deprotonation (Figure 2), which is attributed to efficient photoinduced electron transfer.[35–37] In fact, no emission is detected for the deprotonated form of the dyes. The apparent pK_a values (p$K`_a$) obtained from the emission measurements in solution are very close to those determined from the absorption spectra (Table 2).

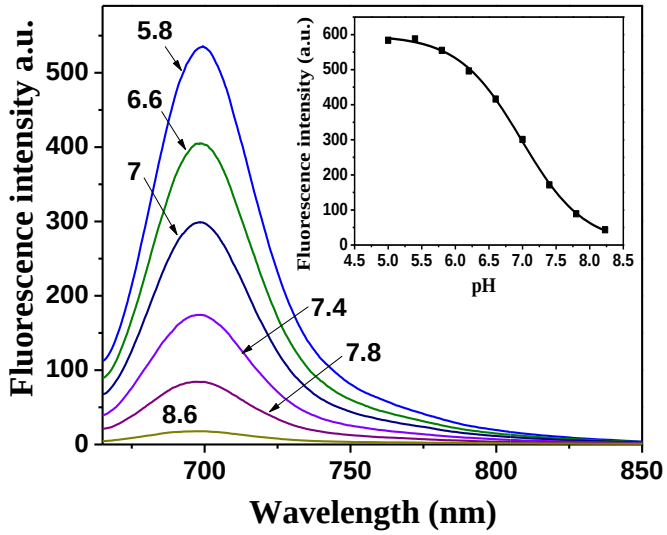

Figure 2. pH dependence of fluorescence for **2** (1.41 × 10^{-6} M) in ethanol/aqueous buffer solution (1:1) and the corresponding calibration curve (insert).

Optical pH sensors were prepared by noncovalent entrapment of the indicators in the hydrogel D4 matrix, which is a highly proton-permeable, uncharged polyurethane derivative with a water uptake capacity of about 50%. The pK_a values obtained for the sensing materials from the absorption measurements were very close to those obtained for the solutions of the indicators (Table 2). Unexpectedly, the apparent pK_a values in D4 as derived from fluorescence data were 0.5–1 pH units lower than those obtained from absorption data (Table 2). This discrepancy can be explained by the fact that the concentration of the indicator is much higher in the hydrogel than in the solution. Therefore, the dye molecules are close enough to enable Förster resonance energy transfer (FRET) from the protonated to the deprotonated form (Figure S3 of the Supporting Information). Considering that FRET is concentration-dependent, this offers another possibility of tuning the dynamic range of the materials. In fact, p$\acute{K}_a$ values derived from the fluorescence data are lower for higher concentration of the indicators in hydrogel D4 (e.g., p$\acute{K}_a$ of 6.65, 6.14, 6.03, and 5.89 for the sensor films containing 0.1, 0.25, 0.5 and 1% of the

indicator **2**), Supporting Information Figure S3c. The p$\acute{K}_a$ values obtained from the absorption measurements (Supporting Information Figure S10b) are 6.92, 6.83, 7.04, and 7.32 for the same concentrations. This increase may be due to different localization patterns of the dye in hydrogel D4, which is known to be composed of the hydrophilic and hydrophobic regions.

Dye leaching out of the sensing matrix may be a problem in the case of physically entrapped indicators. It was tested in the case of **1** by monitoring the absorption of the sensing foils. No evident leaching into the aqueous solution was detectable for the protonated form of the dye. In the case of the charged deprotonated form, the decrease in the absorption was very low (0.8% per 24 h, Figure S5 of the Supporting Information), which is within the experimental error. Consequently, leaching is not critical for the investigated sensors due to the pronounced hydrophobicity of the indicator systems.

We compared the pH-sensing properties of the complexes and the respective ligands. The ligands were virtually nonfluorescent, possibly due to their nonplanar structure. However, distinct changes in the absorption spectra were observed (Figure S4a of the Supporting Information). The pK_a values were ∼1 unit higher than for the corresponding complexes (Supporting Information Figure S4b). For example, the pK_a values were 8.35 and 7.00 for **1** and **2**, but 9.39 and 7.97 for the corresponding ligands. This effect is likely due in part to the lower degree of the π-conjugation between the phenolic substituents and the chromophore core (which is reflected by the smaller shift between the λ_{max} of both forms of the dye compared with the corresponding complexes). The electron-withdrawing effect of the BF_2 group can also contribute here. Despite the absence of fluorescence, the nonchelated dyes can be promising as absorption-based indicators.

Photostability. Photostability is a very important parameter for all optical chemosensors. We investigated solutions of the new pH dyes in dimethylformamide under continuous illumination with an ultrabright 642-nm LED array. Figure 33 demonstrates the photodegradation profiles for the new indicators and for seminaphthorhodafluor decyl ester (SNARF-DE), which is used for comparison. The aza-BODIPY probes were significantly more photostable (about 30-fold) than SNARF-DE under identical conditions. In fact, after 2.5 h of illumination, only 1–8% of the dyes was decomposed compared with SNARF-DE, which degrades almost completely after 60 min of irradiation. The photostability trend for aza-BODIPY probes was 6 > 3 > 4 > 1–2 ∼ 7 > 5–8

(Figure S6 of the Supporting Information). The electron-donating substituents in the aryl rings Ar^1 and Ar^2seem to be responsible for decreased photostability; nevertheless, new pH dyes retain excellent photostability of aza-BODIPY dyes,[38] which makes them particularly suitable for long-duration measurements.

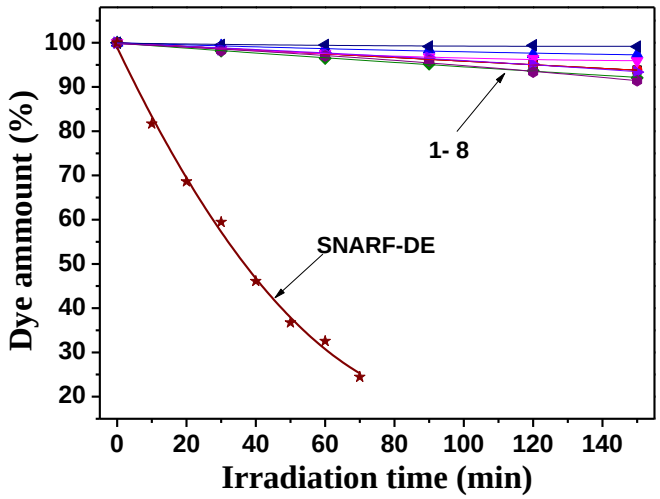

Figure 3. Comparison of photobleaching profiles for aza-BODIPY fluorescent pH probes and SNARF-DE in dimethylformamide determined from the absorption measurements.

Dual-lifetime referenced pH sensor. Fluorescence intensity is a parameter that is easy to measure, but it is influenced by a number of factors, such as the intensity and light field of the excitation source, the sensitivity of the photodetector, and the coloration and turbidity of the measuring media. In contrast, measurements of fluorescence decay time, which is a self-referenced parameter, normally require complicated and expensive equipment. Ratiometric sensing and dual lifetime referencing are popular alternatives. In the latter approach, a referenced material having a long luminescence decay time (typically in the microseconds time domain) is added, and the overall phase shifts are measured in the frequency domain.[39] Since good spectral compatibility (both for excitation and for emission) is essential, a recently reported inorganic phosphor, chromium(III)-doped gadolinium aluminum borate (Cr-GAB)[28] is an excellent candidate for this purpose; its luminescence decay times of about 100 μs, and high chemical and photochemical inertness make it particularly attractive. The spectral compatibility of the indicator (in its protonated form) and the referenced phosphor is very good (Figure 4) because both are efficiently excited by red LEDs and emit in the same spectral window. The resulting pH-sensing material is compatible with a commercially available fiber-optic phase oxygen meter

(Firesting from Pyroscience), which was used for measurements (λ_{exc} ~ 620 nm). The "sensing chemistry" applied on the tip of a glass optical fiber included 0.1% w/w of indicator **1** and 66% w/w Cr-GAB particles and 33% w/w of hydrogel D4. Different concentrations of indicator and Cr-GAB particles were tested to ensure optimal phase shift dynamics (data not shown). Figure 4c shows a calibration plot of the cotangents of the phase angle, cot Φ vs pH for the DLR pH-sensing material. The calibration showed an inflection point at pH 8.12, which is very close to the apparent pK_a value obtained from the spectroscopic investigations. Photostability of the indicator at the fiber optic tip was monitored by applying 5 times stronger light intensity and 10 times longer integration times than in the standard settings. For the acidic form, no evident photobleaching was observed after 2000 measurement points, which corresponds to 100 000 measurement points in the standard settings (Figure S7 of ESI). A very small drift of the phase angle (0.2°) was observed in the basic conditions for the same measurement time. Nevertheless, it can be concluded that the fiber-optic sensors possess excellent photostability and can be used for prolonged measurements without recalibration.

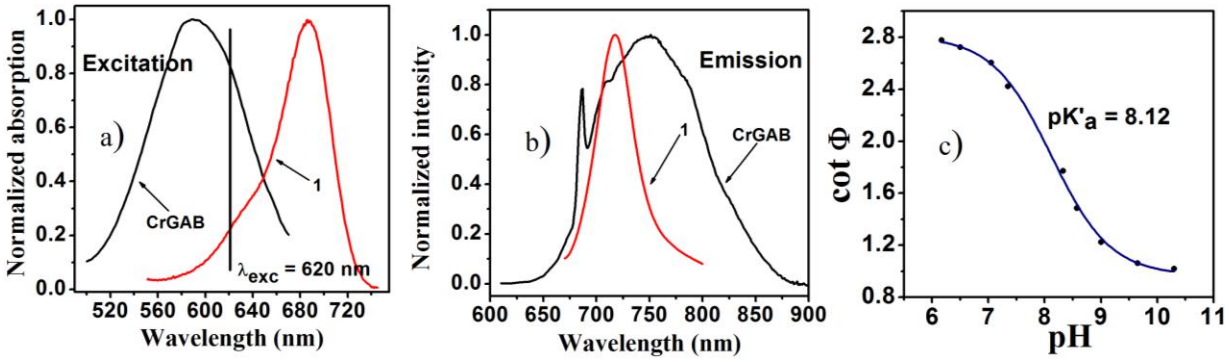

Figure 4. Spectral properties of the luminescent materials used in the pH sensor: (a) excitation spectrum of the Cr-GAB and pH indicator **1** in protonated form; (b) emission spectra of Cr-GAB and pH indicator **1**; (c) calibration plot for the DLR pH sensor containing pH indicator **1** (0.1 %) and Cr-GAB (66 % w/w) in hydrogel D4 at 25 °C (IS = 0.02 M).

Application in marine biology. The new pH sensing materials operate in significantly different dynamic ranges and are, therefore, suitable for a variety of important applications. For example, the apparent pK'_a values of the indicators **2** and **4** make them particularly suitable for biotechnological and biological applications, respectively. On the other side, the apparent pK'_a of about 8 found for indicator **1** almost ideally matches the pH of the seawater. This new sensing

material thus provides a promising alternative to the state-of-the-art optical sensors for seawater pH measurements, which rely on fluorescein derivatives and possess poor photostability.[40,41] We demonstrated this applicability in marine biology by measuring the pH in corals with a fiber-optic pH optode based on the DLR material described above (Figure 5). The pH in corals is affected by both the photosynthetic activity of the algal symbionts in the host tissue, which tend to increase the pH due to their phototsynthetic fixation of inorganic carbon, and the respiratory activity of the coral host cells and hetrotrophic bacteria associated with the coral, the activity of which tends to decrease pH. Although most pH measurements in corals have focused on the exposed tissues,[42] the pH conditions in the gastric cavity (i.e., the coral stomach) are largely unknown; yet, such measurements are highly relevant to understand the microbial processes going on inside corals. Our pH measurements showed a pH gradient of almost 1 pH unit from the coral mouth and into the deepest part of the coral just above the calcium carbonate skeleton (Figure 5b). Evidently, the pH in these parts of the coral was not affected by photosynthetic activity, which was also seen by the absence of any accumulation of O_2 (data not shown).

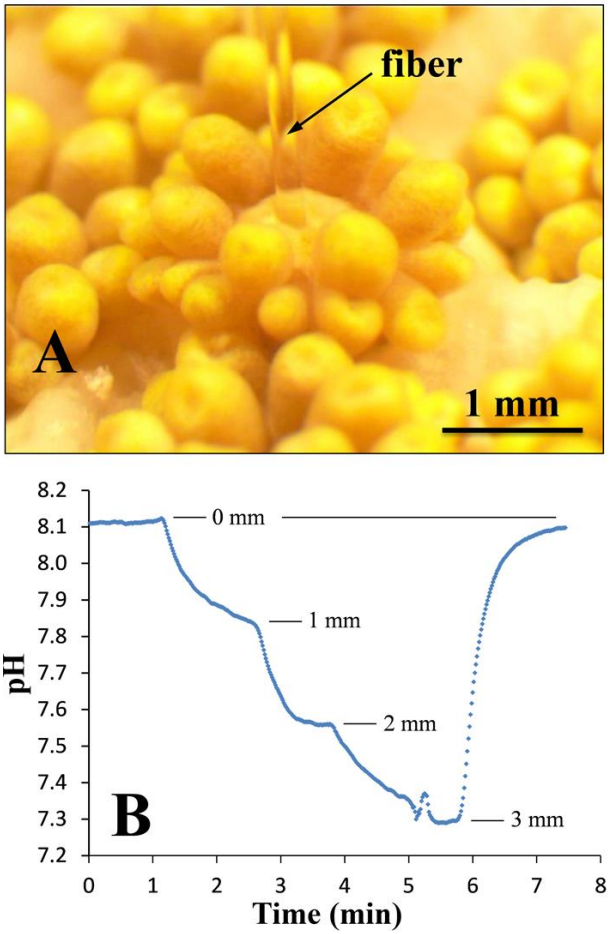

Figure 5. (A) Photographic image of a fiber-optic pH optode based on **1** and Cr-GAB inserted into the mouth opening of a single polyp in the coral (*Goniopora* sp.) under an irradiance of ~150 µmol photons m^{-2} s^{-1}. (B) pH profile in the gastric cavity of the coral showing a pH decrease at increasing distance from the mouth opening. After measurement at 3 mm depth, the pH optode was retracted into the overlaying seawater.

2.4 Conclusion

In conclusion, we prepared and characterized a series of NIR fluorescent pH indicators with potential to suit a diverse range of analytical applications. pH-sensitive functional aza-BODIPY derivatives were obtained via a simple reaction route starting from commercially available compounds. Except for probes **5** and **6**, the new indicators retain the advantages of aza-BODIPY fluorescent probes, such as good brightness and excellent photostability. Variations in both the substitution pattern and the position of hydroxyl functionality allowed manipulation of pK_a values over a wide range, providing valuable information that can be used for future rational

design of the indicator systems. The new sensors have high potential for a variety of biotechnological, biological, environmental, etc. applications. As an example, monitoring of pH inside coral polyps was demonstrated. Ongoing work concerns the covalent immobilization of the indicators into the polymeric network, which will completely suppress their leaching, migration, and aggregation and can lead to even better shelf life stability and operating time of the optical sensors.

2.5 References

1. B. Valeur, *Molecular Fluorescence. Principles and Applications*, Wiley-VCH, Weinheim, Germany, **2002**.
2. R. P. Haugland, *The Handbook. A Guide to Fluorescent Probes and Labeling Technologies*, 10th ed., Molecular Probes, Eugene, Oregon, **2005**, 935.
3. J. Han, K. Burgess, *Chem. Rev.* **2010**, 110, 2709.
4. Zhang W., Tang B., Liu X., Liu Y., Xu K., Ma J., Tong L., Yang G., *Analyst*, **2009**, 134, 367.
5. Tang, B., Yu, F., Li, P. Tong, L., Duan X., Xie T., Wang X., *J. Am. Chem. Soc.*, **2009**, 3016.
6. Almutairi, A., Guillaudeu, S. J., Berezin, M. Y., Achilefu, S., Frechet J. M. J., *J. Am. Chem. Soc.*, **2008**, 130 , 444.
7. Lee, H., Berezin, M.Y., Guo, K., Kao, J., Achilefu, S., *Org. Lett.*, **2009**, 11, 29.
8. Zhang, Z., Achilefu, S., *Chem. Commun.*, **2005**, 47, 5887.
9. Deniz, E., Isbasar, G. C., Bozdemir, O. A. Yildirim, L. T., Siemiarczuk, A., Akkaya E. U., *Org. Lett.*, 10 **2008**, 16, 3401.
10. Hilderbrand, S.A., Kelly, K. A., Nieder, M. Weissleder R., *Bioconjug. Chem.*, **2008**, 19, 1635.
11. Kühl, M., *Meth. Enzymol.*, **2005**, 397, 166.
12. Larsen, M.; Borisov, S. M.; Grunwald, B.; Klimant, I.; Glud, R. N. *Limnol. Oceanogr. Methods* **2011**, *9*, 348.

13. Jeevarajan A. S., Vani S., Taylor T. D., Anderson M. M., *Biotechnol. Bioeng.* **2002**, 78, 467.

14. John G. T., Goelling D., Klimant I., Schneider H., Heinzle E., *J. Dairy Res*. **2003**, 70, 327.

15. Wolfbeis OS, Fürlinger E, Kroneis H, Marsoner H, *Fresenius Anal. Chem.* **1983**, 314, 119.

16. Whitaker JE, Haugland R. P., Prendergas F. G. *Anal. Biochem.* **1991**, 194, 330.

17. Offenbacher H, Wolfbeis OS, Fürlinger E, *Sens. Act. B* **1986**, 9, 73.

18. Zhujun Z, Seitz W R, *Anal. Chim. Acta* **1984,** 160, 47.

19. Xu Z, Rollins A, Alcala R, Marchant E, *J. Biomed. Mater. Res*. **1998**, 39, 9.

20. Weidgans, B. M., Krause, C., Klimant, I., Wolfbeis, O. S., *Analyst*, **2004**, 129, 645.

21. Borisov, S. M., Gatterer, K., Klimant, I., *Analyst*, **2010**, 135, 1711.

22. Cooper, M. E., Gregory, S., Adie, E., Kalinka, S. *J. Fluoresc*. **2002**, 12, 425.

23. Briggs, M. S., Burns, D. D., Cooper, M. E., Gregory, S., *J. Chem. Commun.* **2000**, 23, 2323.

24. J. Killoran, L. Allen, J. F. Gallagher, W. M. Gallagher, D. F. O'Shea, *Chem. Commun.*, **2002**, 1862.

25. J. Killoran, Shane O. McDonnell, J. F. Gallagher and D. F. O'Shea, *New J. Chem.*, **2008**, 32, 483.

26. J. Murtagh, D. O. Frimannsson and D. F. O'Shea, *Org. Lett.*, **2009**, 11, 5386.

27. S. O. McDonnell and D. F. O'Shea, *Org. Lett.*, **2006**, 8, 3493.

28. S. M. Borisov, K. Gaterrer, B. Bitschnau and I. Klimant, *J. Phys. Chem. C*, **2010**, 114, 9118.

29. W. Freyer, S. Mueller, K. Teuchner, *J. Photochem. Photobio. A*, **2004**, 163, 231.

30. M. J. Hall, S. O. McDonnell, J. Killoran, D. F. O'Shea, *J. Org. Chem.* **2005**, 70, 5571.

31. A. Gorman, J. Killoran, C. O'Shea, T. Kenna, W. M. Gallagher, D. F. O'Shea, *J. Am. Chem. Soc.*, **2004**, 126, 10619.

32. Loudet, A., Rakeshwar, B., Wu, L., Burgess, K., *Tetrahedron*, **2008**, 64, 3642.

33. Demas, J. N., Crosby, G. A., *J. Phys. Chem.*, **1971**, 75, 991.

34. Isaacs, N. S., *Physical Organic Chemistry*, 2nd ed. Ed.; Longman Scientific & Technical: Harlow, England, **1995**, 188.

35. Daffy, L. M., de Silva, A.P., Gunaratne, H.Q.M., Huber, C., Lynch, P.L.M., Werner, T., Wolfbeis, O.S., *Chem.-Eur. J.* **1998**, 4, 1810.

36. Werner, T., Huber, C., Heinl, S., Kollmannsberger, M., Daub, J., Wolfbeis, O.S., *Fresenius J. Anal. Chem.* **1997,** 359, 150.

37. de Silva, A.P., Vance, T.P., West, M.E.S., Wright, G.D., *Org. Biomol. Chem.* **2008**, 6, 2468.

38. P. Batat, M. Cantuel, G. Jonusauskas, L. Scarpantonio, A. Palma, D. F. O'Shea, N. D. McClenaghan, *J. Phys. Chem. A*, **2011**, 115, 14034.

39. Huber, C.; Klimant, I.; Krause, C.; Wolfbeis, O. S. *Anal. Chem.* **2001**, 73, 2097.

40. Schröder, C.R., Weidgans, B.M., Klimant, I. *Analyst*, **2005**, 130, 907.

41. Schröder, C. R.; Polerecky, L.; Klimant, I. *Anal. Chem.* **2007**, 79, 60.

42. Kühl, M., Cohen, Y., Dalsgaard, T.,Jørgensen, B. B., Revsbech, N. P. *Mar. Ecol. Progr. Ser.*, **1995**, 117, 159.

2.6 Supporting Information

EXPERIMENTAL

Measurements of pH gradients in the gastric cavity of a symbiont bearing coral (Goniopora sp.)

The coral was sampled from the reef flat off Heron Island, Great Barrier Reef, Australia. After sampling, the coral was kept at Heron Island Research Station in an outdoor aquarium continuously flushed with aerated seawater from the reef flat. Prior to pH measurements, coral specimen was transferred to a flow chamber with aerated seawater (pH ~8.1) at 26 °C and at a flow rate of approximately 3 cm s^{-1}. The coral was illuminated with an incident irradiance of ~150 µmol·photons $m^{-2}·s^{-1}$ from a fiber-optic halogen lamp Schott kl2500 LCD (www.schott.com). The pH optode was mounted in a manual micromanipulator MM33 (Märtzhäuser, www.marzhauser.com) that was attached to a heavy stand. The optode tip was carefully positioned towards and into the mouth opening of a single coral polyp; this was done by observation under a dissection microscope SM-6TZ-54S, Amscope (www.amscope.com) equipped with a CCD camera.

Solution preparation for titration curves

Indicators **1 - 8** were dissolved in THF (10 ml). For absorption measurements 200 µl (90 µl for fluorescence measurements) of this solution was diluted with 25 ml of ethanol. Prior to absorption (fluorescence) measurements ethanolic solution was diluted with aqueous buffer 1:1. Final concentration of solutions were for absorption measurements **1** – 3.19×10^{-6} M, **2** – 3.10×10^{-6} M, **3** – 3.37×10^{-6} M, **4** – 3.27×10^{-6} M, **5** – 3.32×10^{-6} M, **6** – 3.01×10^{-6} M, **7**- 2.55×10^{-6} M, **8** – 3.23×10^{-6} M, and fluorescence measurements **1** – 1.45×10^{-6} M, **2** – 1.41×10^{-6} M, **3** – 1.53×10^{-6} M, **4** – 1.49×10^{-6} M, **5** – 1.51×10^{-6} M, **6** – 1.37×10^{-6} M, **7**- 1.16×10^{-6} M, **8** – 1.47×10^{-6} M.

Synthesis

1-(3-chloro-4-hydroxyphenyl)-3-phenylpropenone (2a): 3'-chloro-4'-hydroxyacetophenone (1 eq, 2 g, 11.7 mmol) and benzaldehyde (1 eq, 1.24 g, 11.7 mmol) were dissolved in absolute ethanol (10 ml). 10 ml of aqueous potassium hydroxide solution (3 eq, 1.96 g, 35.1 mmol) was added dropwise. Resulting solution was stirred for 8-12 hours, during which the product precipitated as the potassium salt. The solution/suspension was poured into 1 M HCl (10 ml), and further concentrated HCl was added until the solution was acidic. Obtained yellow solid was washed with water and used in further synthesis without purification. (2.7 g, 77%)

1-(3-chloro-4-hydroxyphenyl)-4-nitro-3-phenylbutan-1-one (2b): A solution of 1-(3-chloro-4-hydroxyphenyl)-3-phenylpropenone (2a) (1eq, 2 g, 7.7 mmol), nitromethane (20 eq, 8,35 ml, 154.7 mmol) and KOH (1.2 eq, 0.52 g, 9.28 mmol) in EtOH (10 ml) was heated at 60 ºC under reflux for 12 h. After cooling to room temperature, the solvent was removed in vacuo and oily residue obtained was acidified with 4 M HCl and partitioned between EtOAc (50 ml) and H_2O (50 ml). The organic layer was separated, dried over sodium sulfate and evaporated under reduced pressure. The obtained product was used for further synthesis without purification. (2.4 g, 73%)

[5-(3-chloro-4-hydroxyphenyl)-3-phenyl-1H-pyrrol-2-yl]-[5-phenyl-3-phenylpyrrol-2-ylidene]amine (2c): 1-(3-chloro-4-hydroxyphenyl)-4-nitro-3-phenylbutan-1-one (2b) (1 eq, 1 g, 3.7 mmol), 1,3-diphenyl-4-nitro-butan-1-on (1b) (1 eq, 0.99 g, 3.7 mmol) and ammonium acetate (35 eq, 8.03 g, 129 mmol) in butanol (50 ml) were heated under reflux for 24 h. The reaction was cooled to room temperature, the crude product was purified by column chromatography on silica with dichloromethane (after eluting symmetric byproduct with hexane/dichloromethane 3:1 v/v) to yield to product 2c as a blue-black solid. Product was recrystallized from hexane/tetrahydrofuran mixture as green metallic crystals (0.26 g, 17%). ^{1}H NMR (300 MHz, DMSO-d6) δ 8.26-8.27 (d, *J* = 2 Hz, 1H), 8.06-8.13 (t, *J* = 6.5 Hz, 4H), 7.99-8.02 (dd, *J* = 8.7 Hz, 2.1 Hz, 1H), 7.92-7.95 (d, *J* = 7.4 Hz, 2H), 7.83 (s, 1H), 7.32-7.61 (t, *J* = 7.5 Hz, 10H), 7.04-7.06 (d, *J* = 8.6 Hz, 1H). Electron impact-direct insertion-time of flight (EI-DI-TOF) m/z [MH^+] found 499.1473, calculated 499.1451.

BF_2 chelate of [5-(3-chloro-4-hydroxyphenyl)-3-phenyl-1H-pyrrol-2-yl]-[5-phenyl-3-phenylpyrrol-2-ylidene]amine (2): Compound 2c (0.24 g, 0.48 mmol) was dissolved in dry CH_2Cl_2 (50 ml), treated with diisopropylethylamine (10 eq, 0.79 ml, 4.8 mmol) and BF_3 diethyletherate (15 eq, 0.92 ml, 7.2 mmol) and stirred under argon for 24 h. Purification by column chromatography on silica eluting with CH_2Cl_2 and recrystallization from hexane/tetrahydrofurane gave the product 2 as a red metallic solid (0.20 g, 43 %). ^{1}H NMR (300 MHz, DMSO-d6) δ 8.30-8.29 (d, *J* = 2.1 Hz, 1 H), 8.21 – 8.07 (m, 7 H), 7.76 (s, 1 H), 7.58 – 7.45 (m, 10 H), 7.13- 7.16 (d, *J* = 8.7 Hz, 1 H). Electron impact-direct insertion-time of flight (EI-DI-TOF) m/z [MH^+] found 546.1490, calculated 546.1470.

1-(3-methyl-4-hydroxyphenyl)-3-phenylpropenone (3a): 3'-methyl-4'-hydroxyacetophenone (1 eq, 2 g, 14.7 mmol) and benzaldehyde (1 eq, 1.55 g, 11.8 mmol) were dissolved in absolute ethanol (10 ml). 10 ml of aqueous potassium hydroxide solution (3 eq, 1.98 g, 35.4 mmol) was added dropwise. Resulting solution was stirred for 8-12 hours, during which the product precipitated as the potassium salt. The solution/suspension was poured into 1 M HCl (10 ml), and further concentrated HCl was added until the solution was acidic. Obtained yellow solid was washed with water and used in further synthesis without purification. (3.5 g, 93%)

1-(3-methyl-4-hydroxyphenyl)-4-nitro-3-phenylbutan-1-one (3b): A solution of 1-(3-methyl-4-hydroxyphenyl)-3-phenylpropenone (3) (1eq, 2 g, 12.05 mmol), nitromethane (20 eq, 16.6 ml, 240.96 mmol) and KOH (1.2 eq, 0.81 g, 14.46 mmol) in EtOH (10 ml) was heated at 60 ºC under reflux for 12 h. After cooling to room temperature, the solvent was removed in vacuo and oily residue obtained was acidified with 4 M HCl and partitioned between EtOAc (50 ml) and H_2O (50 ml). The organic layer was separated, dried over sodium sulfate and evaporated under reduced pressure. The obtained product was used for further synthesis without purification. (1.33 g, 53%)

[5-(3-methyl-4-hydroxyphenyl)-3-phenyl-1H-pyrrol-2-yl]-[5-phenyl-3-phenylpyrrol-2-ylidene]amine (3c): 1-(3-methyl-4-hydroxyphenyl)-4-nitro-3-phenylbutan-1-one (3a) (1 eq, 1 g, 3.7 mmol), 1,3-diphenyl-4-nitro-butan-1-on (1b) (1 eq, 0.99 g, 3.7 mmol) and ammonium acetate (35 eq, 8.03 g, 129 mmol) in butanol (50 ml) were heated under reflux for 24 h. The reaction was cooled to room temperature, the crude product was purified by column chromatography on silica

with dichloromethane (after eluting symmetric byproduct with hexane/dichloromethane 3:1 v/v) to yield to product 3c as a blue-black solid. Product was recrystalized from hexane/tetrahydrofuran mixture as green metallic crystals (0.26 g, 10%). ^{1}H NMR (300 MHz, DMSO-d6) δ 8.05 – 8.13 (m, 5 H), 7.93- 7.95 (d, *J* = 7.6 Hz, 3 H), 7.80 (s, 1 H), 7.56-7.61 (m, 2 H), 7.32 – 7.51 (m, 8 H), 7.00-7.03 (d, *J* = 8.4 Hz, 1 H), 2.29 (s, 3 H). Electron impact-direct insertion-time of flight (EI-DI-TOF) m/z [MH^+] found 479.1998, calculated 479.1998.

BF_2 chelate of [5-(3-methyl-4-hydroxyphenyl)-3-phenyl-1H-pyrrol-2-yl]-[5-phenyl-3-phenylpyrrol-2-ylidene]amine (3): Compound 3c (0.19 g, 0.39 mmol) was dissolved in dry CH_2Cl_2 (50 ml), treated with diisopropylethylamine (10 eq, 0.65 ml, 3.9 mmol) and BF_3 diethyletherate (15 eq, 0.75 ml, 5.85 mmol) and stirred under argon for 24 h. Purification by column chromatography on silica eluting with CH_2Cl_2 gave the product 3 as a red metallic solid (0.22 g, 66 %). ^{1}H NMR (300 MHz, DMSO-d6) δ 10.74 (s, 1 H), 8.04 – 8.22(m, 8 H), 7.82 (s, 1 H), 7.39 – 7.59 (m, 10 H), 6.97 (m, 1 H), 2.21 (s, 3H). Electron impact-direct insertion-time of flight (EI-DI-TOF) m/z [MH^+] found 526.2020, calculated 526.2017.

1-(3,5-dimethyl-4-hydroxyphenyl)-3-phenylpropenone (4a): 3',5'-dimethyl-4'-hydroxyacetophenone (1 eq, 2 g, 12.1 mmol) and benzaldehyde (1 eq, 1.29 g, 12.1 mmol) were dissolved in absolute ethanol (10 ml). 10 ml of aqueous potassium hydroxide solution (3 eq, 2.04 g, 36.3 mmol) was added dropwise. Resulting solution was stirred for 8-12 hours, during which the product precipitated as the potassium salt. The solution/suspension was poured into 1 M HCl (10 ml), and further concentrated HCl was added until the solution was acidic. Obtained yellow solid was washed with water and used in further synthesis without purification. (3.3 g, 95%)

1-(3,5-dimethyl-4-hydroxyphenyl)-4-nitro-3-phenylbutan-1-one (4b): A solution of 1-(3,5-dimethyl-4-hydroxyphenyl)-3-phenylpropenone (4a) (1eq, 2 g, 7.93 mmol), nitromethane (20 eq, 16.6 ml, 240.96 mmol) and KOH (1.2 eq, 0.81 g, 14.46 mmol) in EtOH (10 ml) was heated at 60 ºC under reflux for 12 h. After cooling to room temperature, the solvent was removed in vacuo and oily residue obtained was acidified with 4 M HCl and partitioned between EtOAc (50 ml) and H_2O (50 ml). The organic layer was separated, dried over sodium sulfate and evaporated under reduced pressure. The obtained product was used for further synthesis without purification. (1.6 g, 65%)

[5-(3,5-dimethyl-4-hydroxyphenyl)-3-phenyl-1H-pyrrol-2-yl]-[5-phenyl-3-phenylpyrrol-2-ylidene]amine (4c): 1-(3,5-dimethyl-4-hydroxyphenyl)-4-nitro-3-phenylbutan-1-one (4b) (1 eq, 1 g, 3.2 mmol), 1,3-diphenyl-4-nitro-butan-1-on (1b) (1 eq, 1 g, 3.2 mmol) and ammonium acetate (35 eq, 8.03 g, 112 mmol) in butanol (50 ml) were heated under reflux for 24 h. The reaction was cooled to room temperature, the crude product was purified by column chromatography on silica with dichloromethane (after eluting symmetric byproduct with hexane/dichloromethane 3:1 v/v) to yield to product 5 as a blue-black solid. Product was recrystallized from hexane/tetrahydrofuran mixture as green metallic crystals (0.43 g, 20%). ^{1}H NMR (300 MHz, DMSO-d6) δ 8.09-8.15 (m, 4H), 7.93-7.96 (m, 2H), 7.89 (s, 2H), 7.81 (s, 1H), 7.31-7.60 (m, 10H). Electron impact-direct insertion-time of flight (EI-DI-TOF) m/z [MH^+] found 493.2198, calculated 493.2154.

BF_2 chelate of [5-(3,5-dimethyl-4-hydroxyphenyl)-3-phenyl-1H-pyrrol-2-yl]-[5-phenyl-3-phenylpyrrol-2-ylidene]amine (4): Compound 4c (0.19 g, 0.39 mmol) was dissolved in dry CH_2Cl_2 (50 ml), treated with diisopropylethylamine (10 eq, 0.65 ml, 3.9 mmol) and BF_3 diethyletherate (15 eq, 0.75 ml, 5.85 mmol) and stirred under argon for 24 h. Purification by column chromatography on silica eluting with CH_2Cl_2 gave the product 4 as a red metallic solid (0.28 g, 62 %). ^{1}H NMR (300 MHz, DMSO-d6) δ 9.66 (s, 1H), 8.06 – 8.22 (m, 6H), 8.01 (s, 2H), 7.82 (s, 1H), 7.42 – 7.58 (m, 9 H), 7.40 (s, 1H), 2.26 (s, 6 H). Electron impact-direct insertion-time of flight (EI-DI-TOF) m/z [MH^+] found 540.2192, calculated 540.2173.

1-phenyl-4-nitro-3-(4-hydroxyphenyl)-butan-1-one (5a): A solution of 1-phenyl-3-(4-hydroxyphenyl)-propenone (1eq, 2 g, 8.9 mmol), nitromethane (20 eq, 10.8 ml, 178.3 mmol) and KOH (1.2 eq, 0.59 g, 10.68 mmol) in EtOH (10 ml) was heated at 60 ºC under reflux for 12 h. After cooling to room temperature, the solvent was removed in vacuo and oily residue obtained was acidified with 4 M HCl and partitioned between EtOAc (50 ml) and H_2O (50 ml). The organic layer was separated, dried over sodium sulfate and evaporated under reduced pressure. The obtained product was used for further synthesis without purification. (1.5 g, 60%)

[5-phenyl-3-(4-hydroxyphenyl)-1H-pyrrol-2-yl]-[5-phenyl-3-phenylpyrrol-2-ylidene]amine (5b): 1-phenyl-4-nitro-3-(4-hydroxyphenyl)-butan-1-one (5a) (1 eq, 1 g, 3.5 mmol), 1,3-diphenyl-4-nitro-butan-1-on (1b) (1 eq, 1 g, 3.5 mmol) and ammonium acetate (35 eq, 7.6 g, 122

mmol) in butanol (50 ml) were heated under reflux for 24 h. The reaction was cooled to room temperature, the crude product was purified by column chromatography on silica with dichloromethane (after eluting symmetric byproduct with hexane/dichloromethane 3:1 v/v) to yield to product 6b as a blue-black solid. Product was recrystallized from hexane/tetrahydrofuran mixture as green metallic crystals (0.32 g, 20%). ^{1}H NMR (300 MHz, DMSO-d6) δ 8.14 – 7.99 (m, 8 H), 7.66 – 7.38 (m, 11 H), 6.88- 6.85 (d, *J* = 8.7 Hz, 2 H). Electron impact-direct insertion-time of flight (EI-DI-TOF) m/z [MH^+] found 465.1876, calculated 465.1841.

BF_2 chelate of [5-phenyl-3-(4-hydroxyphenyl)-1H-pyrrol-2-yl]-[5-phenyl-3-phenylpyrrol-2-ylidene]amine (5): Compound 5b (0.22 g, 0.47 mmol) was dissolved in dry CH_2Cl_2 (50 ml), treated with diisopropylethylamine (10 eq, 0.61 ml, 4.7 mmol) and BF_3 diethyletherate (15 eq, 0.9 ml, 7.05 mmol) and stirred under argon for 24 h. Purification by column chromatography on silica eluting with CH_2Cl_2 and recrystallization from hexane/tetrahydrofurane gave the product 5 as a red metallic solid (0.17 g, 36 %). ^{1}H NMR (300 MHz, DMSO-d6) δ 10.22 (s, 1H), 8.08-8.13 (d, *J* = 13 Hz, 8 H), 7.45-7.56 (m, 11 H), 6.92-6.95 (d, *J* = 8.5 Hz, 2 H). Electron impact-direct insertion-time of flight (EI-DI-TOF) m/z [MH^+] found 512.1888, calculated 512.186.

1-(3-hydroxyphenyl)-3-phenylpropenone (6a): 3'-hydroxyacetophenone (1 eq, 2 g, 14.7 mmol) and benzaldehyde (1 eq, 1.56 g, 14.7 mmol) were dissolved in absolute tetrahydrofurane (10 ml). Sodium hydride (3 eq, 1.06 g, 44.1 mmol) was added dropwise. Resulting solution was stirred for 8-12 hours, during which the product precipitated as the potassium salt. The solution/suspension was poured into 1 M HCl (10 ml), and further concentrated HCl was added until the solution was acidic. Obtained yellow solid was washed with water and used in further synthesis without purification. (2.98 g, 91%)

1-(3-hydroxyphenyl)-4-nitro-3-phenylbutan-1-one (6b): A solution of 1-(3-hydroxyphenyl)-3-phenylpropenone (3) (1eq, 2 g, 7 mmol), nitromethane (20 eq, 7.57 ml, 140.2 mmol) and KOH (1.2 eq, 0.47 g, 8.4 mmol) in EtOH (10 ml) was heated at 60 ºC under reflux for 12 h. After cooling to room temperature, the solvent was removed in vacuo and oily residue obtained was acidified with 4 M HCl and partitioned between EtOAc (50 ml) and H_2O (50 ml). The organic layer was separated, dried over sodium sulfate and evaporated under reduced pressure. The obtained product was used for further synthesis without purification. (0.99 g, 60%)

[5-(3-hydroxyphenyl)-3-phenyl-1H-pyrrol-2-yl]-[5-phenyl-3-phenylpyrrol-2-ylidene]amine (6c): 1-(3-hydroxyphenyl)-4-nitro-3-phenylbutan-1-one (6b) (1 eq, 1 g, 3.5 mmol), 1,3-diphenyl-4-nitro-butan-1-on (1b) (1 eq, 0.94 g, 3.5 mmol) and ammonium acetate (35 eq, 7.6 g, 122.5 mmol) in butanol (50 ml) were heated under reflux for 24 h. The reaction was cooled to room temperature, the crude product was purified by column chromatography on silica with dichloromethane (after eluting symmetric byproduct with hexane/dichloromethane 3:1 v/v) to yield to product 6c as a blue-black solid. Product was recrystalized from hexane/tetrahydrofuran mixture as green metallic crystals (0.20 g, 17%). ^{1}H NMR (300 MHz, Chloroform-d) δ 6.97-7.00 (dd, *J* = 9.7 Hz, 1H), 7.39-7.66 (m, 13H), 7.71 (m, 1H), 8.10-8.12 (d, *J* = 7.3 Hz, 6H). Electron impact-direct insertion-time of flight (EI-DI-TOF) m/z [MH^+] found 465.1853, calculated 465.1841.

BF_2 chelate of [5-(3-hydroxyphenyl)-3-phenyl-1H-pyrrol-2-yl]-[5-phenyl-3-phenylpyrrol-2-ylidene]amine (6): Compound 6c (0.19 g, 0.4 mmol) was dissolved in dry CH_2Cl_2 (50 ml), treated with diisopropylethylamine (10 eq, 0.7 ml, 4 mmol) and BF_3 diethyletherate (15 eq, 0.81 ml, 6 mmol) and stirred under argon for 24 h. Purification by column chromatography on silica eluting with CH_2Cl_2 and recrystallization from hexane/tetrahydrofurane gave the product 6 as a red metallic solid (0.08 g, 36 %). ^{1}H NMR (300 MHz, Chloroform-d) δ 8.02-8.09 (m, 6H), 7.59-7.61 (t, *J* = 2.3 Hz, 1H), 7.44-7.56 (m, 10H), 7.34-7.39 (t, *J* = 8 Hz, 1H), 6.97-7.01 (m, 3H). Electron impact-direct insertion-time of flight (EI-DI-TOF) m/z [MH^+] found 512.193, calculated 512.186.

1-phenyl-4-nitro-3-(4-methoxyphenyl)-butan-1-one (7a): A solution of 1-phenyl-3-(4-methoxyphenyl)-propenone (1 eq, 2 g, 8.4 mmol), nitromethane (20 eq, 10.25 ml, 168 mmol) and KOH (0.2 eq, 0.09 g, 1.7 mmol) in EtOH (10 ml) was heated at 60 ºC under reflux for 12 h. After cooling to room temperature, the solvent was removed in vacuo and oily residue obtained was partitioned between EtOAc (50 ml) and H_2O (50 ml). The organic layer was separated, dried over sodium sulfate and evaporated under reduced pressure. The obtained product was used for further synthesis without purification. (2.5 g, 82%)

[5-(4-hydroxyphenyl)-3-phenyl-1H-pyrrol-2-yl]-[5-(4-methoxyphenyl)-3-phenylpyrrol-2-ylidene]amine (7b): Compound 7a (1eq, 1.0 g, 4.4 mmol), compound 1b (1eq, 0.93 g, 4.4 mmol)

and ammonium acetate (35 eq, 9.55 g, 154 mmol) in butanol (50 ml) were heated under reflux for 24 h. The reaction was cooled to room temperature, the crude product was purified by column chromatography on silica with dichloromethane (after eluting symmetric byproduct with toluene/dichloromethane 3:1 v/v) to yield to product 7b as a blue-black solid. Product was recrystallized from hexane/tetrahydrofuran mixture as green metallic crystals (0.13 g, 8%). ^{1}H NMR (300 MHz, DMSO-d6) δ 8.08-8.10 (d, *J* = 7.3 Hz, 4 H), 7.97-8.01 (dd, *J* = 8.7, 3.3 Hz, 4 H), 7.60 (s, 1 H), 7.53 (s, 1 H), 7.34 – 7.49 (m, 2H), 7.18-7.21 (d, *J* = 8.8 Hz, 2 H), 7.01-7.04 (d, *J* = 8.7 Hz, 2 H), 3.89 (s, 3 H). Electron impact-direct insertion-time of flight (EI-DI-TOF) m/z [MH^+] found 495.1984, calculated 495.1947.

BF_2 chelate of [5-(4-hydroxyphenyl)-3-phenyl-1H-pyrrol-2-yl]-[5-(4-methoxyphenyl)-3-phenylpyrrol-2-ylidene]amine (7): Compound 7b (0.1 g, 0.20 mmol) was dissolved in dry CH_2Cl_2 (50 ml), treated with diisopropylethylamine (10 eq, 0.39 ml, 2 mmol) and BF_3 diethyletherate (15 eq, 0.38 ml, 3 mmol) and stirred under argon for 24 h. Purification by column chromatography on silica eluting with CH_2Cl_2 and recrystallization from hexane/tetrahydrofurane gave the product 7 as a red metallic solid (0.079 g, 53 %). ^{1}H NMR (300 MHz, DMSO-d) δ 8.11-8.19 (m, 8 H), 7.68 (s, 1 H), 7.42-7.57 (m, 7 H), 7.12-7.15 (d, *J* = 9.0 Hz, 2 H), 6.87-6.90 (d, *J* = 8.9 Hz, 2 H), 3.88 (s, 3 H). Electron impact-direct insertion-time of flight (EI-DI-TOF) m/z [MH^+] found 542.203, calculated 542.196.

1-(4-methoxyphenyl)-4-nitro-3-(4-methoxyphenyl)-butan-1-one (8a). A solution of 1-(4-methoxyphenyl)-3-(4-methoxyphenyl)-propenone (1 eq, 2 g, 8.4 mmol), nitromethane (20 eq, 10.25 ml, 168 mmol) and KOH (0.2 eq, 0.09 g, 1.68 mmol) in EtOH (10 ml) was heated at 60 ºC under reflux for 12 h. After cooling to room temperature, the solvent was removed in vacuo and oily residue obtained was partitioned between EtOAc (50 ml) and H_2O (50 ml). The organic layer was separated, dried over sodium sulfate and evaporated under reduced pressure. The obtained product was used for further synthesis without purification. (2.2 g, 92%)

[5-(4-hydroxyphenyl)-3-phenyl-1H-pyrrol-2-yl]-[5-(4-methoxyphenyl)-3-(4-methoxy phenyl)-pyrrol-2-ylidene]amine (8b): Compound 8a (1eq, 1.0 g, 4.4 mmol), compound 1b (1eq, 0.93 g, 4.4 mmol) and ammonium acetate (35 eq, 9.55 g, 154 mmol) in butanol (50 ml) were heated under reflux for 24 h. The reaction was cooled to room temperature, the crude

product was purified by column chromatography on silica eluting with dichloromethane (after eluting symmetric byproduct with toluene/dichloromethane 3:1 v/v) to yield to product 8b as a blue-black solid. Product was recrystallized from hexane/tetrahydrofuran mixture as green metallic crystals (0.39 g, 20%). ^{1}H NMR (300 MHz, DMSO-d6) δ 8.08-8.13 (m, 4H), 7.92 – 7.95 (m, 2 H), 7.87 (s, 2 H), 7.78 (s, 1 H), 7.54-7.59 (t, 2 H), 7.32-7.50 (m, 8 H), 2.31 (s, 2 H). Electron impact-direct insertion-time of flight (EI-DI-TOF) m/z [MH^+] found 525.2096, calculated 525.2053.

BF_2 chelate of [5-(4-hydroxyphenyl)-3-phenyl-1H-pyrrol-2-yl]-[5-(4-methoxyphenyl)-3-(4-methoxy phenyl)-pyrrol-2-ylidene]amine (8): Compound 8b (0.22 g, 0.42 mmol) was dissolved in dry CH_2Cl_2 (50 ml), treated with diisopropylethylamine (10 eq, 0.71 ml, 4.2 mmol) and BF_3 diethyletherate (15 eq, 0.8 ml, 6.3 mmol) and stirred under argon for 24 h. Purification by column chromatography on silica eluting with CH_2Cl_2 and recrystallization from hexane/tetrahydrofurane gave the product 8 as a red metallic solid (0.19 g, 78 %). ^{1}H NMR (300 MHz, DMSO-d6) δ 10.46 (s, 1 H), 8.08 - 8.20 (m, 8 H), 7.46-7.59 (m, 5 H), 7.08-7.11 (dd, *J* = 12.9, 9.0 Hz, 4 H), 6.92-6.95 (d, *J* = 8.9 Hz, 2 H), 3.89 (s, 3 H), 3.87 (s, 3 H). Electron impact-direct insertion-time of flight (EI-DI-TOF) m/z [MH^+] found 572.2072, calculated 572.2129.

BF_2 chelate of [5-(4-hydroxyphenyl)-3-phenyl-1H-pyrrol-2-yl]-[5-phenyl-3-phenylpyrrol-2-ylidene]amine (1).

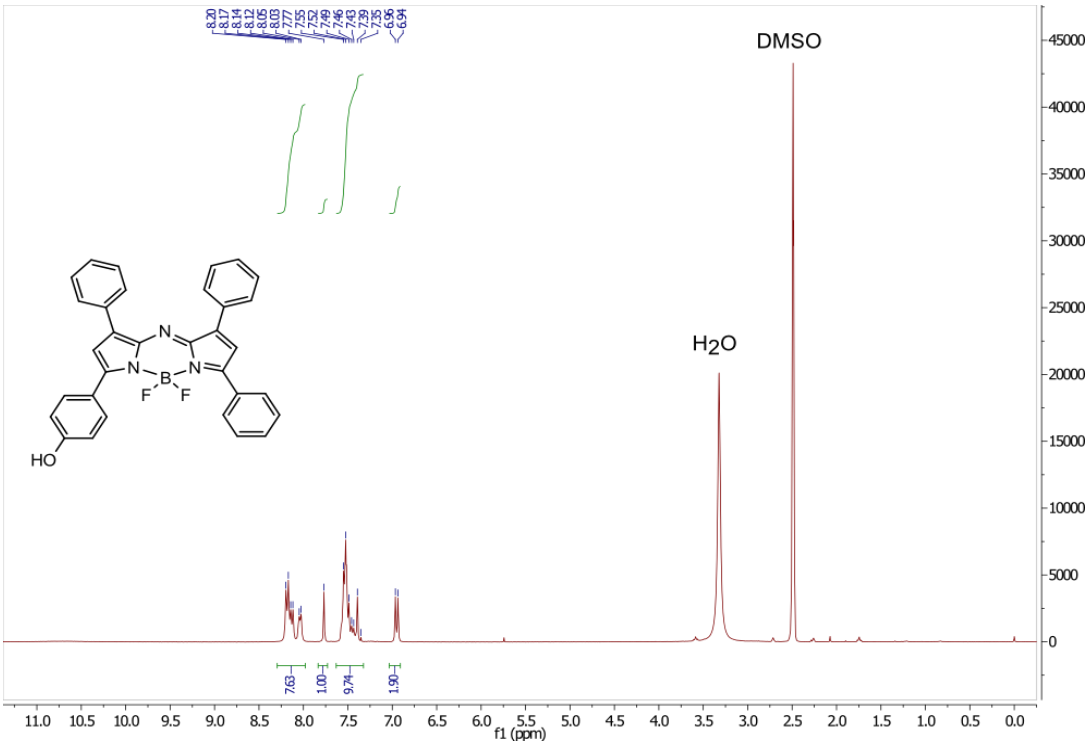

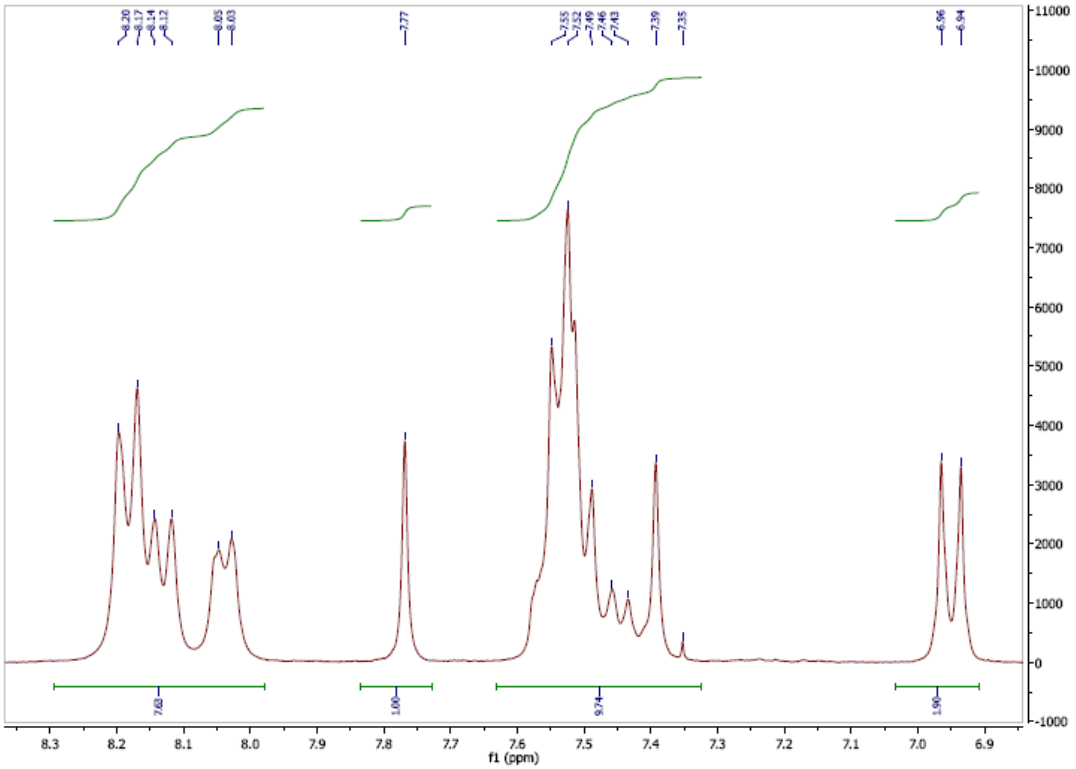
8.20
8.17
8.14
8.12
8.05
8.03
7.77
7.55
7.52
7.49
7.46
7.43
7.39
7.35
6.96
6.94
7.63
1.00
9.74
1.90
f1 (ppm)

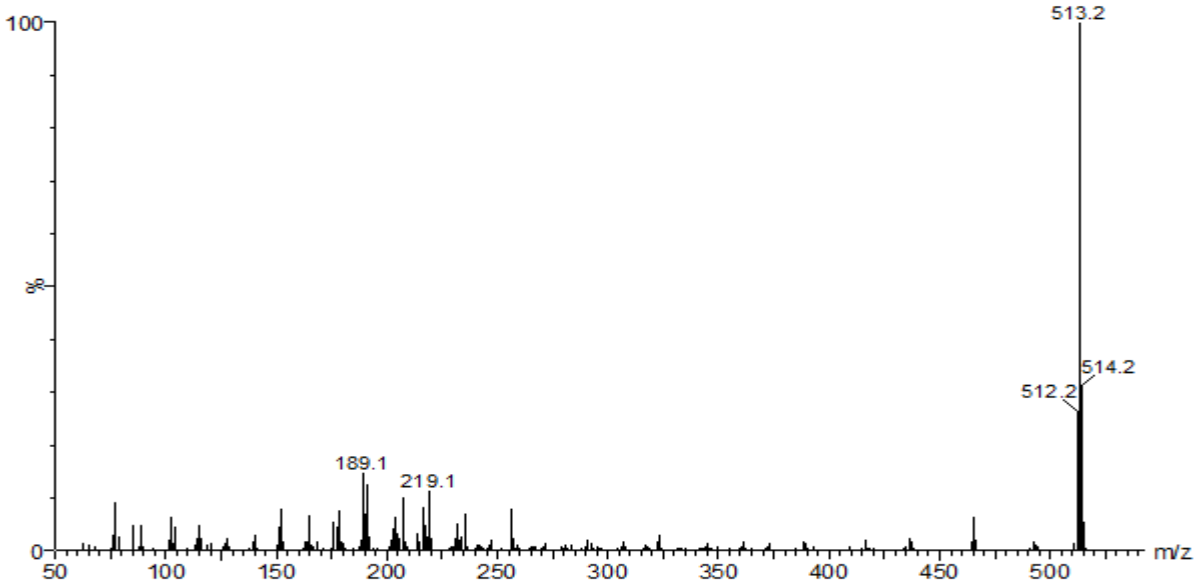
100
%
0
513.2
514.2
512.2
189.1
219.1
m/z
50
100
150
200
250
300
350
400
450
500

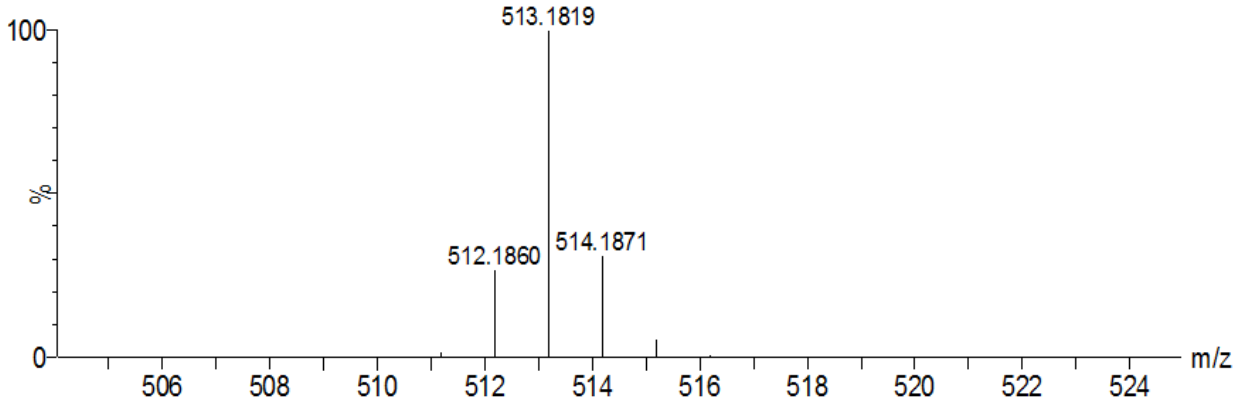

Figure S1. ^{1}H NMR and mass spectra of **1** in DMSO.

BF_2 chelate of [5-(3-chloro-4-hydroxyphenyl)-3-phenyl-1H-pyrrol-2-yl]-[5-phenyl-3-phenylpyrrol-2-ylidene]amine (2)

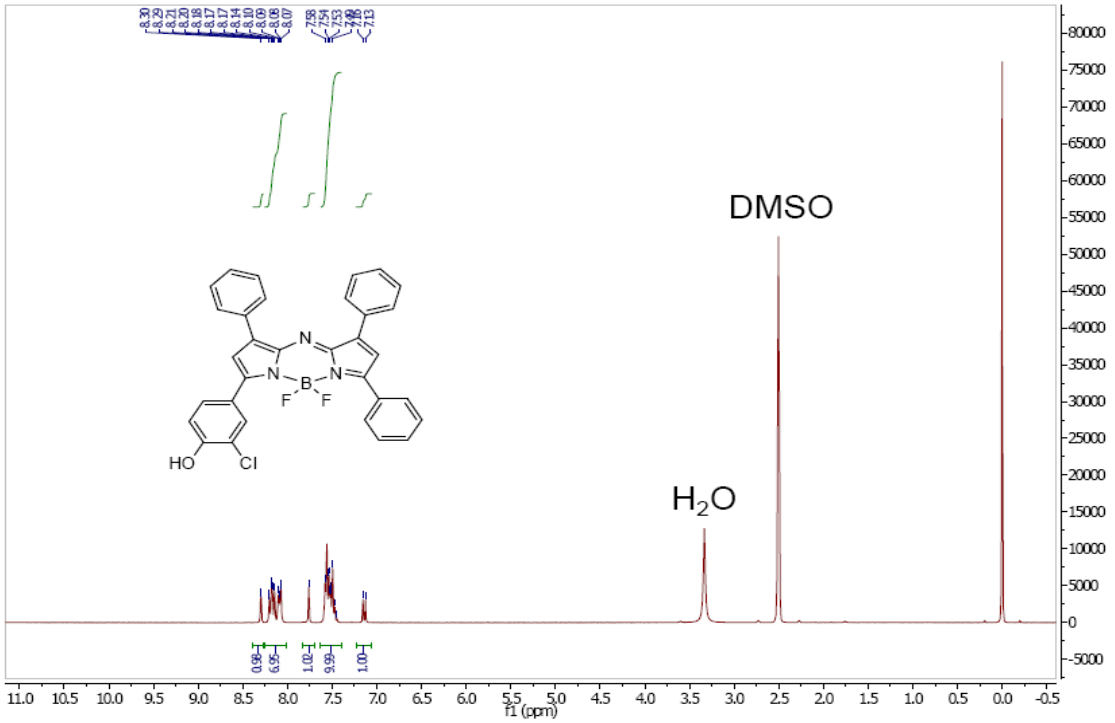

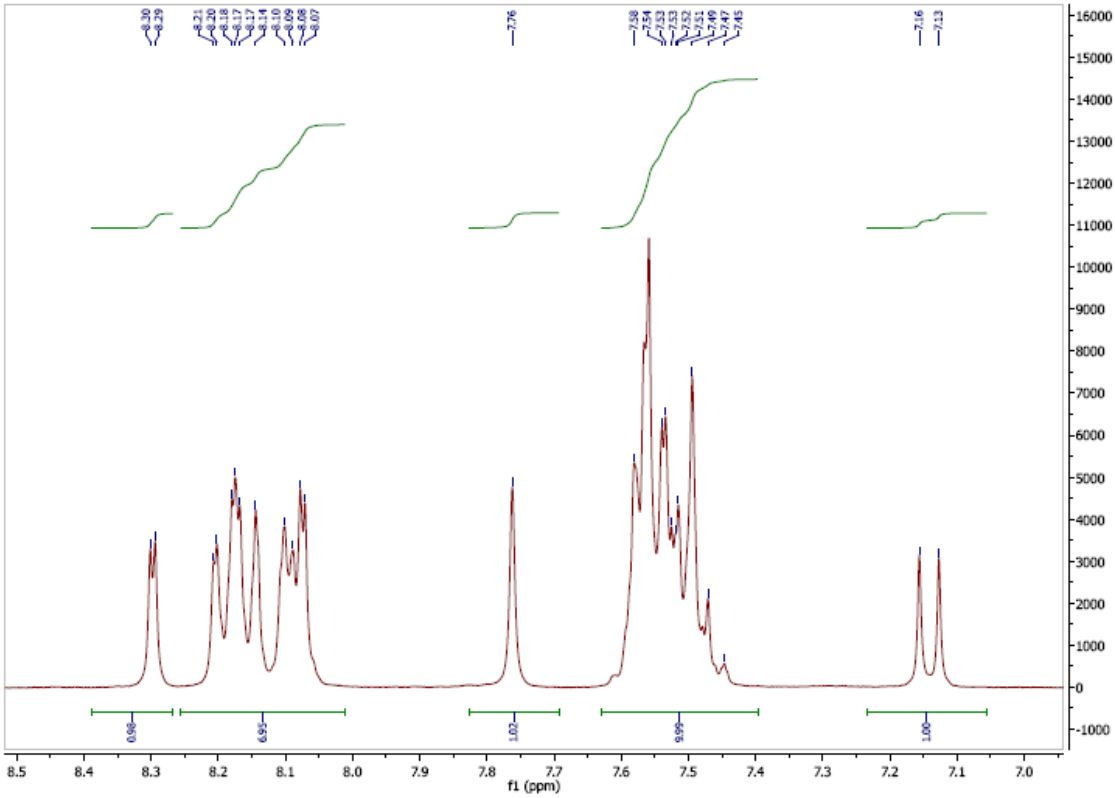

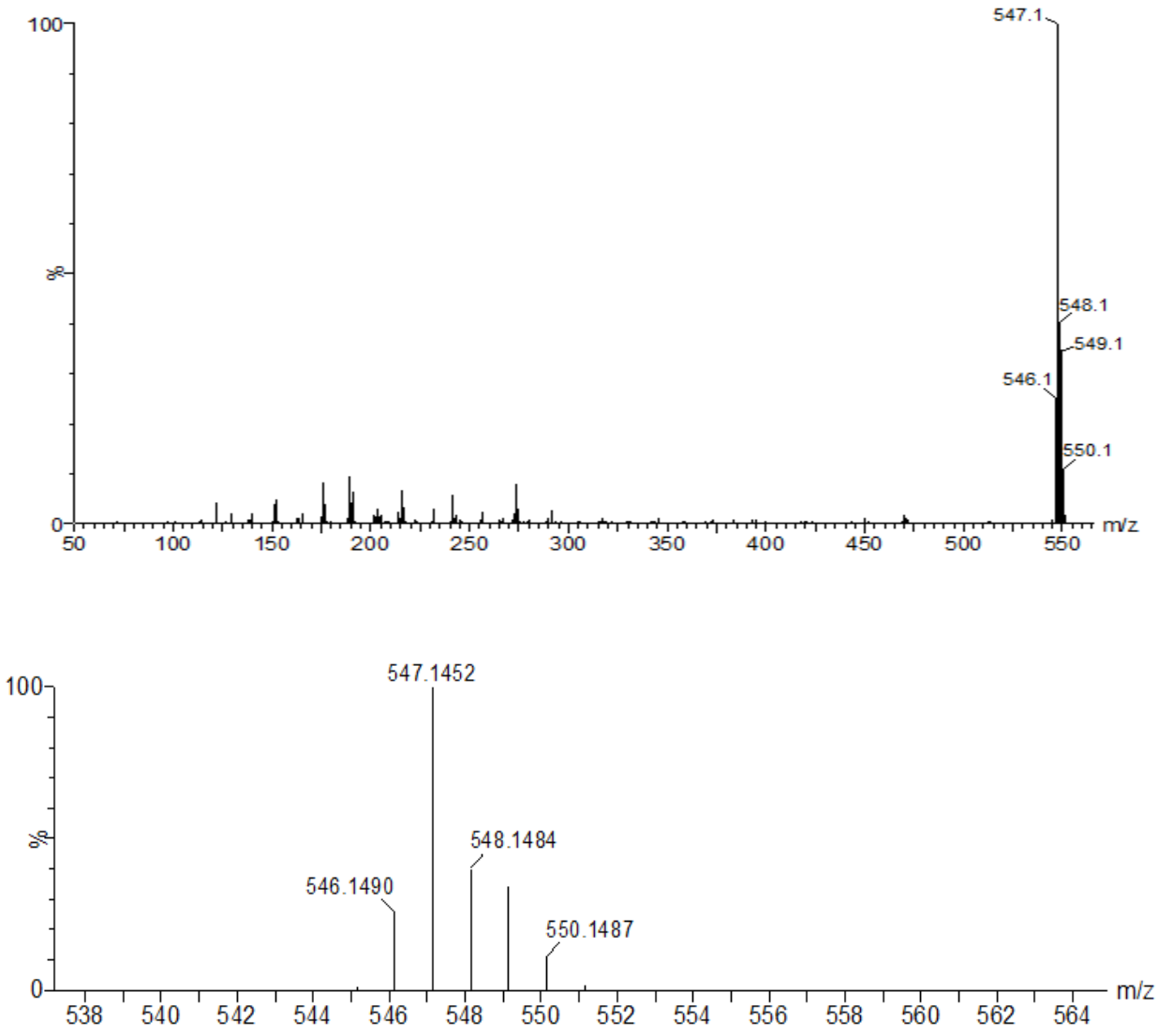

Figure S2. ^{1}H NMR and mass spectra of **2** in DMSO.

BF_2 chelate of [5-(3-methyl-4-hydroxyphenyl)-3-phenyl-1H-pyrrol-2-yl]-[5-phenyl-3-phenylpyrrol-2-ylidene]amine (3)

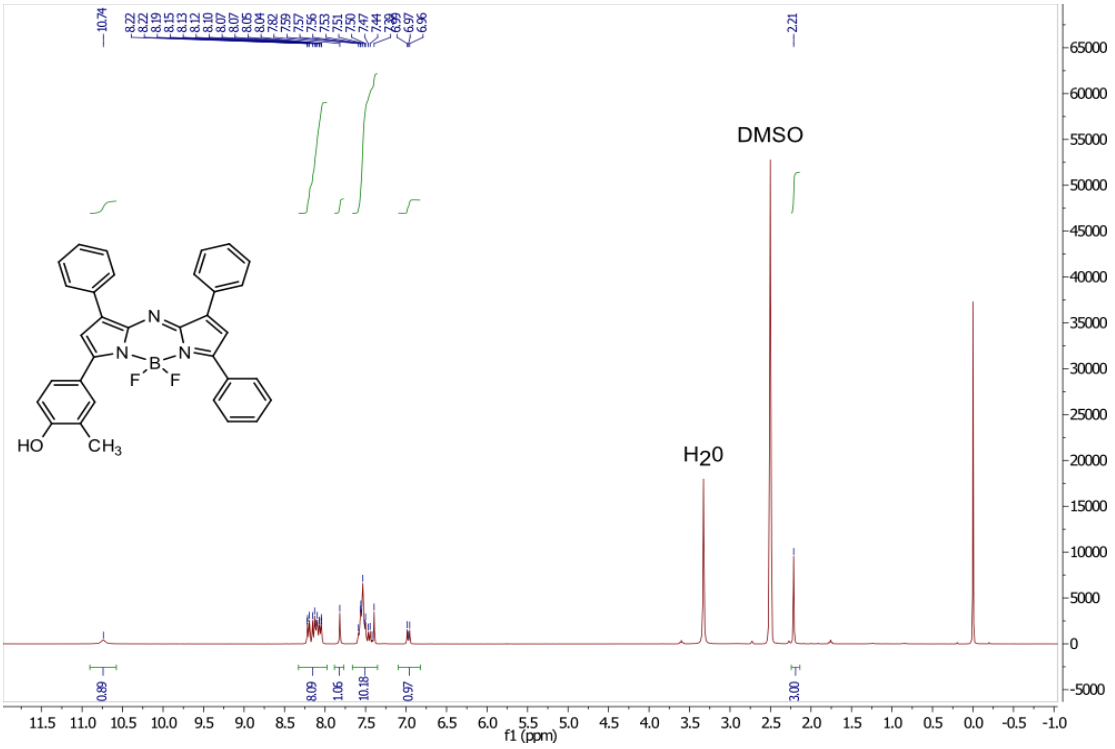

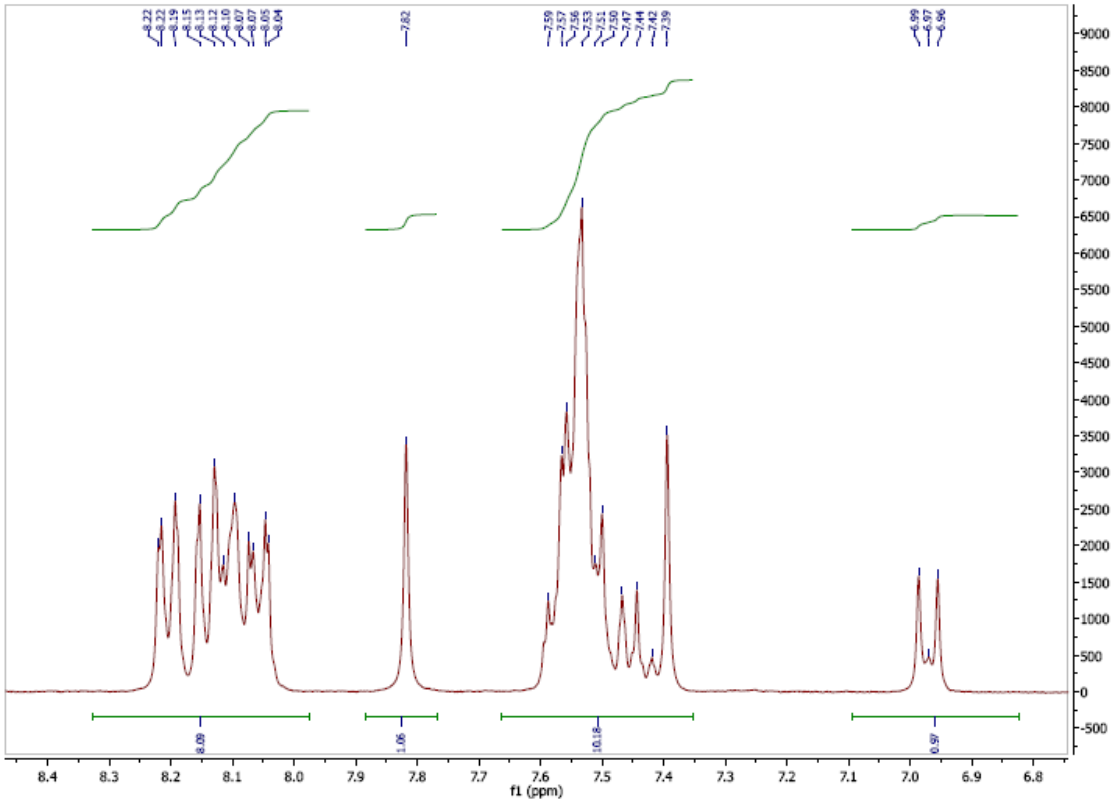
8.22
8.22
8.19
8.15
8.13
8.12
8.10
8.07
8.07
8.05
8.04
7.82
7.59
7.57
7.56
7.53
7.51
7.50
7.47
7.44
7.42
7.39
6.99
6.97
6.96
8.09
1.06
10.18
0.97
f1 (ppm)

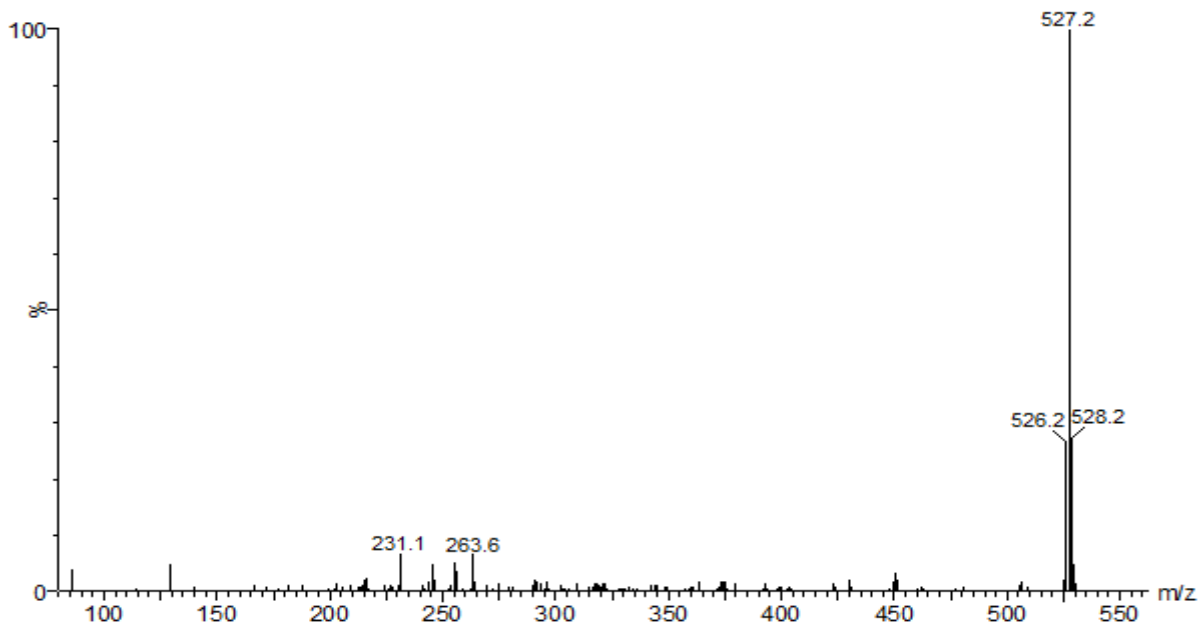
100
%
0
527.2
526.2
528.2
231.1
263.6
m/z
100
150
200
250
300
350
400
450
500
550

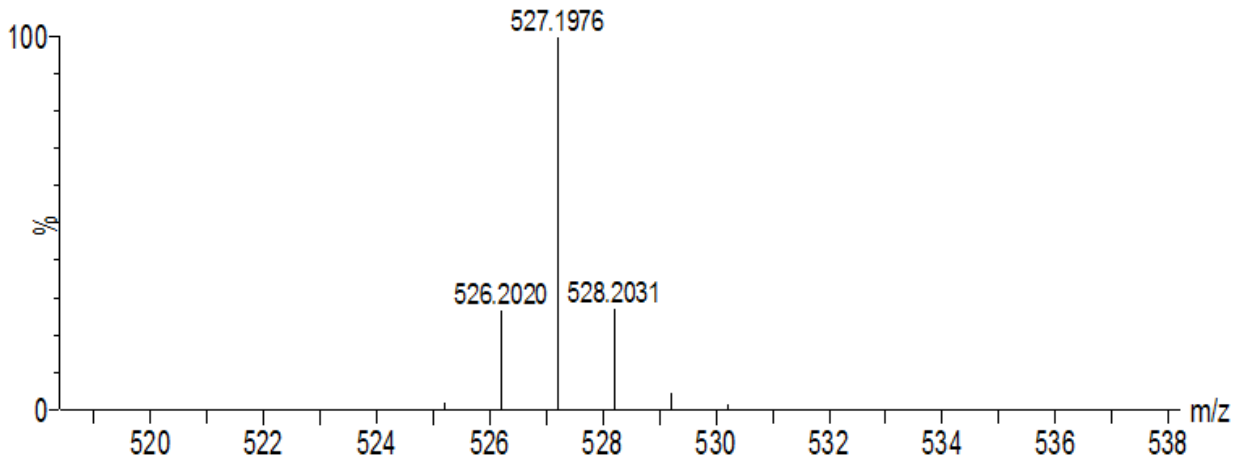

Figure S3. ^{1}H NMR and mass spectra of **3** in DMSO.

BF_2 chelate of [5-(3,5-dimethyl-4-hydroxyphenyl)-3-phenyl-1H-pyrrol-2-yl]-[5-phenyl-3-phenylpyrrol-2-ylidene]amine (4)

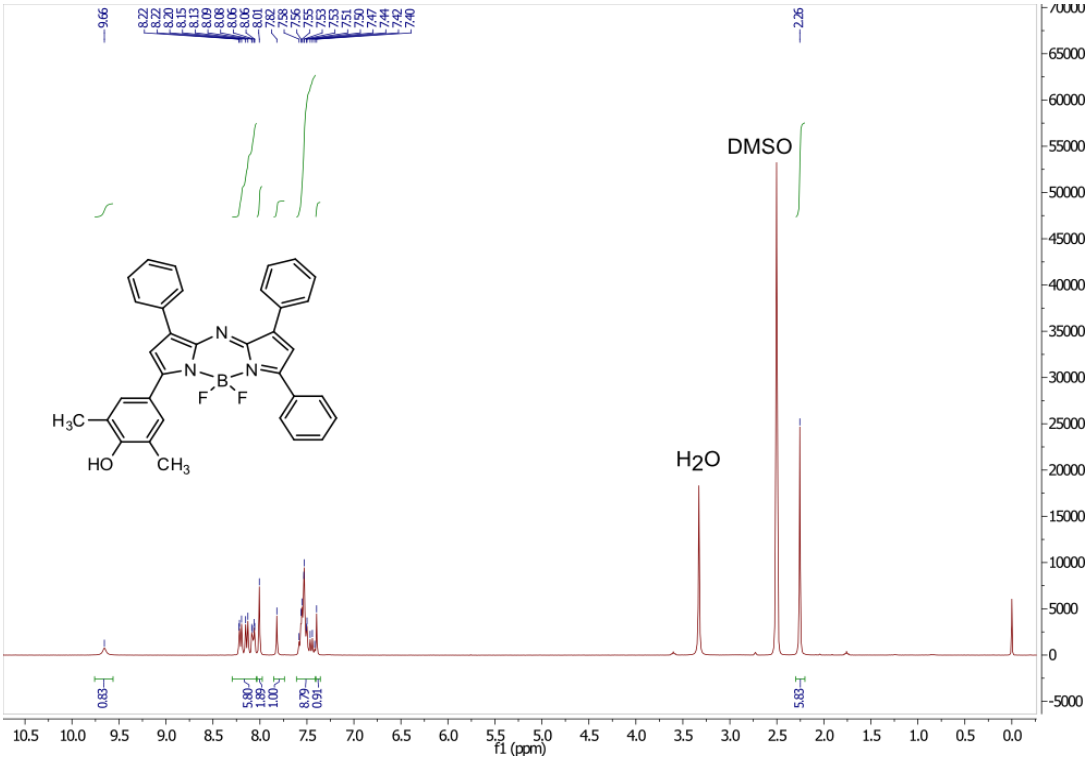

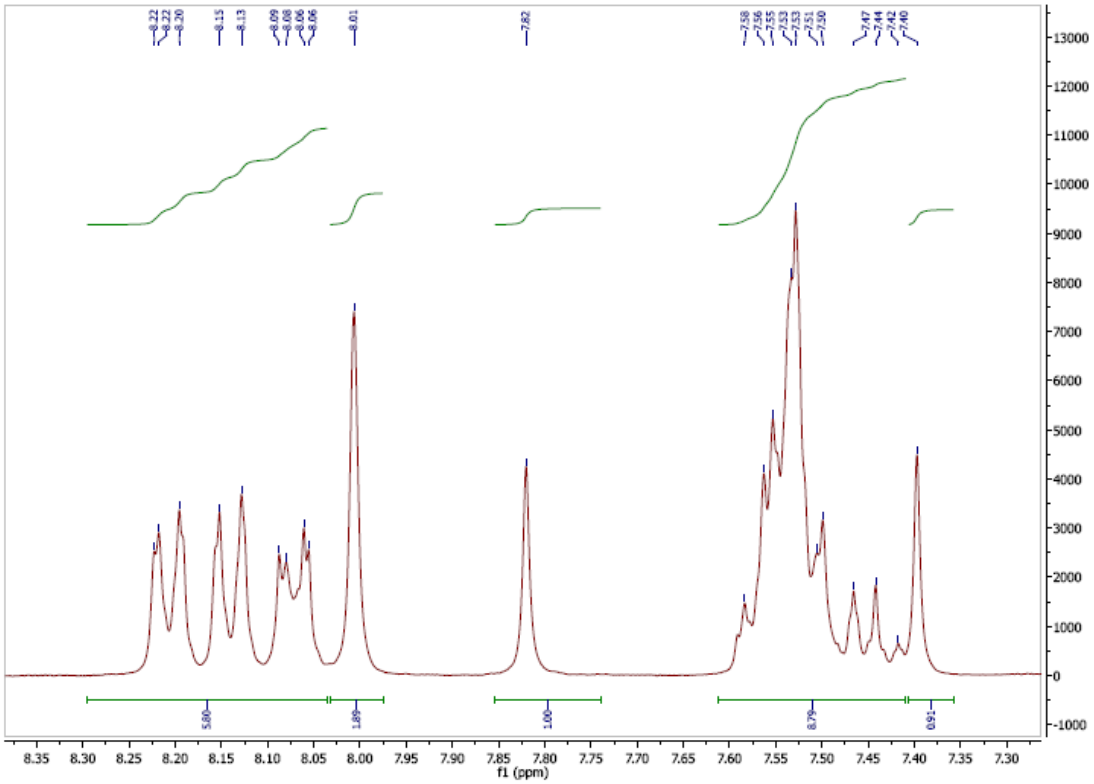

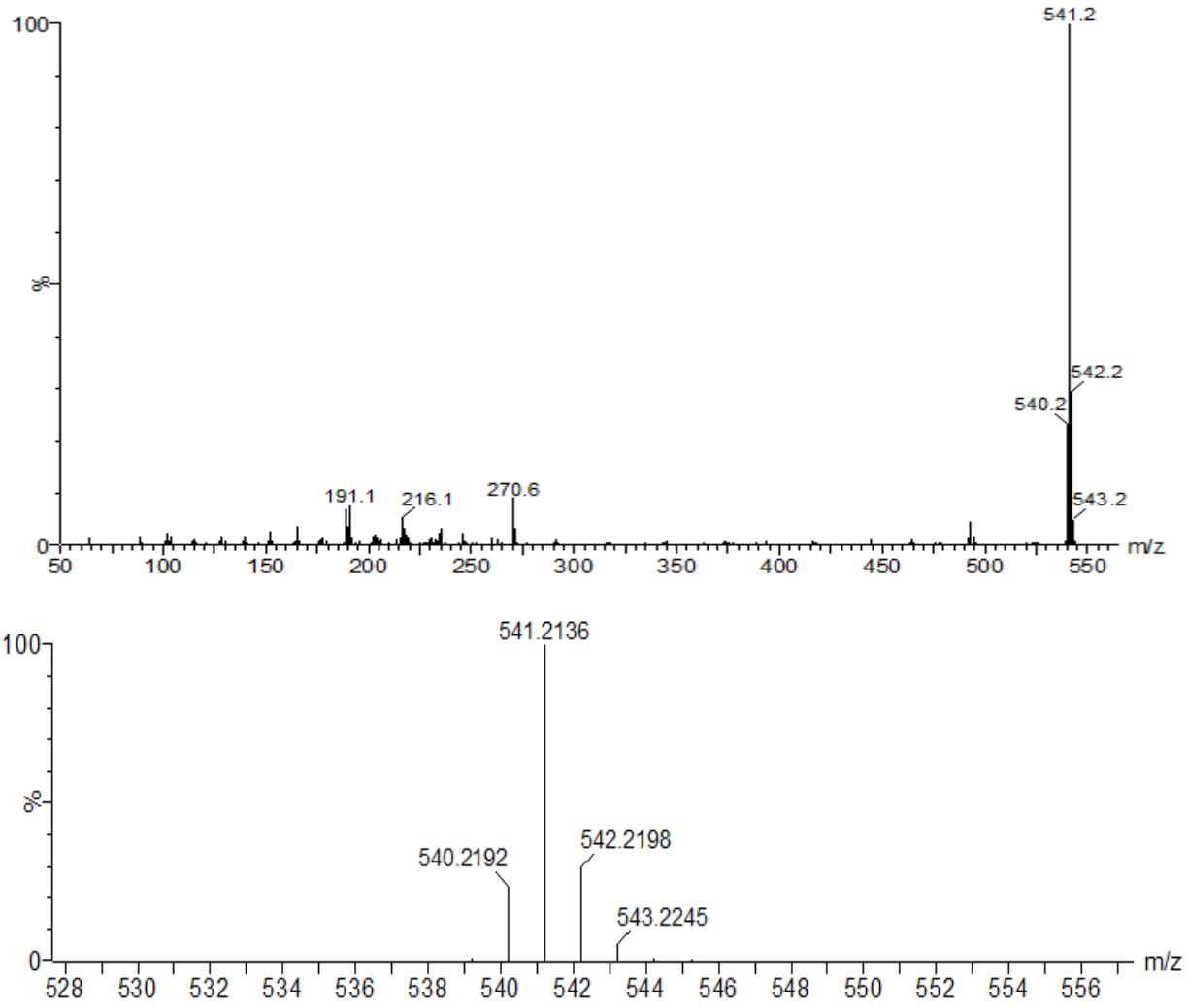

Figure S4. ^{1}H NMR and mass spectra of **4** in DMSO.

BF_2 chelate of [5-phenyl-3-(4-hydroxyphenyl)-1H-pyrrol-2-yl]-[5-phenyl-3-phenylpyrrol-2-ylidene]amine (5)

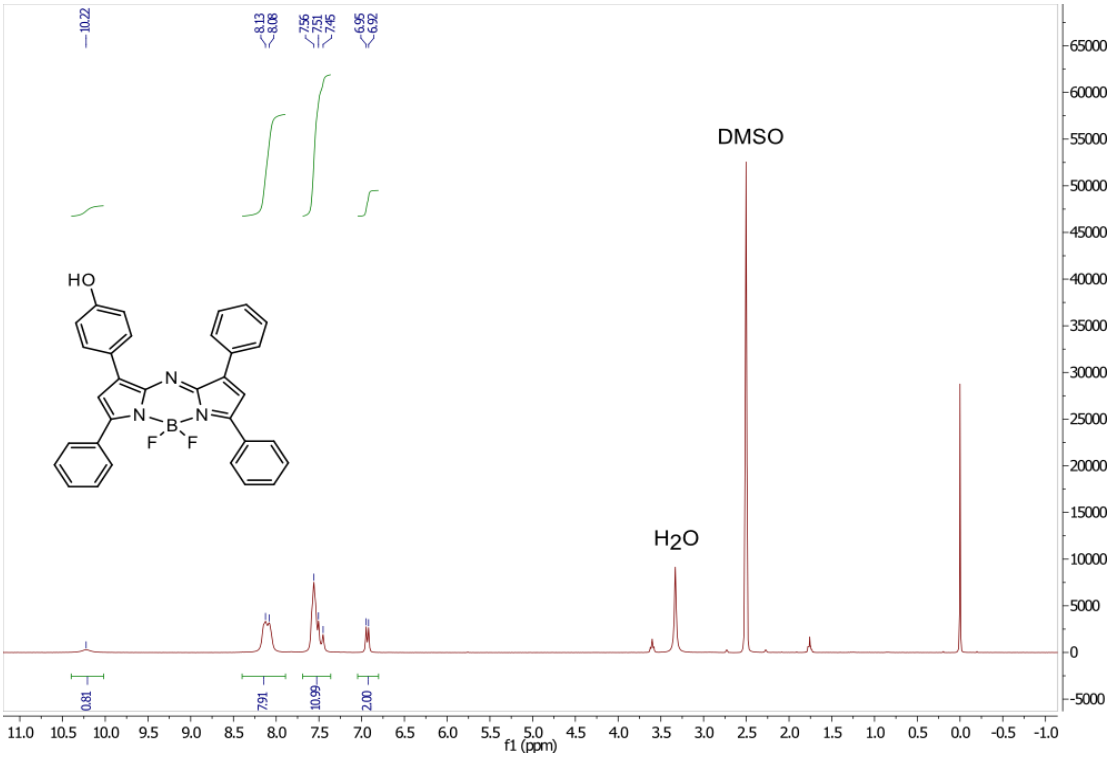

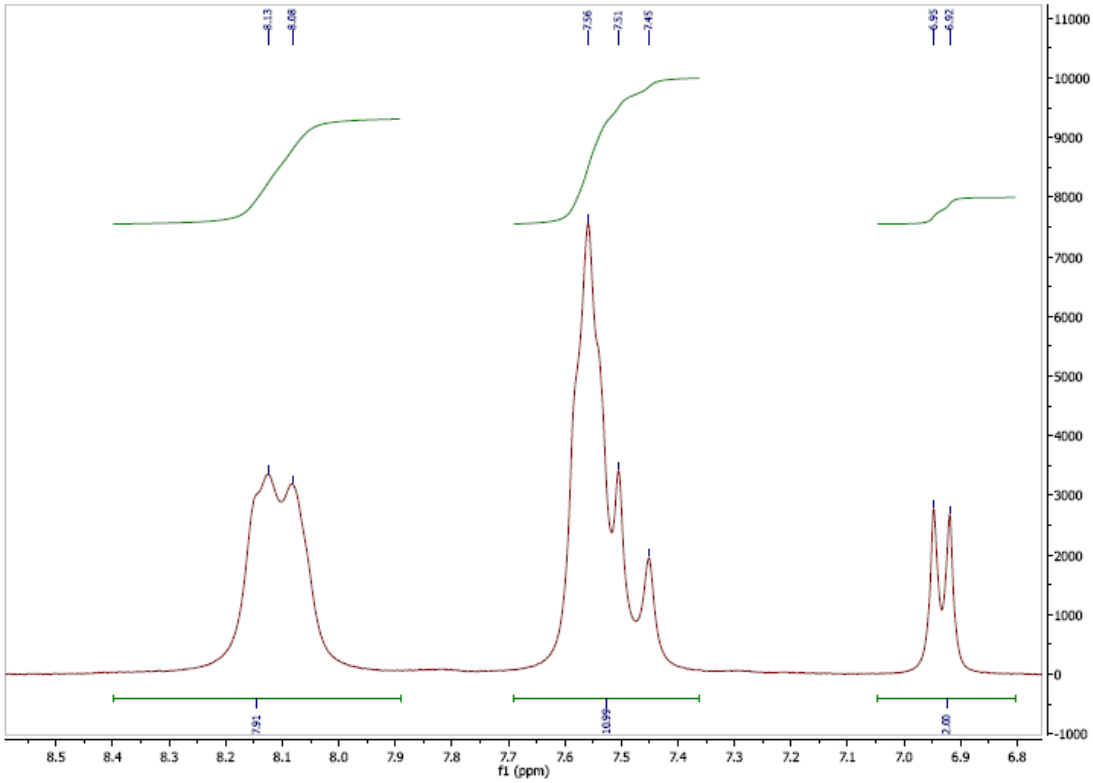

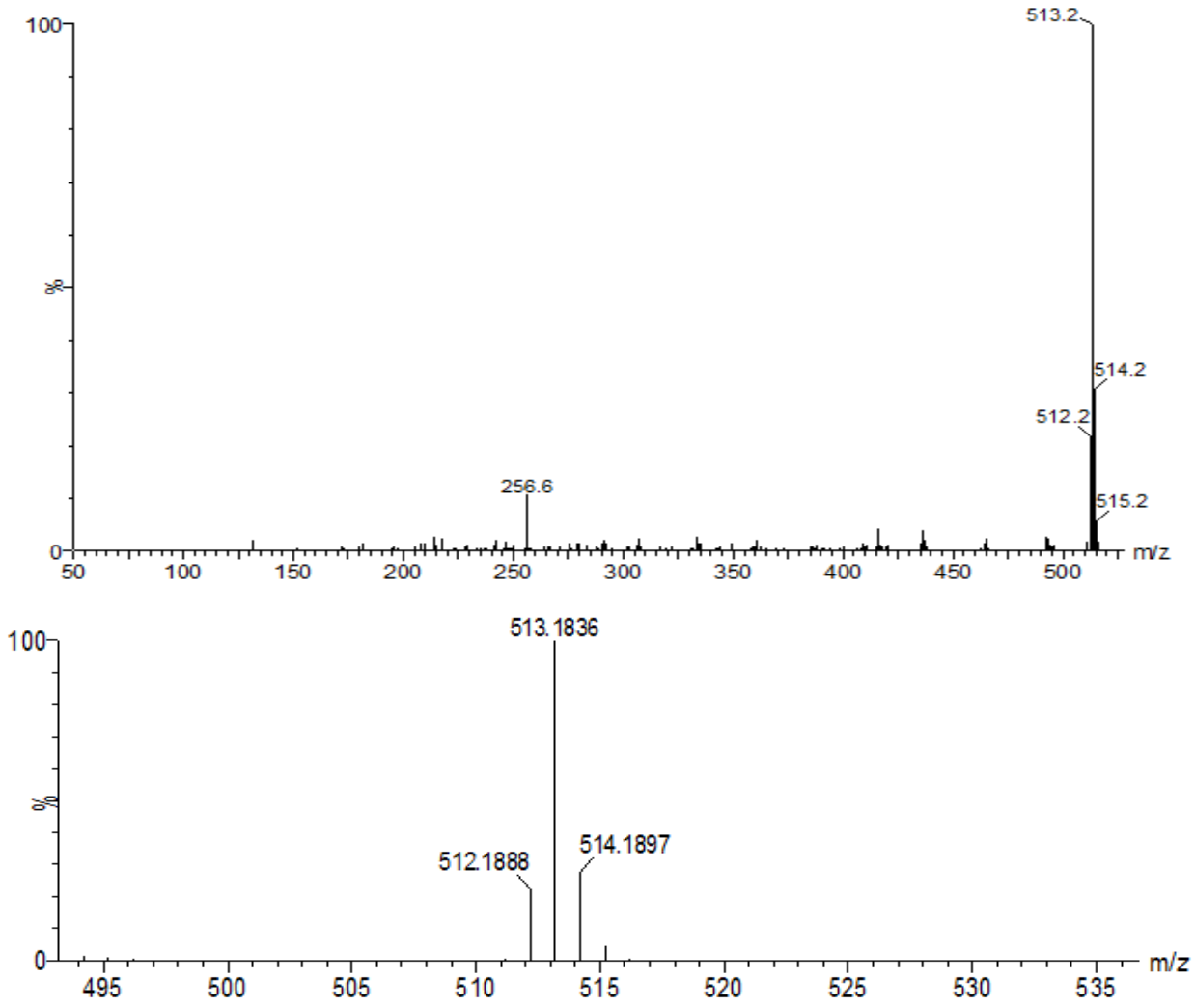

Figure S5. ^{1}H NMR and mass spectra of **5** in DMSO.

BF_2 chelate of [5-(3-hydroxyphenyl)-3-phenyl-1H-pyrrol-2-yl]-[5-phenyl-3-phenylpyrrol-2-ylidene]amine (6)

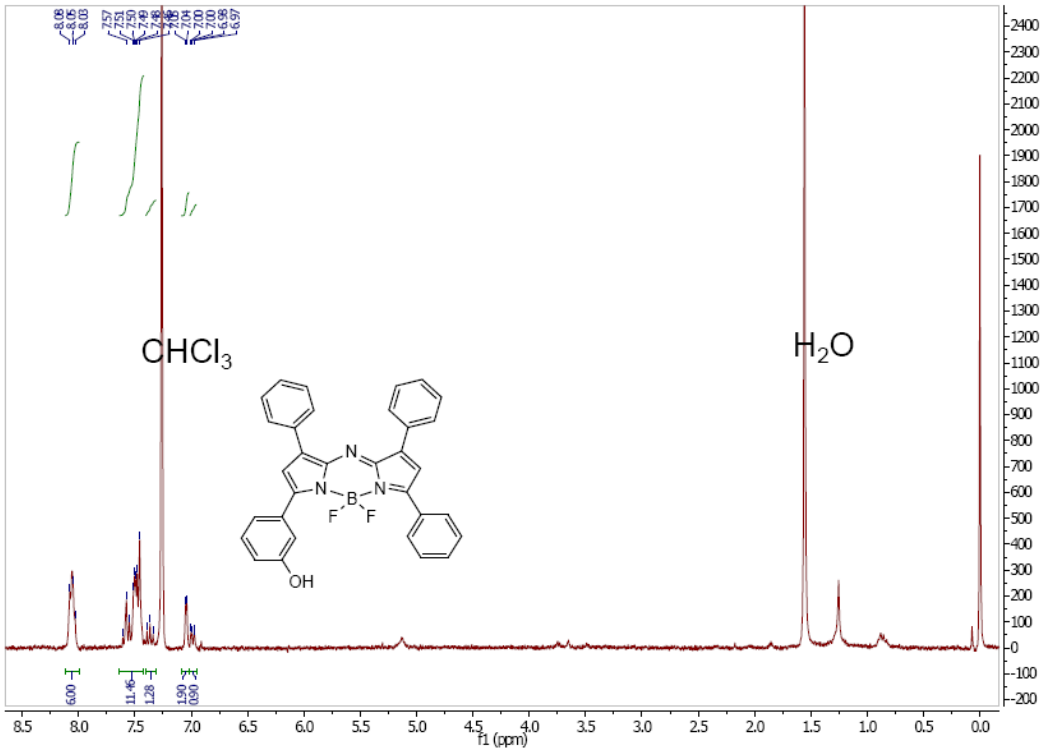

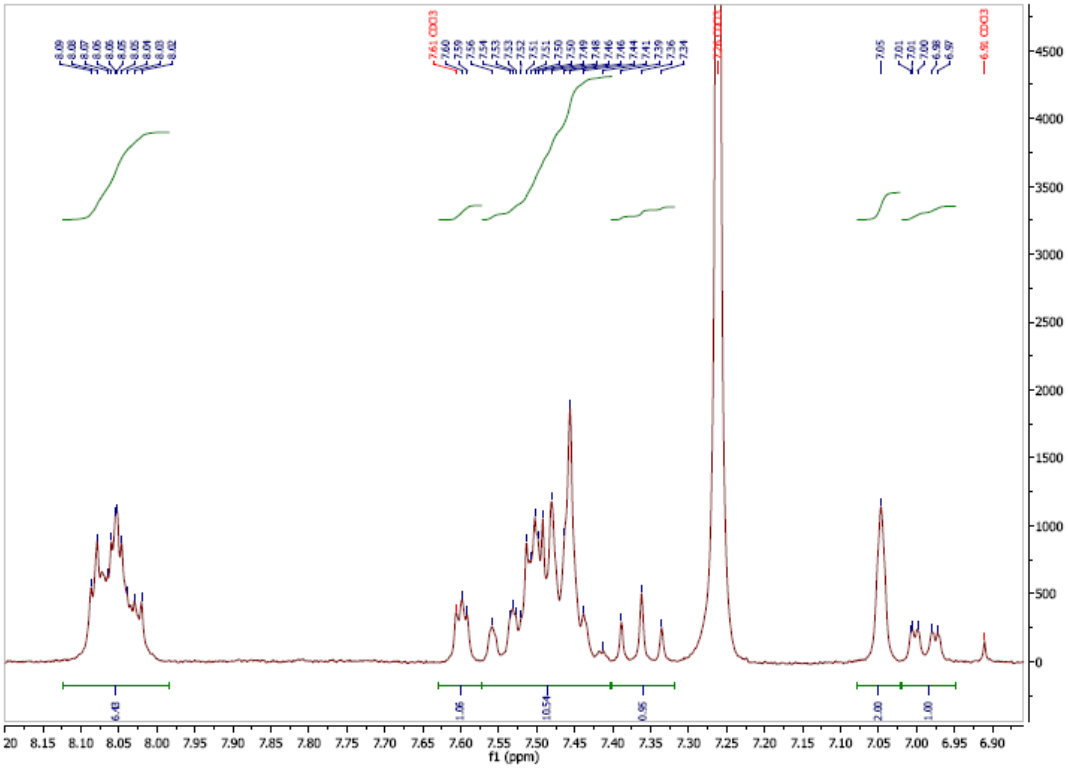

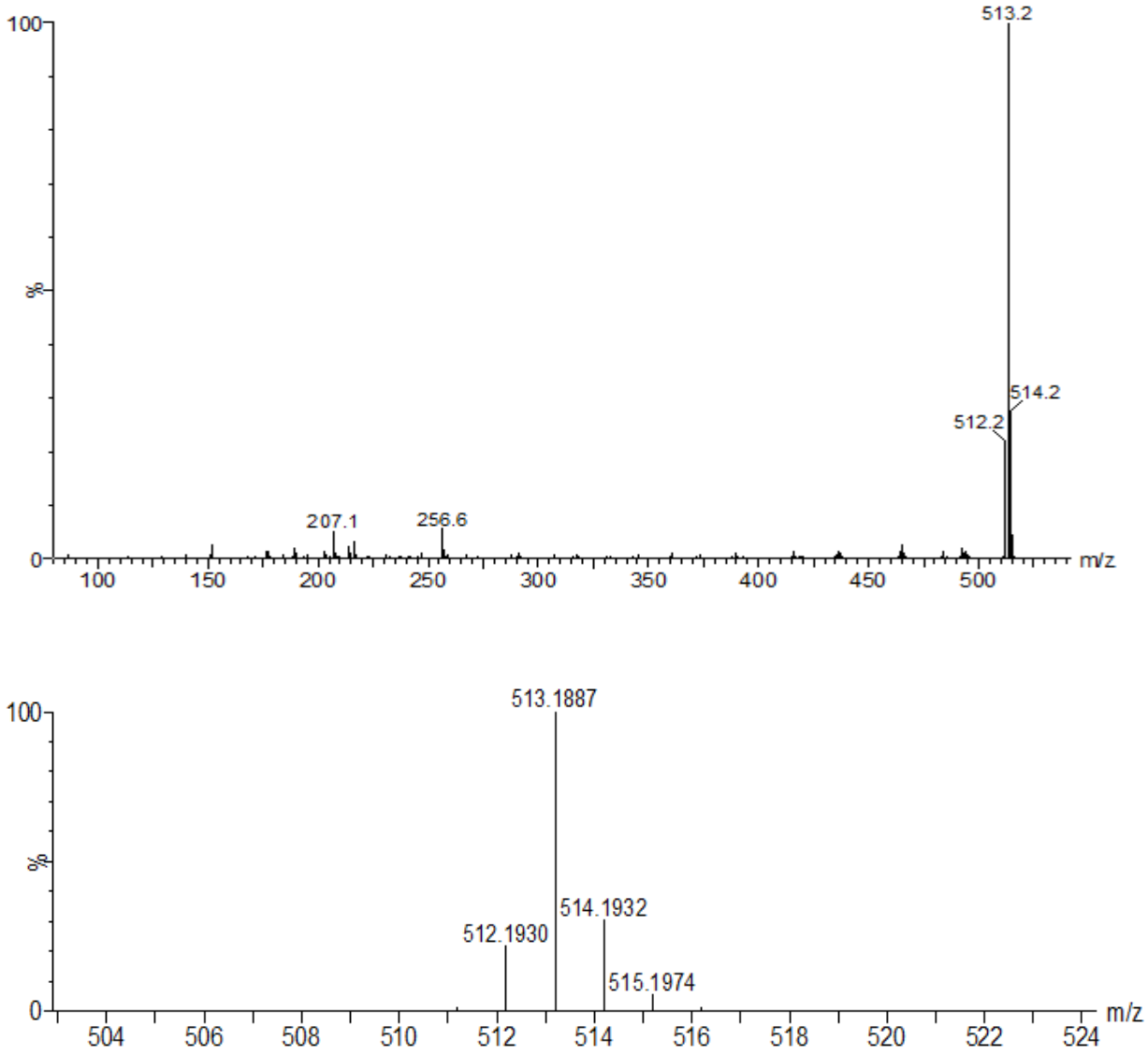

Figure S6. ^{1}H NMR and mass spectra of **6** in $CDCl_3$.

BF_2 chelate of [5-(4-hydroxyphenyl)-3-phenyl-1H-pyrrol-2-yl]-[5-(4-methoxyphenyl)-3-phenylpyrrol-2-ylidene]amine (7)

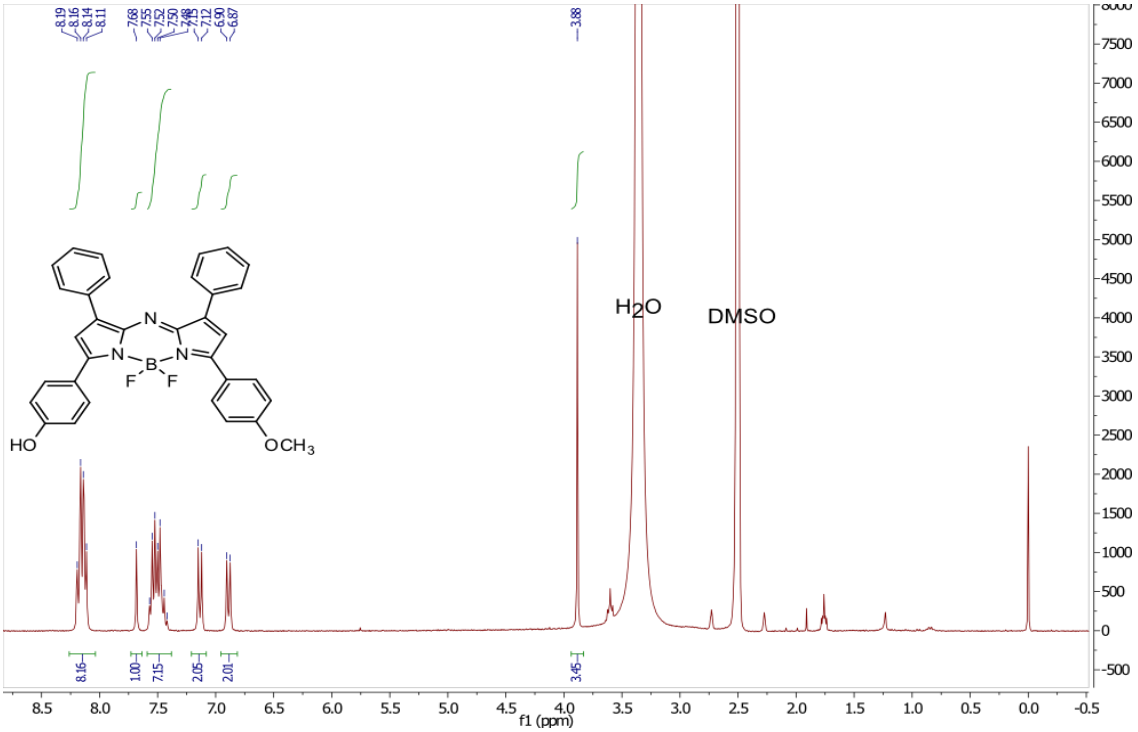

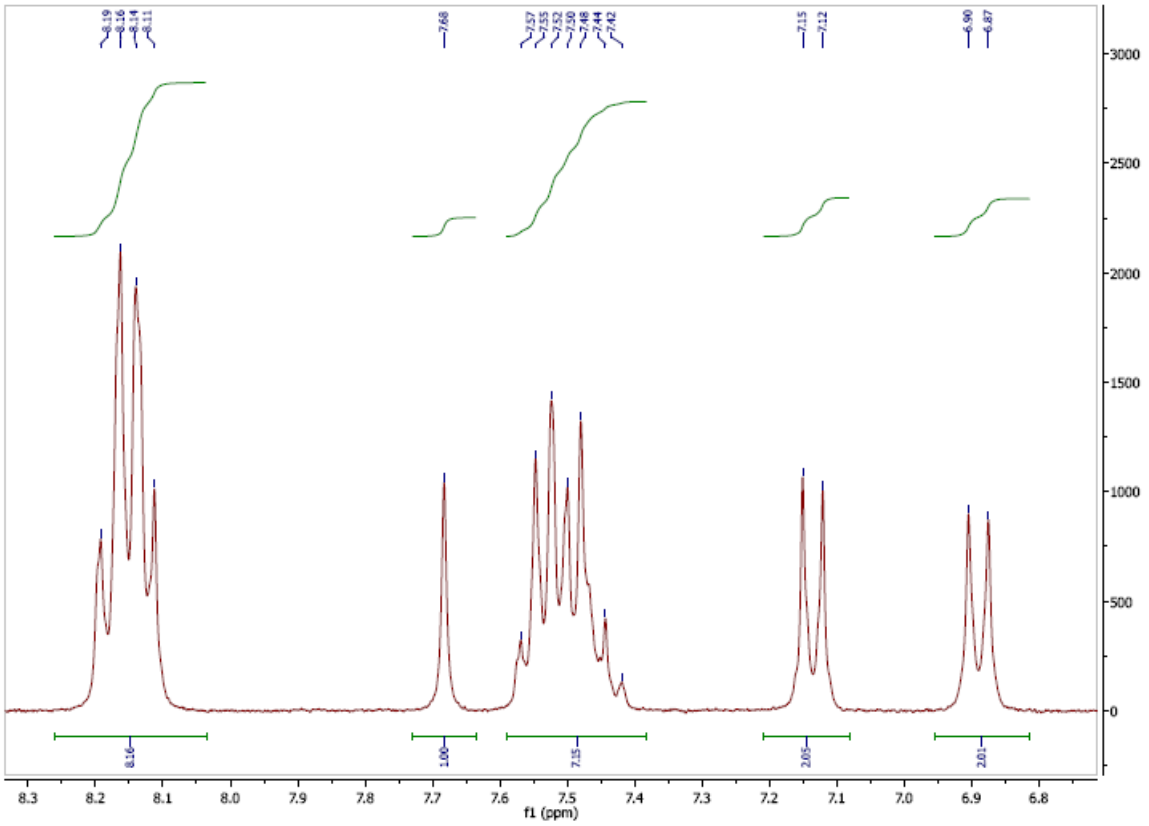
8.19
8.16
8.14
8.11
7.68
7.57
7.55
7.52
7.50
7.48
7.44
7.42
7.15
7.12
6.90
6.87
3000
2500
2000
1500
1000
500
0
8.16
1.00
7.15
2.05
2.01
8.3
8.2
8.1
8.0
7.9
7.8
7.7
7.6
7.5
7.4
7.3
7.2
7.1
7.0
6.9
6.8
f1 (ppm)

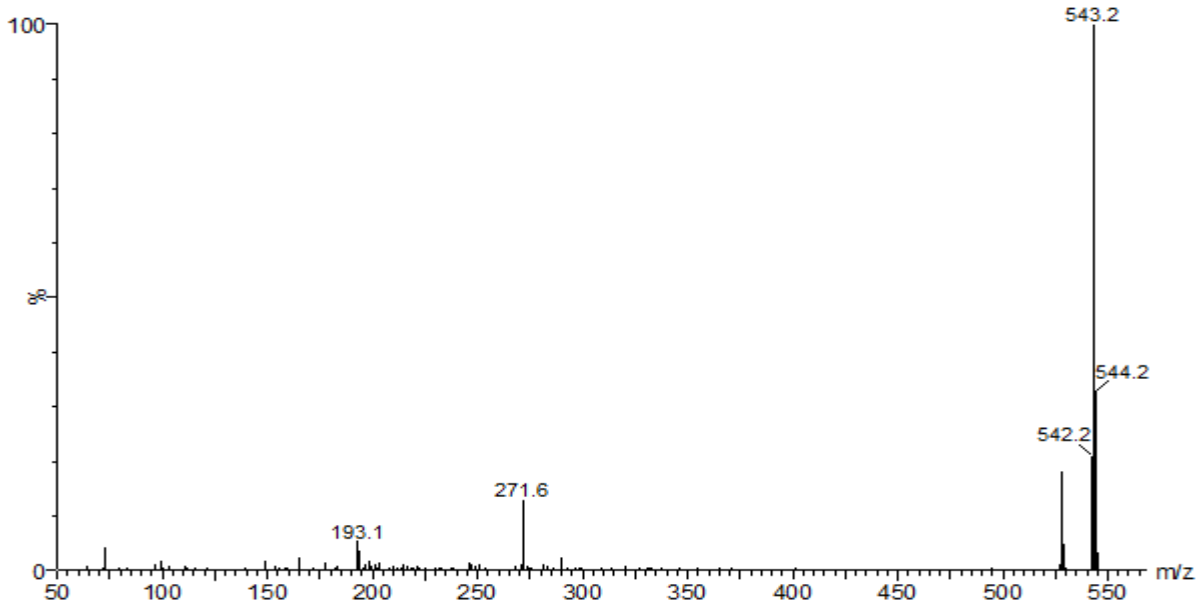
100
%
0
543.2
544.2
542.2
271.6
193.1
50
100
150
200
250
300
350
400
450
500
550
m/z

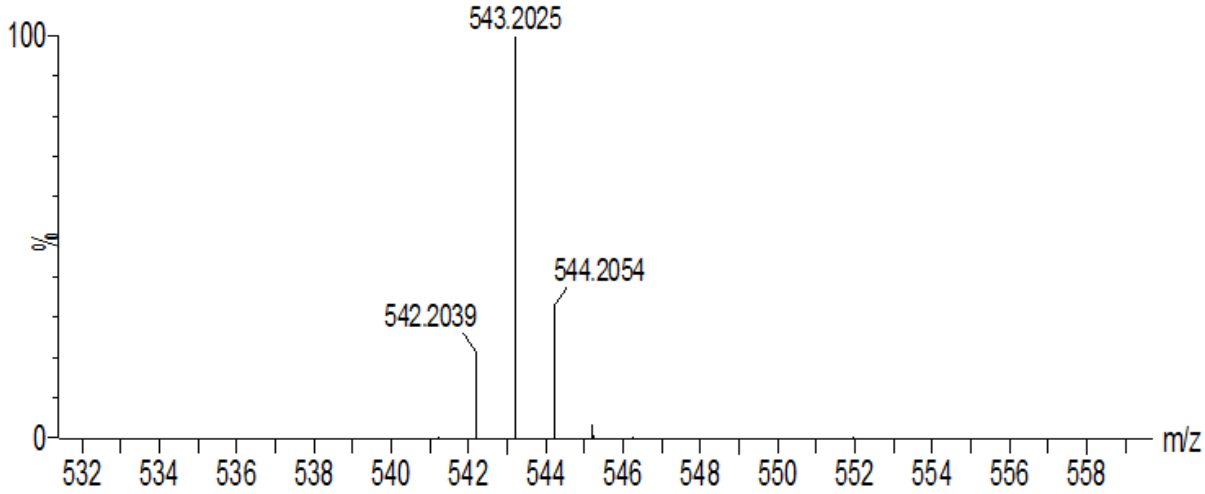

Figure S7. ^{1}H NMR and mass spectra of **7** in DMSO.

BF_2 chelate of [5-(4-hydroxyphenyl)-3-phenyl-1H-pyrrol-2-yl]-[5-(4-methoxyphenyl)-3-phenylpyrrol-2-ylidene]amine (8)

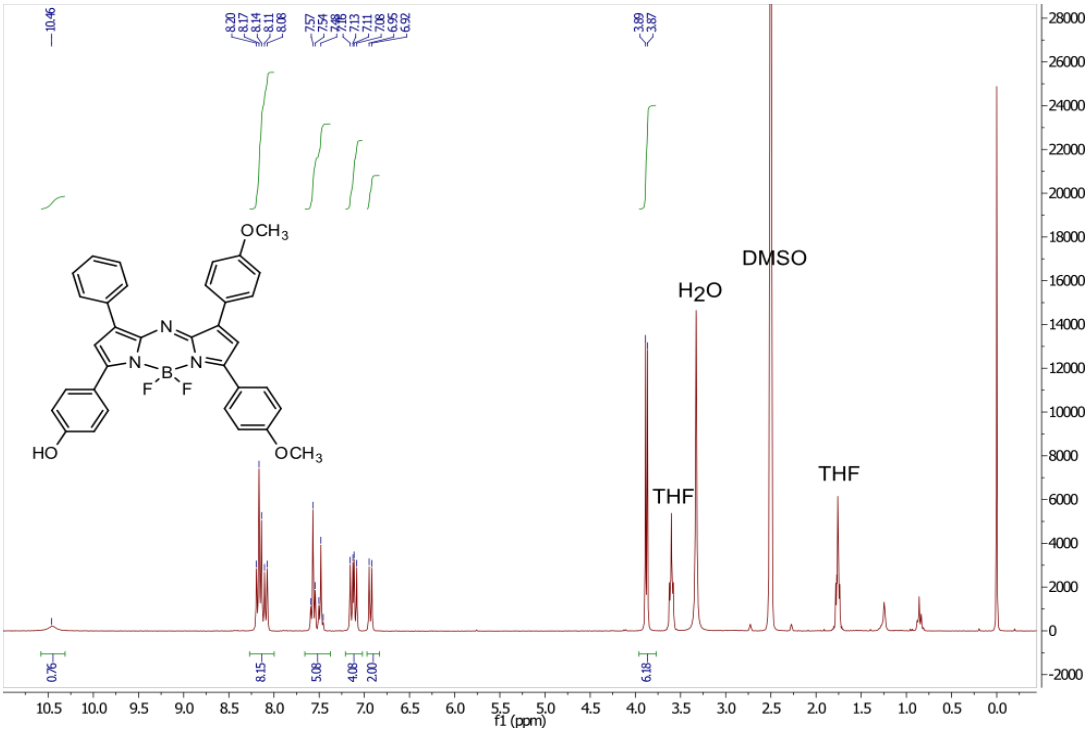

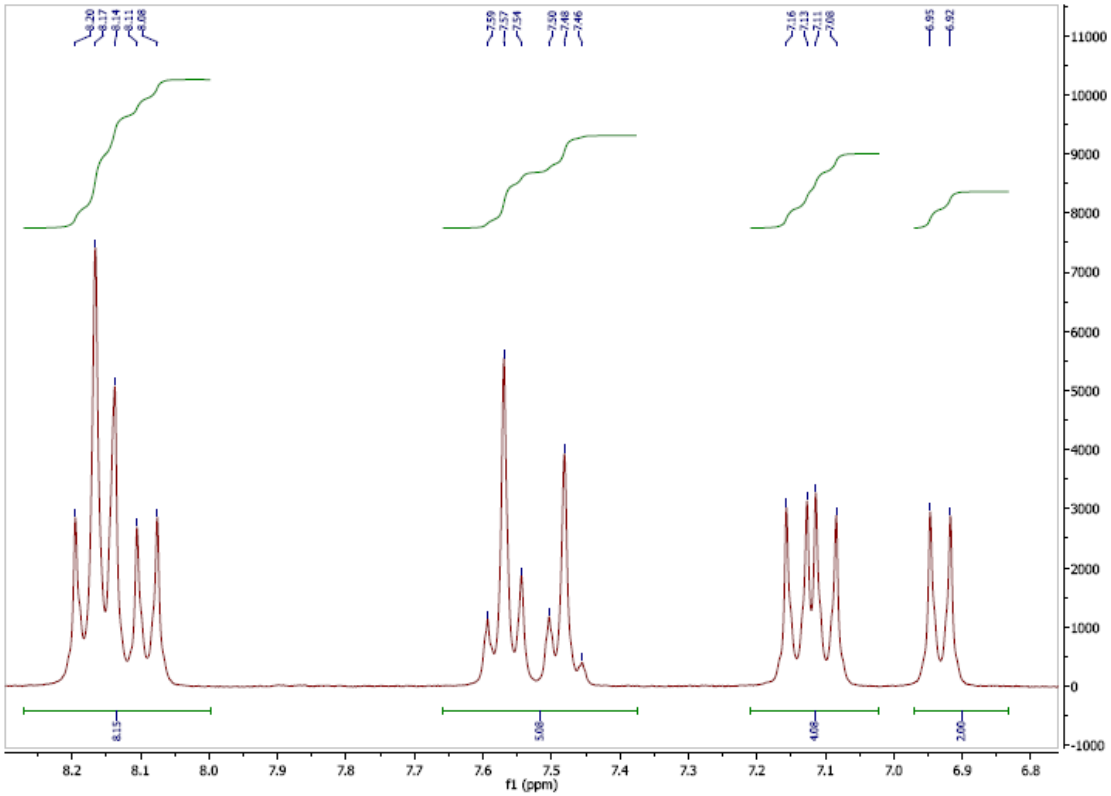

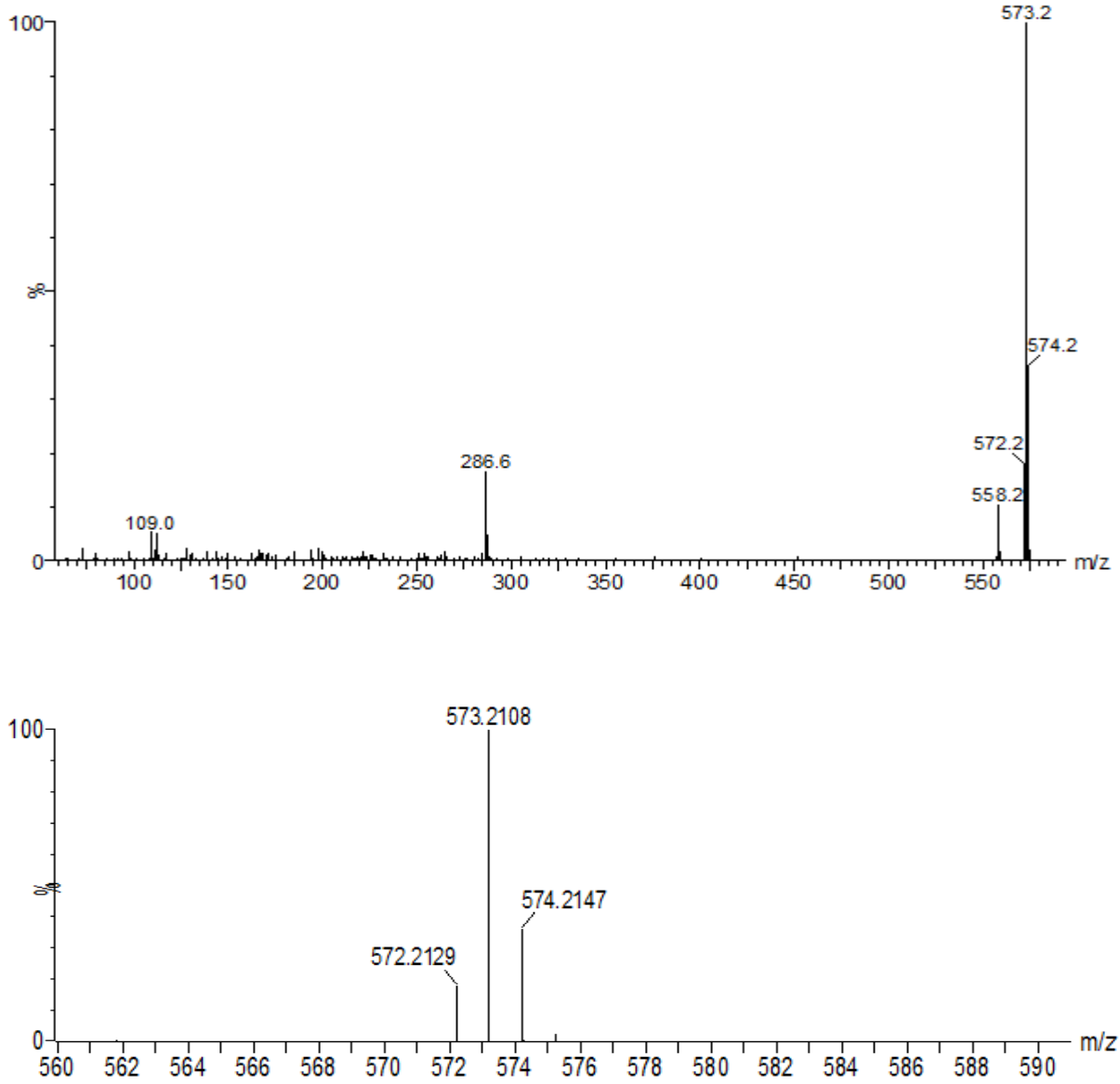

Figure S8. ^{1}H NMR and mass spectra of **8** in DMSO.

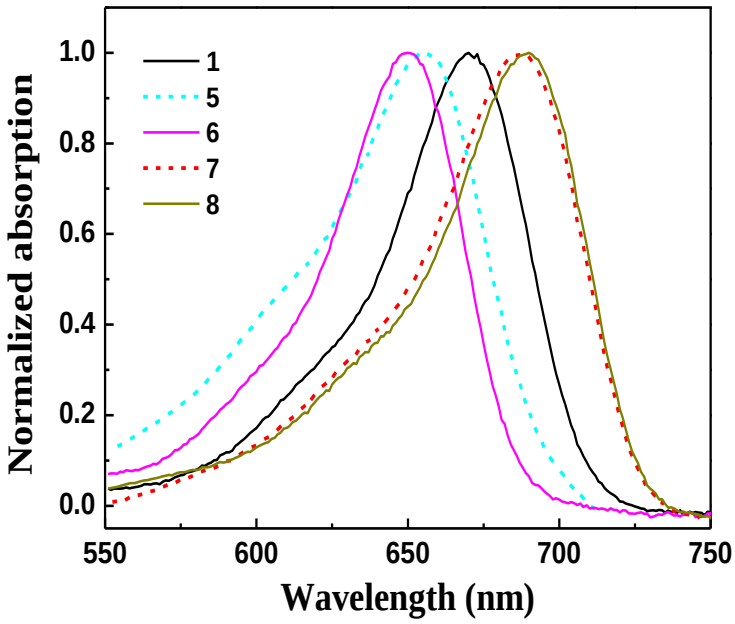

Figure S9. Normalized absorption spectra of pH sensor dye no. **1**, **5**, **6**, **7** and **8** in EtOH/H_2O, IS=0.02 M.

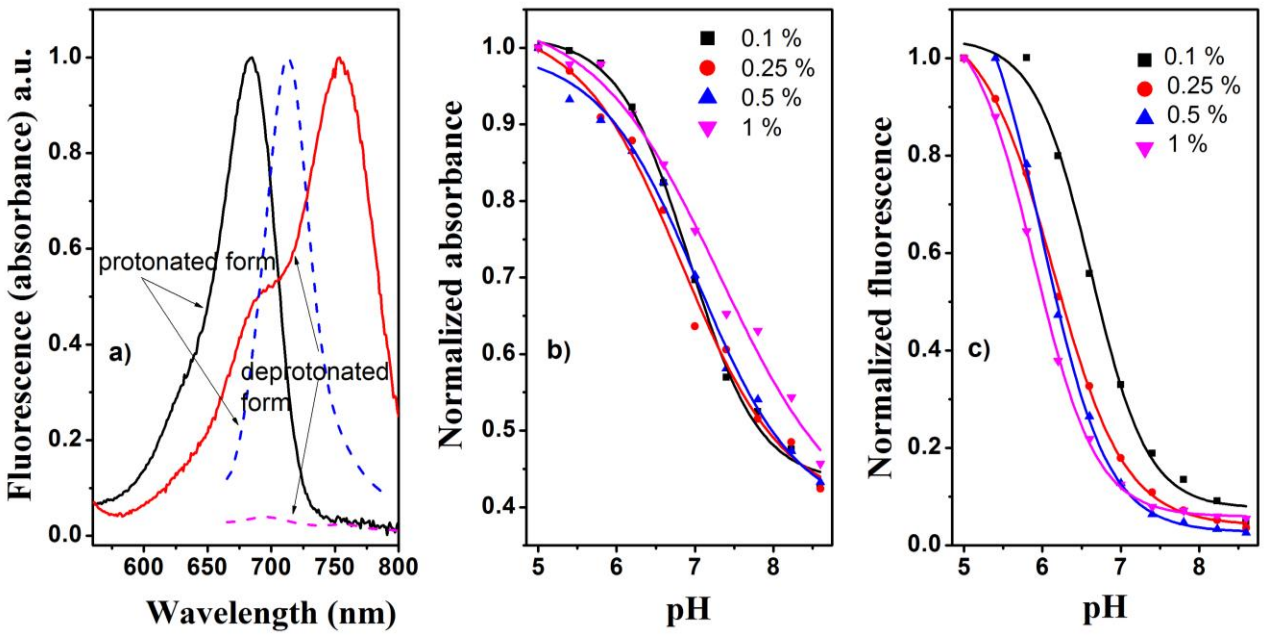

Figure S10. a) Absorbance (solid lines) and fluorescence spectra (dashed lines) of **2** in hydrogel D4 (excited at 650 nm), absorption (b) and fluorescence (c) calibration plots for different concentrations of indicator **2** in hydrogel D4.

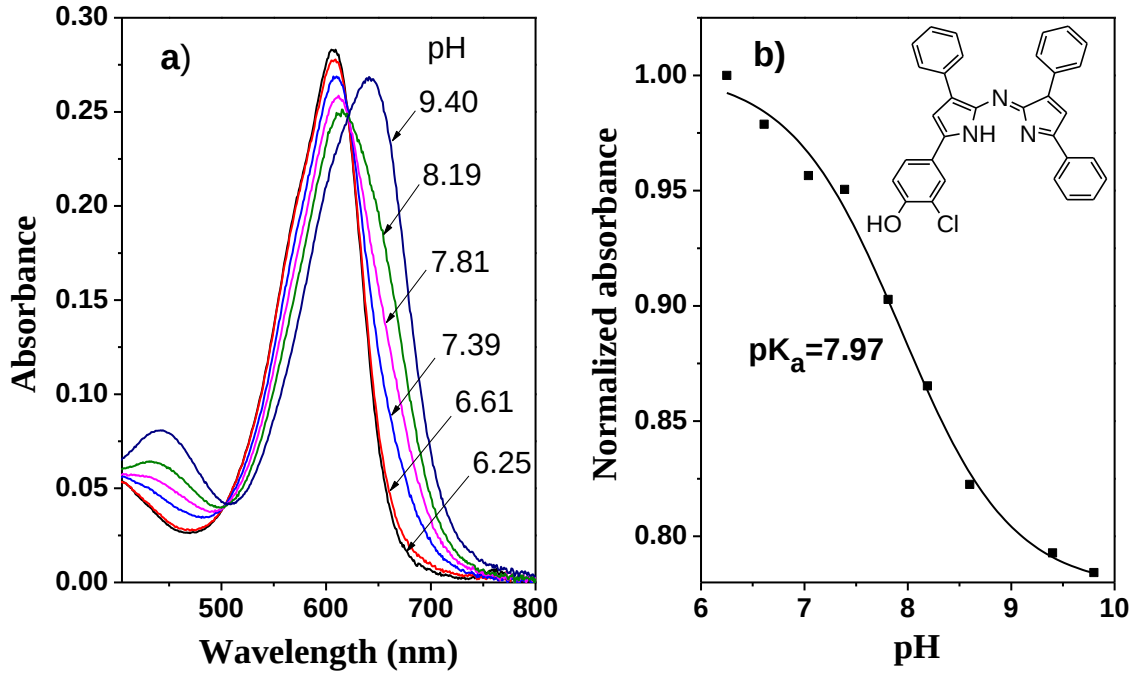

Figure S11. a) pH dependence of absorbance (left) and calibration curve (right) for azadipyrromethene corresponding to the pH indicator **2** in ethanol/aqueous buffer solution.

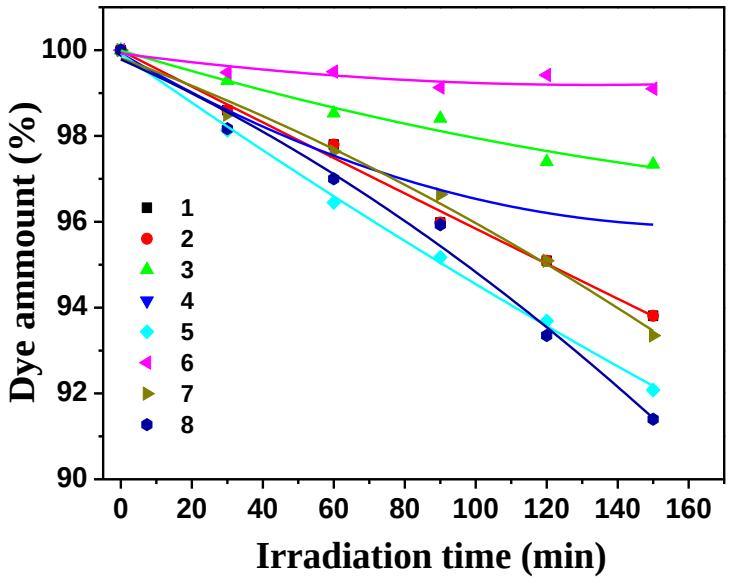

Figure S12. Photobleaching profiles for aza-BODIPY fluorescent pH probes in dimethylformamide determined from the absorption measurements.

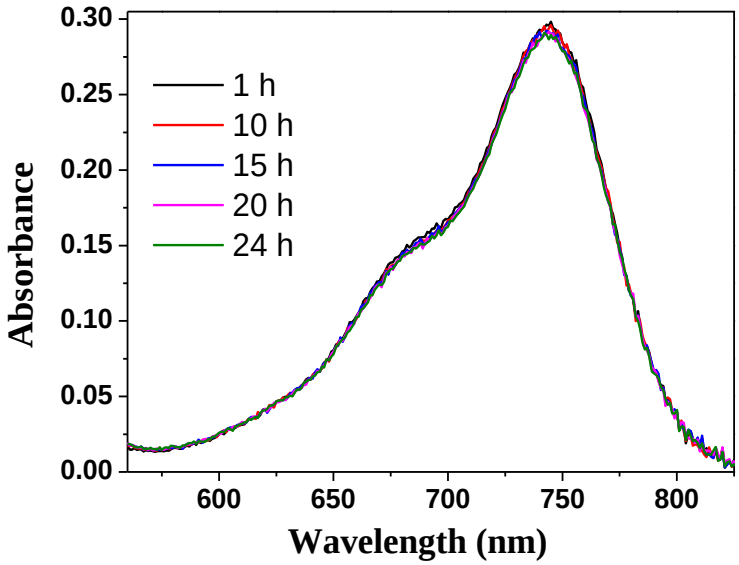

Figure S13. Leaching of aza-BODIPY pH probe **1** determined from the absorption measurements. (pH 10, IS=0.02 M)

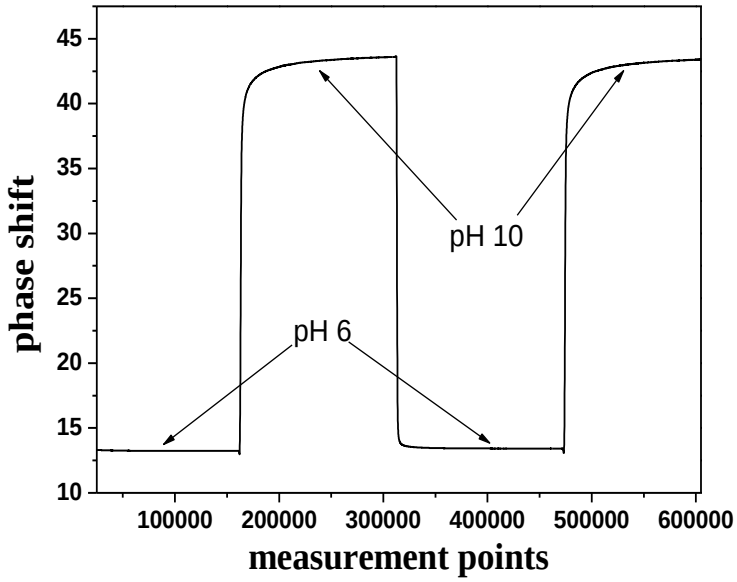

Figure S14. Photobleaching of aza-BODIPY pH probe **1** in microsensor film (100% light intensity, 200 ms integration time, IS=0.02 M).

Chapter 2

NIR optical carbon dioxide sensors based on highly photostable dihydroxy-aza-BODIPY dyes

Susanne Schutting[a], Tijana Jokic[a], Martin Strobl[a], Sergey M. Borisov[a], Dirk de Beer[b] and Ingo Klimant[a]*

[a] Institute of Analytical Chemistry and Food Chemistry, Graz University of Technology, NAWI Graz, Stremayrgasse 9, 8010 Graz, Austria

[b] Max-Planck-Institute of Marine Microbiology, Celsiusstrasse 1, 28359 Bremen, Germany

A new class of pH-sensitive indicator dyes for optical carbon dioxide sensors based on di-OH-aza-BODIPYs is presented. These colorimetric indicators show absorption maxima in the near infrared range (λ_{max} 670–700 nm for the neutral form, λ_{max} 725–760 nm for the mono-anionic form, λ_{max} 785–830 nm for the di-anionic form), high molar absorption coefficients of up to 77 000 M^{-1} cm^{-1} and unmatched photostability. Depending on the electron-withdrawing or electron-donating effect of the substituents the pK_a values are tunable (8.7–10.7). Therefore, optical carbon dioxide sensors based on the presented dyes cover diverse dynamic ranges (0.007–2 kPa; 0.18–20 kPa and 0.2–100 kPa), which enables different applications varying from marine science and environmental monitoring to food packaging. The sensors are outstandingly photostable in the absence and presence of carbon dioxide and can be read out *via* absorption or *via* the luminescence-based ratiometric scheme using the absorption-modulated inner-filter effect. Monitoring of the carbon dioxide production/consumption of a Hebe plant is demonstrated.

3.1 Introduction

Carbon dioxide is one of the most important parameters in many scientific and industrial fields, such as medicine,[1–3] marine science,[4–7] food packaging,[8] bio processing[9,10] or environmental and industrial monitoring.[11] Routine techniques of CO_2 quantification like infrared (IR) spectroscopy, gas chromatography (GC) or the Severinghaus electrode are well established, but suffer from different drawbacks.[12,13] For instance IR spectroscopy is mainly used for gas

samples,[14,15] because of strong interferences of water and the Severinghaus electrode is strongly affected by osmotic effects. Carbon dioxide chemosensors are a promising alternative,[16–23] among which the so-called "plastic type" sensors are the most common ones.[24–31] The core of this type of sensor is a pH-sensitive indicator dye. It is embedded in a polymer matrix together with a base (mainly a quaternary ammonium base) and responds to carbon dioxide by changing its spectral properties according to the degree of protonation. Read-out of these sensors can be carried out *via* absorption or luminescence intensity. In the case of a fluorescent indicator dye, referencing of the fluorescence intensity is necessary to achieve reliable results. This can be realized by using an analyte-insensitive reference dye with different spectral properties from the indicator, either a different emission spectrum or a different luminescence decay time. Although necessary in many cases, the addition of reference materials can cause dramatic ratio changes when photobleaching of one dye (reference or indicator) or both occurs. Therefore, self-referencing indicator dyes are highly desired for ratiometric read-out. However, only a few self-referencing dyes (absorption and fluorescence intensity) have been published so far.[32–38] Optical carbon dioxide sensors are also of great interest in biological applications. Here, indicators with absorption/fluorescence intensity maxima in the infrared (IR) or near-infrared (NIR) region are preferred, because of several advantages, *e.g.* low light scattering, dramatically reduced autofluorescence and availability of low-cost excitation sources and photodetectors. Recently our group has presented pH-sensitive BF_2-chelated tetraarylazadipyrromethene indicators (aza-BODIPYs).[38] This indicator class represents an interesting alternative to the state-of-the-art dyes for biological applications as SNARF indicators[39] or cyanine dyes.[40,41] The aza-BODIPYs showed absorption/fluorescence intensity spectra in the near-infrared region and were highly photostable. Although pH-sensitive, these dyes could not be used for optical carbon dioxide sensors. Here, the formation of the ion pair was irreversible and the indicator could not be protonated anymore, even at 100% CO_2. In this study we present a new class of pH-sensitive indicator dyes suitable for optical carbon dioxide sensors, the di-OH-aza-BODIPYs containing two de-/protonatable hydroxyl groups. It will be shown that the pK_a values of the di-OH-aza-BODIPYs can be tuned by using different substituents with either the electron-withdrawing or the electron-donating effect. Luminescence-based ratiometric read-out can be realized *via* the

absorption-modulated inner-filter effect.[42–45] An application example demonstrating the carbon dioxide production/consumption of a Hebe plant will also be presented.

3.2 Experimental

Materials. Ethyl cellulose (EC49, ethoxyl content 49%), thymol-blue (A.C.S. reagent), *m*-cresol-purple (indicator grade), poly(styrene-*co*-divinylbenzene)microspheres (8 μm mean particle size; PS-microparticles), 3′-chloro-4′-hydroxyacetophenone, ammonium acetate, benzaldehyde, *N*,*N*-diisopropylethylamine (DIPEA), dry dichloromethane, boron trifluoride diethyl etherate, MOPS buffer salt, sodium sulfate (anhydrous) and tetraoctylammonium hydroxide solution (TOAOH, 20% in methanol) were obtained from Sigma-Aldrich (www.sigmaaldrich.com). Deuterated dimethyl sulfoxide (DMSO-d_6) was purchased from Euriso-top (www.eurisotop.com). Perfluorodecalin (98%; *cis* and *trans*), 1-butanol (99%, BuOH) and nitromethane were received from ABCR (Germany, www.abcr.de), Hyflon AD 60 from Solvay (www.solvay.com). Nitrogen, 2% oxygen in nitrogen, 5% carbon dioxide in nitrogen, 0.2% carbon dioxide in nitrogen, argon and carbon dioxide (all of 99.999% purity) were obtained from Air Liquide (Austria, www.airliquide.at). Toluene, ethanol (EtOH), tetrahydrofuran (THF), hydrochloric acid (37%), dichloromethane (DCM) and hexane were purchased from VWR (Austria, www.vwr.com). 3′-methyl-4-hydroxyacetophenone, 4′-butoxyacetophenone and 2-fluoro-4-hydroxyacetophenone were from TCI Europe (www.tcichemicals.com). Poly(ethylene terephthalate) (PET) support Melinex 505 was obtained from Pütz (Germany, www.puetz-folien.com). Potassium chloride, potassium carbonate (pro analysi), potassium hydroxide and silica gel 60 (0.063–0.200 mm) were received from Merck (www.merck.at). Sodium hydroxide, ethyl acetate, the buffer salts CHES, MES and CAPS were purchased from Roth (www.carlroth.com). De-ionized water was filtered *via* a Barnstead NANOpure ultrapure water system. 1-(4-Hydroxyphenyl)-4-nitro-3-phenylbutan-1-one (compound **1b**) was synthesized according to Jokic *et al.*[38] Silanized Egyptian blue particles were prepared according to the literature procedure.[46]

Synthesis of 3,7-bis(4-butoxyphenyl)-5,5-difluoro-1,9-diphenyl-5*H*-4λ^4,5λ^4-dipyrrolo[1,2-*c*:2′,1′-*f*][1,3,5,2]triazaborinine (di-butoxy-complex).

*(E)-1-(4-Butoxyphenyl)-3-phenylprop-2-en-1-one (compound **a**).* 4′-Butoxyacetophenone (1 eq., 2.00 g, 15.5 mmol) was dissolved in absolute ethanol (15 ml). Benzaldehyde (1 eq., 1580 µl, 15.5 mmol) and potassium hydroxide (3 eq., 2.61 g, 46.4 mmol in 5 ml H_2O) were added to the solution and the reaction was stirred at room temperature for 12 h. Then, the reaction solution/suspension was acidified with 0.1 M HCl and the resulting precipitate was collected by filtration and was washed with water three times (3 × 100 ml). The precipitate was dried on a rotary evaporator and was used for the next step without further purification (3.87 g, 89.2%). *1-(4-Butoxyphenyl)-4-nitro-3-phenylbutan-1-one (compound **b**).* A solution of (*E*)-1-(4-butoxyphenyl)-3-phenylprop-2-en-1-one (1 eq., 3.87 g, 13.8 mmol), nitromethane (20 eq., 14.8 ml, 276 mmol) and KOH (0.3 eq., 0.232 g, 4.1 mmol) in 30 ml of absolute ethanol was heated under reflux for 12 h. After cooling to room temperature the solvent was removed on a rotary evaporator. The resulting oily residue was acidified with 0.1 M HCl and was partitioned with ethyl acetate and water in a separating funnel. The organic layer was separated, dried over sodium sulfate and the solvent was removed under reduced pressure (4.035 g, 85.7%). *(5Z)-5-(4-Butoxyphenyl)-N-(5-(4-butoxyphenyl)-3-phenyl-2H-pyrrol-2-ylidene)-3-phenyl-1H-pyrrol-2-amine (**c**).* Compound **b** (1 eq., 2.5 g, 7.33 mmol) and ammonium acetate (35 eq., 19.77 g, 256 mmol) were dissolved in 50 ml of 1-butanol and the reaction solution was heated under reflux for 24 h. The reaction was cooled to room temperature and the solvent was removed under reduced pressure. Then, the solid was redissolved in DCM and washed with water three times (3 × 100 ml). The crude solid was purified by column chromatography on silica gel, eluting with DCM/cyclohexane (1 : 1 v/v). The product was recrystallized from a hexane–THF mixture to give metallic blue crystals (983 mg, 45.4%). ^{1}H NMR (300 MHz, $CDCl_3$) δ 8.06 (d, J = 7.1 Hz, 4H), 7.88–7.83 (m, 4H), 7.44–7.31 (m, 6H), 7.11 (s, 2H), 7.02 (d, J = 8.8 Hz, 4H), 4.06 (t, J = 6.5 Hz, 4H), 1.91–1.72 (q, J = 8.5 Hz, 4H), 1.6–1.48 (m, 4H), 1.01 (t, J = 7.4 Hz, 6H). *3,7-Bis(4-butoxyphenyl)-5,5-difluoro-1,9-diphenyl-5H-4λ^4,5λ^4-dipyrrolo[1,2-c:2′,1′-f][1,3,5,2]triazaborinine.* Compound **c** (1 eq., 300 mg, 0.51 mmol) was dissolved in 200 ml of dry DCM. *N*,*N*-Diisopropylethylamine (DIPEA, 10 eq., 839 µl, 5.06 mmol) and boron trifluoride diethyl etherate (15 eq., 953 µl, 7.58 mmol) were added and the reaction solution was stirred

under nitrogen for 12 h. The green solution was washed with water three times (3 × 200 ml) and dried over anhydrous sodium sulfate. The crude product was purified by column chromatography on silica gel, eluting with DCM/cyclohexane (1 : 1 v/v). The product was recrystallized from a hexane–THF mixture to give metallic red needles (179 mg, 55.2%). ^{1}H NMR (300 MHz, $CDCl_3$) δ 8.09–8.05 (m, 8H), 7.49–7.38 (m, 6H), 7.04–6.98 (m, 6H), 4.07–4.02 (t, J = 6.4 Hz, 4H), 1.58–1.45 (q, J = 14.4 Hz, 4H), 1.62–1.42 (m, 4H), 1.02–0.97 (t, J = 7.4 Hz, 6H). Electron impact-direct insertion-time of flight (DI-EI-TOF):m/z of $[M]^+$ was found to be 641.3007, calc. 641.3032.

Synthesis of 4,4′-(5,5-difluoro-1,9-diphenyl-5*H*-4λ^4,5λ^4-dipyrrolo[1,2-*c*:2′,1′-*f*][1,3,5,2]triazaborinine-3,7-diyl)bis(2-chlorophenol) (di-Cl-di-OH-complex).

*1-(3-Chloro-4-hydroxyphenyl)-3-phenylpropenone (compound **1a**).* 3′-Chloro-4′-hydroxyacetophenone (1 eq., 2 g, 11.7 mmol) and benzaldehyde (1 eq., 1.24 g, 11.7 mmol) were dissolved in 10 ml of ethanol absolute. 10 ml of aqueous potassium hydroxide solution (3 eq., 1.96 g, 35.1 mmol) were added dropwise. The resulting solution was stirred for 8–12 h, during which the product precipitated as a potassium salt. The solution/suspension was poured into 10 ml of hydrochloric acid (1 M) and further concentrated hydrochloric acid was added until the solution became acidic. The obtained yellow solid was washed with water and used for further synthesis without purification (2.33 g, 77%).

*1-(3-Chloro-4-hydroxyphenyl)-4-nitro-3-phenylbutan-1-one (compound **1b**).* A solution of compound **1a** (1 eq., 2 g, 7.7 mmol), nitromethane (20 eq., 8.35 ml, 154.7 mmol) and potassium hydroxide (1.2 eq., 0.52 g, 9.28 mmol) in 10 ml of ethanol was heated at 60 °C under reflux for 12 h. After cooling to room temperature, the solvent was removed *in vacuo* and the oily residue obtained was acidified with hydrochloric acid (4 M) and partitioned between ethyl acetate (50 ml) and de-ionized water (50 ml). The organic layer was separated, dried over anhydrous sodium sulfate and evaporated under reduced pressure. The obtained product was used for further synthesis without purification (2.4 g,97.2%).

*[5-(3-Chloro-4-hydroxyphenyl)-3-phenyl-1H-pyrrol-2-yl]-[5-(3-chloro-4-hydroxyphenyl)-3-phenylpyrrol-2-ylidene]amine (compound **1c**).* Compound **1b** (1 eq., 2.02 g, 8.76 mmol) and

ammonium acetate (35 eq., 19.03 g, 307 mmol) in 50 ml of 1-butanol were heated under reflux for 24 h. The reaction was cooled to room temperature, the salt was removed by extraction with de-ionized water/DCM and the product was purified by column chromatography on silica gel, eluting with 5% ethyl acetate/DCM (after eluting impurities with hexane, 20% DCM/hexane, 1% ethyl acetate/DCM and 2% ethyl acetate/DCM) to yield **1c** as a blue-black solid. The product was recrystallized from a hexane–THF mixture to give metallic green crystals (0.097 g, 5.77%). ^{1}H NMR (300 MHz, DMSO-d_6) δ 8.09 (d, J = 7.6 Hz, 6H), 7.90 (d, J = 8.5 Hz, 2H), 7.62 (s, 2H), 7.54–7.32 (m, 6H), 7.19 (d, J = 8.5 Hz, 2H). EI-DI-TOF: m/z $[MH]^+$ found 549.1007, calc. 549.1011.

4,4′-(5,5-Difluoro-1,9-diphenyl-5H-4λ^4,5λ^4-dipyrrolo[1,2-c:2′,1′-f][1,3,5,2]triazaborinine-3,7-diyl)bis(2-chlorophenol) (di-Cl-di-OH-complex). Compound **1c** (0.017 g, 0.07 mmol) was dissolved in 50 ml of dry DCM, treated with DIPEA (10 eq., 0.053 ml, 0.32 mmol) and boron trifluoride diethyletherate (15 eq., 0.061 ml, 0.48 mmol) and stirred under argon for 24 h. Purification was carried out *via* column chromatography on silica gel, eluting with 2% ethanol/DCM (after eluting impurities with DCM). Recrystallization from hexane–THF gave the final product di-Cl-di-OH-complex as a metallic red solid (0.008 g, 44%). ^{1}H NMR (300 MHz, DMSO-d_6) δ 8.29 (s, 2H), 8.16 (d, J = 7.0 Hz, 4H), 8.03 (d, J = 8.7 Hz, 2H), 7.65 (s, 2H), 7.60–7.41 (m, 6H), 7.13 (d, J = 8.7 Hz, 2H). EI-DI-TOF: $m/z$$[MH]^+$ found 597.0968, calc. 597.0999.

Synthesis of 4,4′-(5,5-difluoro-1,9-diphenyl-5*H*-4λ^4,5λ^4-dipyrrolo[1,2-*c*:2′,1′-*f*][1,3,5,2]triazaborinine-3,7-diyl)bis(3-fluorophenol) (di-F-di-OH-complex). The synthesis was performed analogously to that of the di-Cl-di-OH-complex, but starting from 2′-fluoro-4′-hydroxyacetophenone (728 mg). Steps 1 and 2 yielded 1.033 g (90.2%) and 1.28 g (99.4%) of the crude product, respectively. After synthesis step 3, the crude product was purified by column chromatography on silica gel, eluting with 4% THF/DCM to yield [5-(2-fluoro-4-hydroxyphenyl)-3-phenyl-1*H*-pyrrol-2-yl]-[5-(2-fluoro-4-hydroxyphenyl)-3-phenylpyrrol-2-ylidene]amine **2c** as a blue-black solid. The product was recrystallized from a hexane–THF mixture to give metallic green crystals (0.23 g, 20.9%).^{1}H NMR (300 MHz, DMSO-d_6) δ 8.04–8.06 (d, J = 7.0 Hz, 6H), 7.35–7.47 (m, 8H), 6.78–6.86 (m, 4H). DI-EI-TOF: m/z of $[M]^+$ found 517.1626, calc. 517.1602.

4,4′-(5,5-Difluoro-1,9-diphenyl-5H-4λ⁴,5λ⁴-dipyrrolo[1,2-c:2′,1′-f][1,3,5,2]triazaborinine-3,7-diyl)bis(3-fluorophenol) (di-F-di-OH-complex). 4,4′-(5,5-Difluoro-1,9-diphenyl-5*H*-4λ⁴,5λ⁴-dipyrrolo[1,2-*c*:2′,1′-*f*][1,3,5,2]triazaborinine-3,7-diyl)bis(3-fluorophenol) (di-F-di-OH-complex) was synthesized using the same procedure. Purification was carried out *via* column chromatography on silica gel, eluting with 4% THF/DCM. Recrystallization from hexane–THF gave the final product di-F-di-OH-complex as a metallic red solid (0.044 g, 19.6%). ^{1}H NMR (300 MHz, DMSO-d_6) δ 8.12 (d, J = 7.0 Hz, 4H), 7.82 (t, J = 8.7 Hz, 2H), 7.56–7.48 (q, J = 9.4, 7.9 Hz, 6H), 7.31 (d, J = 3.4 Hz, 2H), 6.77 (d, J = 10.7 Hz, 4H). DI-EI-TOF: m/z of $[M]^+$ found 565.1615, calc. 565.1591.

Synthesis of 4,4′-(5,5-difluoro-1,9-diphenyl-5*H*-4λ⁴,5λ⁴-dipyrrolo[1,2-*c*:2′,1′-*f*][1,3,5,2]triazaborinine-3,7-diyl)diphenol (di-OH-complex). Compound **3a** 1-(4-hydroxyphenyl)-3-phenylpropenone was commercially available. Further synthesis steps were performed analogously to the synthesis steps of the di-Cl-di-OH-complex. The synthesis of compound **3b** gave 2.06 g (80%) of the crude product, starting from 2.02 g of 4′-hydroxychalcone. The crude **3c** was purified by column chromatography on silica gel, eluting with 4% THF/DCM to yield [5-(4-hydroxyphenyl)-3-phenyl-1*H*-pyrrol-2-yl]-[5-(4-hydroxyphenyl)-3-phenylpyrrol-2-ylidene]amine as a blue-black solid. The product was recrystallized from a hexane–THF mixture to give metallic green crystals (0.41 g, 23.5%). ^{1}H NMR (300 MHz, DMSO-d_6), δ 8.09 (d, J = 7.3 Hz, 4H), 7.93 (d, J = 8.6 Hz, 4H), 7.53 (s, 2H), 7.42 (m, 6H), 7.01 (d, J = 8.6 Hz, 4H). EI-DI-TOF: m/z $[MH]^+$ found 481.1773, calc. 481.179. *Purification of 4,4′-(5,5-difluoro-1,9-diphenyl-5H-4λ⁴,5λ⁴-dipyrrolo[1,2-c:2′,1′-f][1,3,5,2]triazaborinine-3,7-diyl)diphenol.* Purification of 4,4′-(5,5-difluoro-1,9-diphenyl-5*H*-4λ⁴,5λ⁴-dipyrrolo[1,2-*c*:2′,1′-*f*][1,3,5,2]triazaborinine-3,7-diyl)diphenol was carried out *via* column chromatography on silica gel, eluting with DCM/ethyl acetate (4 : 1). Recrystallization from hexane–THF gave the final product di-OH-complex as a metallic red solid (0.26 g, 57.8%). ^{1}H NMR (300 MHz, DMSO-d_6) δ 8.13 (dd, J = 18.6, 8.0 Hz, 8H), 7.65–7.39 (m, 8H), 6.95 (d, J = 8.8 Hz, 4H). EI-DI-TOF: m/z $[MH]^+$found 529.1771, calc. 529.1779.

Synthesis of 4,4`-(5,5-difluoro-1,9-diphenyl-5H-4λ$^4$,5λ$^4$-dipyrrolo-[1,2-c:2`,1`-f][1,3,5,2]triazaborinine-3,7-diyl)bis(2-methylphenol) (di-CH_3-di-OH-complex).

The synthesis was carried out analogously to that of the di-Cl-di-OH-complex, starting from 3′-methyl-4′-hydroxyacetophenone (1.88 g). Steps 1 and 2 yielded 2.77 g (93%) and 1.84 g (53%) of the crude product, respectively. After synthesis step 3, the crude product was purified by column chromatography on silica gel, eluting with 5% ethyl acetate/DCM (after eluting impurities with hexane/DCM 1 : 1, DCM) to yield [5-(3-methyl-4-hydroxyphenyl)-3-phenyl-1*H*-pyrrol-2-yl]-[5-(3-methyl-4-hydroxyphenyl)-3-phenylpyrrol-2-ylidene]amine **4c** as a blue-black solid. The product was recrystallized from a hexane–THF mixture to give metallic green crystals (0.091 g, 5.8%). ^{1}H NMR (300 MHz, DMSO-d_6) δ 8.10 (d, J = 7.3 Hz, 4H), 7.91–7.75 (m, 4H), 7.57–7.33 (m, 8H), 7.00 (d, J = 8.4 Hz, 2H), 2.29 (s, 6H). EI-DI-TOF: m/z $[MH]^+$ found 509.2086, calc. 509.2103.

Purification of 4,4′-(5,5-difluoro-1,9-diphenyl-5H-4λ^4,5λ^4-dipyrrolo[1,2-c:2′,1′-f][1,3,5,2]triazaborinine-3,7-diyl)bis(2-methylphenol). Purification of 4,4′-(5,5-difluoro-1,9-diphenyl-5*H*-4λ^4,5λ^4-dipyrrolo[1,2-*c*:2′,1′-*f*][1,3,5,2]triazaborinine-3,7-diyl)bis(2-methylphenol) was carried out *via* column chromatography on silica gel, eluting with 5% ethyl acetate/DCM (after eluting impurities with DCM, 1% ethyl acetate/DCM and 2% ethyl acetate/DCM). Recrystallization from hexane–THF gave the final product di-CH_3-di-OH-complex as a metallic red solid (0.04 g, 40%). ^{1}H NMR (300 MHz, DMSO-d_6) δ 8.16 (d, J = 7.2 Hz, 4H), 8.08–7.90 (m, 4H), 7.52 (m, 8H), 6.95 (d, J = 8.5 Hz, 2H), 2.22 (s, 6H). EI-DI-TOF: m/z $[MH]^+$ found 557.2082, calc. 557.2092.

Staining of PS-microparticles

0.50 g of PS-particles were dispersed in a solution of 5 mg of (1% w/w in respect to the PS-particles) the di-butoxy-complex in 10 ml of tetrahydrofuran (THF) and stirred for 1.5 h. Then 8 ml of de-ionized water were added dropwise. After 10 min of stirring the dispersion was transferred rapidly into a beaker with 50 ml of de-ionized water. The dispersion was again stirred for 10 min. Then the particles were filtered through a cellulose filter and rewashed with 20 ml of ethanol. Afterwards the particles were transferred into a milling cup and were overlaid with a

mixture of ethanol/de-ionized water (1 : 1) to reduce friction and to enhance heat dissipation during grinding in the planet mill. The particles were washed with ethanol and dried in the oven at 70 °C.

Sensor preparation

Absorption: a "cocktail" containing 100 mg of ethyl cellulose and 1 mg of dye (1% w/w with respect to the polymer) dissolved in a toluene : ethanol mixture (6 : 4 v/v, 1.9 g) was purged with carbon dioxide. Afterwards 100 µl of tetraoctylammonium hydroxide solution (20% w/w TOAOH in MeOH) were added. The "cocktail" was knife-coated on a dust-free PET support. A sensing film of ~7 µm thickness was obtained after evaporation of the solvent. For luminescence-based measurements a second layer was added to the absorption-based sensing foils. To prepare the "cocktail" for the second layer, 0.180 g of Hyflon AD 60 were dissolved in 2.820 g of perfluorodecalin, which was washed prior to use with 1 mol l^{-1} potassium carbonate solution. Then 0.360 g of Egyptian blue powder (200% w/w with respect to the polymer) and 0.054 g of stained PS-particles (30% w/w with respect to the polymer) were dispersed homogeneously in the Hyflon solution. The thickness of this layer after evaporation of the solvent was estimated to be ~4.5 µm.

Methods

^{1}H NMR spectra were recorded on a 300 MHz instrument (Bruker) in DMSO-d_6 with TMS as standard. Absorption spectra were recorded on a Cary 50 UV-Vis spectrophotometer (Varian). The determination of the molar absorption coefficients was carried out as an average of three independent measurements. Fluorescence spectra were recorded on a Fluorolog3 fluorescence spectrometer (Horiba) equipped with a NIR-sensitive photomultiplier R2658 from Hamamatsu (300–1050 nm). Photobleaching experiments were performed by irradiating the sensor foils in a glass cuvette with the light of a high-power 10 W LED array (λ_{max} 458 nm, 3 LEDs, www.LED-TECH.de) operated at 6 W input power. A lens (Edmund Optics) was used to focus the light of the LED array on the glass cuvette (photon flux: ~3900 µmol s^{-1} m^{-2} as determined using a Li-250A light meter from Li-COR). The photodegradation profiles were obtained by monitoring the absorption spectra of a sensor foil based on the respective dye. The cuvette was flushed with either carbon dioxide gas for the mono-anionic form, or with nitrogen for the di-anionic form and

sealed. Thymol-blue and *m*-cresol-purple were used for comparison. In the case of the anionic form of thymol-blue, *m*-cresol-purple, the di-OH-complex and the di-CH_3-di-OH-complex (di-anionic forms) sodium hydroxide was placed at the bottom of the cuvette to capture carbon dioxide traces. Gas calibration mixtures were obtained using a gas mixing device from MKS (www.mksinst.com). The gas mixture was humidified to about 85% relative humidity, using silica gel soaked with a saturated potassium chloride solution, prior to entering the calibration chamber. Temperature was controlled by a cryostat ThermoHaake DC50. Dyed particles were filtered through cellulose filters type 113A from Roth (www.carlroth.com). Particle milling was carried out using an 80 ml milling cup, zirconia spheres (Ø 5 mm) and a Pulverisette 6 planet mill from Fritsch (www.fritsch.de). For the determination of the pK_a values titration curves in aqueous buffer/ethanol mixtures (1 : 1) were measured and the average value of the point of inflection obtained was used. For the production/consumption measurements of carbon dioxide two Firesting-Mini devices and an oxygen trace sensor from PyroScience (www.pyro-science.com) were used. Illumination of the sample was performed using 3 commercially available halogen bulb lamps with an averaged photon flux of ~217 µmol s^{-1} m^{-2} per lamp. The plant was positioned in a glass desiccator, which was flushed with a gas mixture of 2% oxygen in nitrogen.

3.3 Results and Discussion

Synthesis

As reported by Jokic *et al.*[38] there are two ways for the preparation of azadipyrromethenes to obtain either asymmetrical[47] or symmetrical[48] chromophores. The previously published asymmetrical dyes bearing one hydroxyl group were proved to be promising pH indicators.[38] Unfortunately, they were found to be unsuitable for optical carbon dioxide sensors. The ion pair built between the hydroxyl group and the tetraoctylammonium base was comparatively strong. Even after exposure of the sensors to pure carbon dioxide, the amount of CO_2 was not enough to achieve re-protonation of the indicators and only after exposure to strong acid vapors (*e.g.* hydrochloric acid) the indicators were irreversibly re-protonatable. Dissociation of both hydroxyl groups in symmetrical azadipyrromethenes was expected to be more difficult compared to the mono-hydroxy derivatives since two ion pairs with bulky cations would be built

upon deprotonation. Therefore, this new class of pH indicators potentially suitable for CO_2 sensing was investigated. The starting point of our synthesis was diaryl-α,β-unsaturated ketones (chalcones) either commercially available or readily made by an aldol condensation of the corresponding aldehyde and acetophenone (Scheme 1). The Michael addition of nitromethane to the chalcones, using KOH as a base, yields 1,3-diaryl-4-nitrobutan-1-ones in essentially quantitative yields. Their condensation with ammonium acetate in refluxing butanol gave azadipyrromethenes. Finally, the azadipyrromethenes were converted to the corresponding BF_2 chelates *via* reaction with BF_2-etherate using diisopropylethylamine as a base at room temperature for 24 h, giving yields ranging from 20 to 70%.

Scheme 1. 4-step-synthesis scheme for the di-OH-aza-BODIPY-complexes.

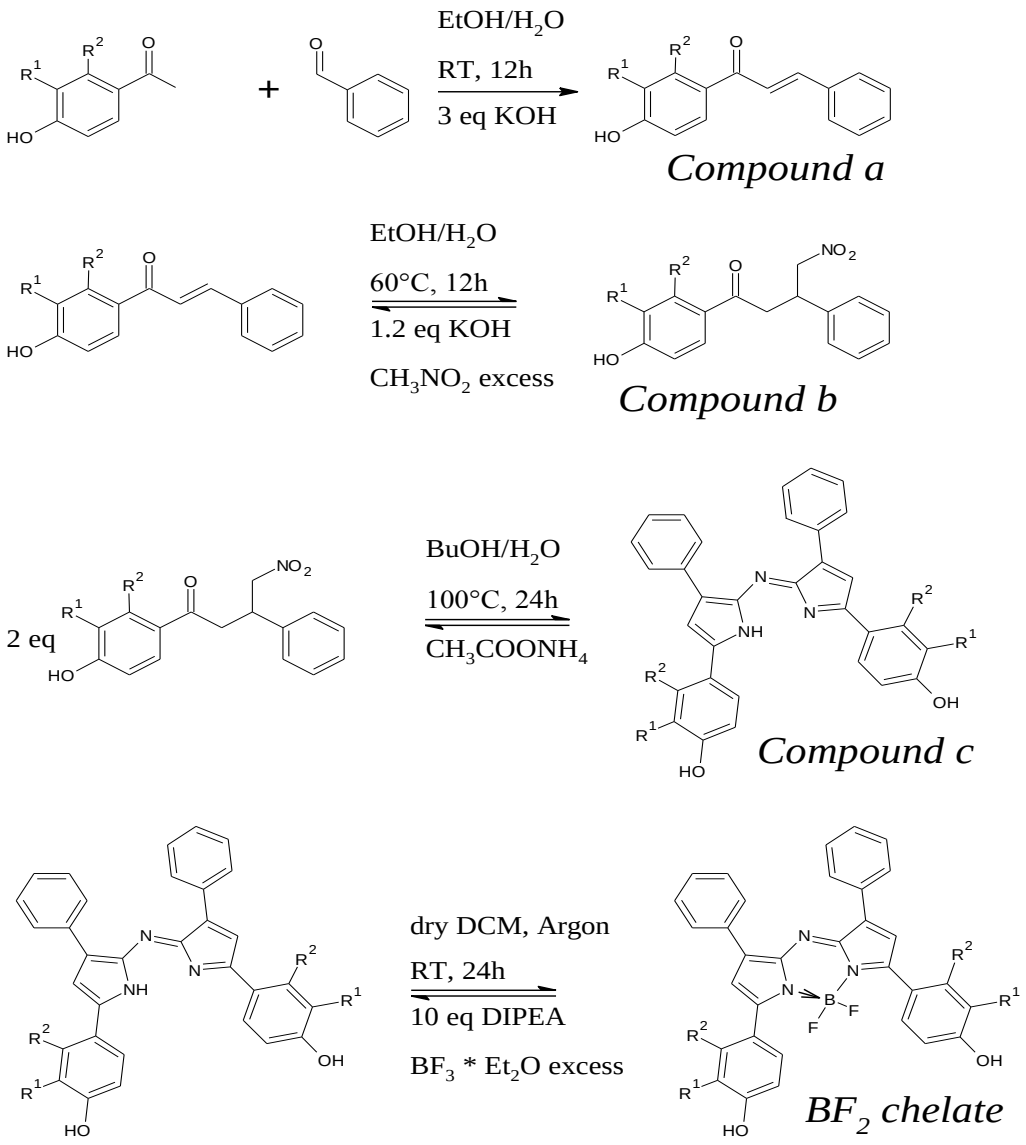

di-OH-complex: $R^1 = R^2 = H$

di-F-di-OH-complex: $R^1 = H$, $R^2 = F$

di-Cl-di-OH-complex: $R^1 = Cl$, $R^2 = H$

di-CH_3-di-OH-complex: $R^1 = CH_3$, $R^2 = H$

Photophysical properties

Dissolved in an ethanol/aqueous buffer mixture (1 : 1) all di-OH-aza-BODIPY dyes showed absorption spectra corresponding to the two protonation steps of the hydroxyl groups (Fig. 1). The neutral forms showed maxima at 670–700 nm and the mono-anionic forms at 725–760 nm. The di-anionic forms were again bathochromically shifted for approximately 60 nm (λ_{max} 785–830 nm). Generally, the di-CH_3-di-OH-complex bearing electron-donating methyl groups showed absorption maxima shifted to higher wavelengths compared to the non-substituted di-OH-complex (Table 1). In contrast, complexes bearing electron-withdrawing groups displayed absorption maxima at shorter wavelengths.

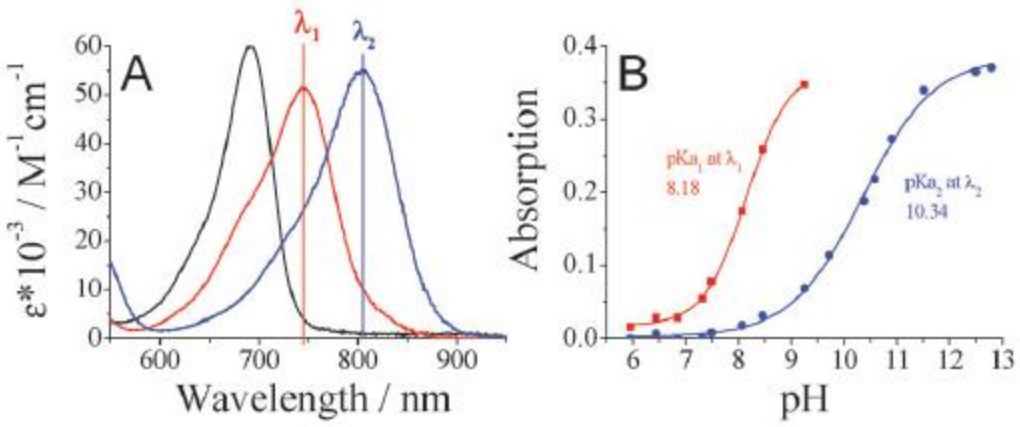

Fig. 1 (A) Absorption spectra of the neutral (black line, pH 6.4), the mono-anionic (red line, pH 9.3) and the di-anionic (blue line, pH 12.8) forms of the di-OH-complex dissolved in the ethanol/aqueous buffer mixture (1:1) at 25°C and (B) the titration curves for p*K*a$_1$ determined at 745 nm (red) and pKa$_2$ at 805 nm (blue), respectively.

An overview of the spectroscopic properties of the presented dyes is given in Table 1. Molar absorption coefficients are rather high: 55 000–77 000 M^{-1} cm^{-1}. pK_a determination was carried out in a mixture of ethanol/aqueous buffer solution (1 : 1). For all di-OH-aza-BODIPY dyes two protonation steps can be observed (Table 1). Here, the complex with electron-donating methyl groups in the *ortho*-position to the hydroxyl groups showed the highest pK_a values, followed by the non-substituted di-OH-complex. Electron-withdrawing chlorine atoms located in the

proximity of the hydroxyl groups (*ortho*-position) have the strongest impact on the pK_a values, whereas the electron-withdrawing effect of fluorine atoms in the *meta*-position is significantly lower.

Table 1. Absorption maxima, molar absorption coefficients (ε) and pK_a values of the di-OH-aza-BODIPY-complexes dissolved in ethanol/aqueous buffer mixture (1:1), as well as the absorption maxima for optical CO_2 sensors (EC49) based on the respective aza-BODIPY-complexes.

	neutral form		**mono-anionic form**			**di-anionic form**	
	λmax (ε*10^{-3}) EtOH/aqu. buffer 1:1 [nm ($M^{-1}cm^{-1}$)]	**pKa$_1$** EtOH/ aqu. buffer 1:1	**λmax (ε*10^{-3})** EtOH/aqu. buffer 1:1 [nm ($M^{-1}cm^{-1}$)]	**λmax** EC49 [nm]	**pKa$_2$** EtOH/ aqu. buffer 1:1	**λmax (ε*10^{-3})** EtOH/aqu. buffer 1:1 [nm ($M^{-1}cm^{-1}$)]	**λmax** EC49 [nm]
di-CH_3-di-OH	701 (76.8)	8.40	762 (65.5)	775	10.68	827 (70.7)	908
di-OH	692 (59.9)	8.18	745 (51.3)	772	10.34	805 (55.2)	876
di-F-di-OH	669 (51.1)	7.32	725 (46.7)	760	9.35	784 (52.8)	860
di-Cl-di-OH	688 (61.4)	6.52	752 (52.6)	781	8.72	808 (57.9)	890

Carbon dioxide sensors

The pH-sensitive di-OH-aza-BODIPY dyes were embedded in an ethyl cellulose matrix (EC49) along with tetraoctylammonium hydroxide as a base to obtain optical carbon dioxide sensors. Clearly, the sensors showed well-observable spectral changes in the near infrared (NIR) range according to the protonation of the di-anionic form giving the mono-anionic form (Fig. 2). The neutral forms of the di-OH-complexes showed slight fluorescence in solution, and the sensors based on the indicators did not show detectable fluorescence, neither for the mono-anionic nor for the di-anionic form. Compared to the measurements in solution the CO_2 sensors based on the di-OH-aza-BODIPY dyes showed significantly bathochromically shifted absorption spectra with

maxima at 760–780 nm for their mono-anionic forms and maxima at 860–910 nm for their di-anionic forms. Generally, a similar trend for the absorption maxima of the CO_2 sensors based on the respective complexes was observed (Table 1). Here, the shift between the mono-anionic and the di-anionic form was enlarged to over 100 nm. This fact is advantageous for optical sensors, because peak separation becomes easier.

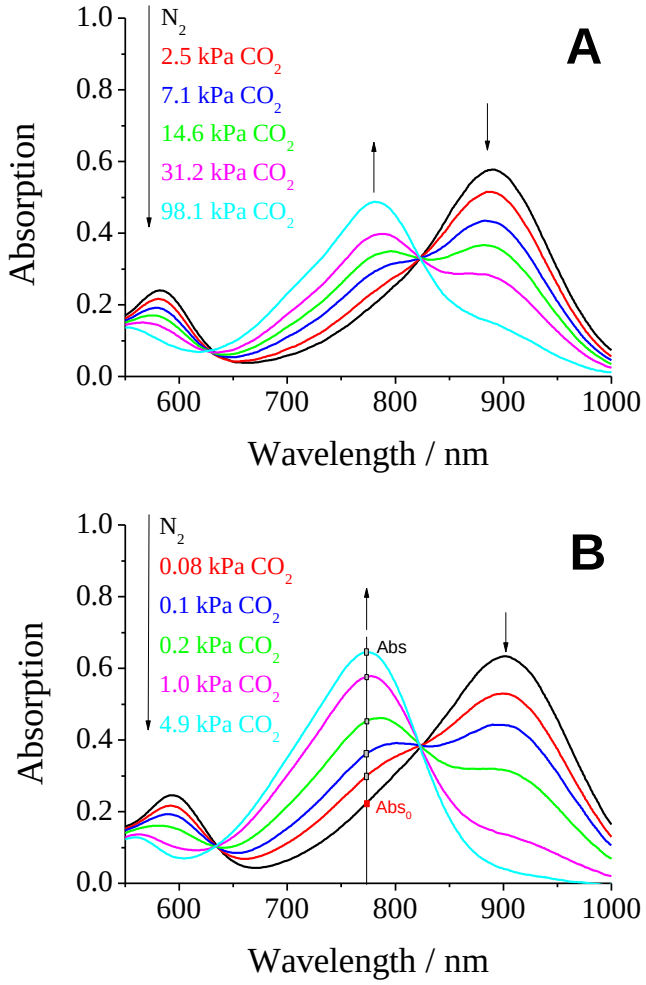

Fig. 2 Absorption spectra of optical carbon dioxide sensors based on (A) the di-Cl-di-OH-complex and (B) the di-CH_3-di-OH-complex in EC49 (base: TOAOH) at 25 °C at various pCO_2 values.

Despite the fact that all di-OH-aza-BODIPY dyes showed two protonation steps in aqueous solution, only one protonation step was observed in optical sensors based on these indicators. In

fact, in the absence of carbon dioxide both hydroxyl groups build ion pairs with the quaternary ammonium base and the spectra of the di-anionic forms are observable. The mono-anionic form is built in the presence of carbon dioxide and is stable even at 100% CO_2. Spectra of the neutral forms are not observable anymore (Fig. 2). Therefore, the pK_{a2} values measured in solution are most relevant for optical carbon dioxide sensors based on the di-OH-aza-BODIPY dyes. Indeed, these values correlate very well with the sensitivities of the optical CO_2 sensors (Table 1 and Fig. 3). The sensitivity increases in the following order: di-Cl-di-OH < di-F-di-OH < di-OH < di-CH_3-di-OH. Notably, for the most sensitive sensor based on di-CH_3-di-OH about 25% of the overall signal change is observed already at atmospheric pCO_2 which is, to the best of our knowledge, one of the highest sensitivities reported so far. Di-F-di-OH and di-Cl-di-OH complexes bearing electron-withdrawing groups displayed diminished pK_{a2} values of 9.35 and 8.72, respectively, and enabled measurements up to 100% CO_2. These great differences in sensitivity lead to a broad range of applications, varying from food packaging and capnography for di-F-di-OH and di-Cl-di-OH complexes to environmental monitoring for di-OH and di-CH_3-di-OH complexes. Fig. 3 shows the increasing absorption of the mono-anionic form in relation to the absorption at 0 kPa (Abs–Abs_0) carbon dioxide (see Fig. 2B). The higher the sensitivity of the sensor, the steeper the respective calibration curves, as shown in Fig. 3, and the lower the amount of carbon dioxide necessary to fully protonate the sensor. Sensors based on the di-Cl-di-OH-complex and the di-F-di-OH-complex showed limits of detection (LOD) of 0.19 kPa and 0.18 kPa, respectively. However, determining the LOD value for very sensitive sensors can be very challenging. For measurements of low levels of carbon dioxide the measuring system (gas mixer, gas lines, flow cell, *etc.*) has to be completely decarbonized, which is very difficult to achieve in reality. Especially for atmospheric levels ofpCO_2 (0.04 kPa ≈ 400 ppm in the gas phase ≈13.6 μmol l^{-1} in water at 298.15 K) and below, traces of environmental carbon dioxide disturbed the measurements for sensors based on the di-CH_3-di-OH-complex and the di-OH-complex. Hence, the determined LODs for these two complexes (0.011 kPa for di-OH and 0.007 kPa for di-CH_3-di-OH) were only rough estimations.

Photodegradation profiles of the carbon dioxide sensors were obtained from the absorption spectra after illuminating the sensor foils with a high-power LED array (λ_{max} 458 nm). For comparison, the state-of-the-art indicator dyes such as *m*-cresol-purple, thymol-blue and HPTS were used (ESI,† Fig. S1). The photostability of both the mono-anionic and the di-anionic form

were investigated. Therefore, the cuvette was filled either with pure carbon dioxide (mono-anionic form) or with pure nitrogen (di-anionic form). Clearly, all of the di-OH-aza-BODIPY dyes showed outstanding photostability, much better than the reference indicators embedded in the same ethyl cellulose matrix. After 1.5 h of illumination the presented dyes showed hardly any photobleaching effects for both the mono-anionic and di-anionic forms, whereas *m*-cresol-purple (neutral form), thymol-blue (neutral form) and HPTS (only anionic form) were degraded to less than 80%. The anionic forms of *m*-cresol-purple and thymol-blue were even less photostable than there neutral forms (ESI,† Fig. S1).

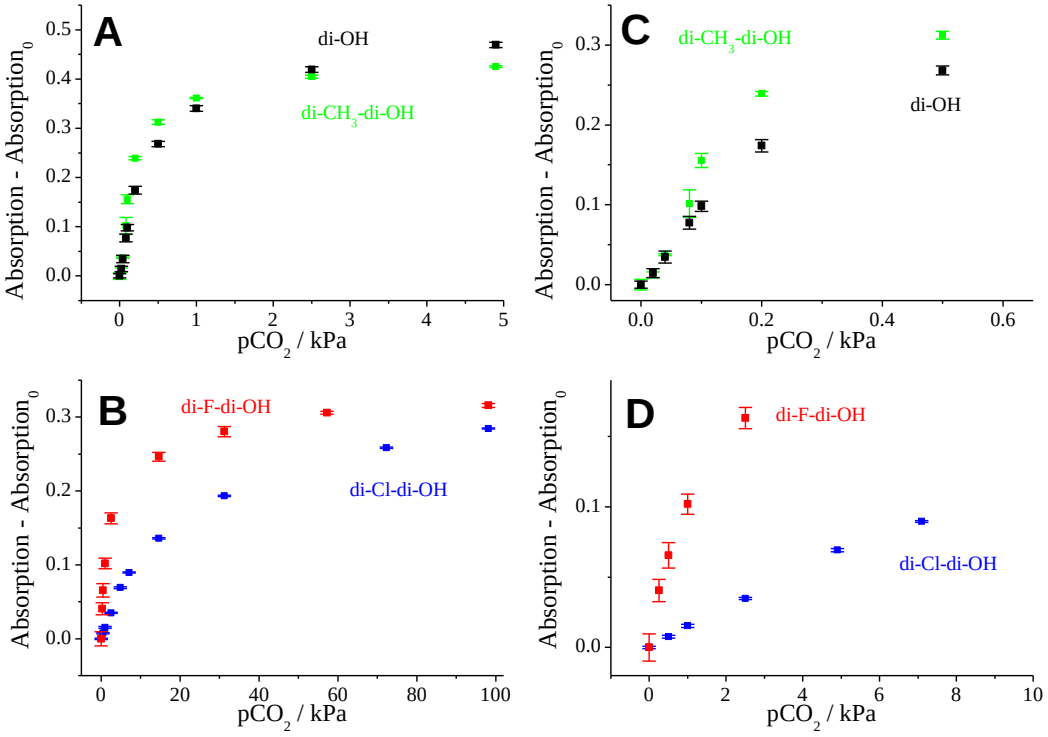

Fig. 3 (A) Calibration curves (absorption – absorption at 0 kPa of the mono-anionic form) for the carbon dioxide sensors based on di-OH-complex (black) and di-CH_3-di-OH-complex (green) and (B) di-Cl-di-OH-complex (blue) and di-F-di-OH-complex (red) 25°C under humid conditions with the respective "zoom-in" sections (C and D).

Luminescence-based ratiometric read-out using IFE (inner filter effect) based sensors

Read-out of the planar optodes and fibre-optic sensors based on colorimetric systems is significantly more challenging than that of the luminescent systems. The inner-filter effect (IFE) was made use of in order to enable read-out *via* luminescence. Additionally to the first layer containing the absorption-based indicator dye along with TOAOH in ethyl cellulose, a second layer containing the secondary emitters was used.[42] It included the pH-insensitive di-butoxy-complex entrapped in PS-particles as a fluorophore and Egyptian blue (EB) as a phosphor, both embedded in Hyflon AD 60. The absorption spectra of the di-OH-complex and the emission spectra of the secondary emitters are shown in Fig. 4A. Here, the broad emission band of the phosphor (EB) overlaps with the absorption spectrum of the di-anionic form of the indicator and the emission band of the fluorophore (di-butoxy-aza-BODIPY-complex) overlaps with the absorption spectrum of the mono-anionic form of the indicator. The isosbestic point of the di-OH-indicator is located at 610 nm and represents an ideal wavelength for exciting the secondary emitters matching the maxima of the red LEDs available (605, 617 nm). The fluorescence spectra of the sensor based on the combination of EB, the di-butoxy-complex and the non-substituted di-OH indicator are shown in Fig. 4B. Emission peaks in the absence (λ_{max} 913 nm) and presence (λ_{max} 738 nm) of carbon dioxide were well observable. Hence, luminescence-based ratiometric read-out becomes possible. This can be realized either by using two emission filters isolating the respective components or by measuring the luminescence phase shift. In fact, the phase shift for luminescent Egyptian blue is 55.8° at 2000 Hz and the phase shift of the fluorophore is 0 at this modulation frequency.

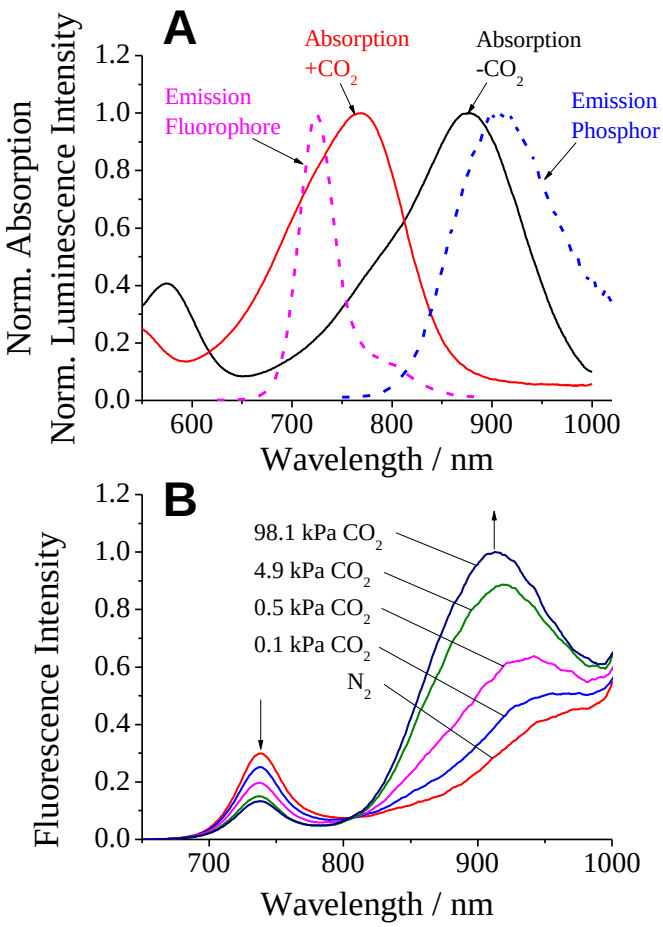

Figure 4. (A) Respective emission spectra (λ_{exc} 610 nm) of Egyptian Blue (EB; blue dashed line; "Emission Phosphor") and the di-butoxy-complex (dissolved in tetrahydrofuran; magenta dashed line; "Emission Fluorophore"); absorption spectra of the sensor based on the di-OH-complex in absence (black line) and in presence (red line) of carbon dioxide at 25°C. (B) Emission spectra (λ_{exc} 610 nm) of a carbon dioxide sensor based on the di-OH-complex and inner-filter-effect read-out at 25 °C under humidified conditions.

Carbon dioxide production/consumption of a Hebe plant. The applicability of the presented carbon dioxide sensors is demonstrated by showing the respiration of a Hebe plant. The Hebe plant in soil, a carbon dioxide sensor based on the di-CH_3-di-OH-complex and an oxygen trace sensor were placed in a desiccator. The desiccator was purged for 15 min with a gas mixture of 2% oxygen in nitrogen (in order to achieve better dynamics when measuring with an optical oxygen sensor compared to air saturation) and then closed tightly. During the measurement the

setup was alternately kept in darkness and illuminated for 30 min using three halogen lamps. According to these illumination sequences the production/consumption of carbon dioxide was observed (Fig. 5). In darkness an increase of carbon dioxide occurred due to respiration, whereas during illumination the concentration of CO_2 decreased. Over the whole measurement more CO_2 was produced than consumed which may be due to stress-induced respiration of the Hebe plant. Corresponding to the applied light sequences also the oxygen concentration was affected. Note that over the whole experiment the oxygen concentration was increasing which can be explained by slow diffusion of oxygen into the desiccator. Surprisingly, oxygen concentration did not increase significantly during the light phase, but it increased abruptly immediately after the light was switched off, reaching a plateau after about 30 min (Fig. 5). This effect may be attributed to the storage of generated oxygen in the plant and its release in the beginning of the dark phase. After this time the equilibrium between oxygen consumption during respiration and oxygen diffusion from outside is reached. As can be seen, the same phenomenon is observed if both the light and dark cycles are extended to 60 min (see hours 2 to 4 in Fig. 5). The above plant behavior is beyond the scope of the paper and calls for more detailed investigation.

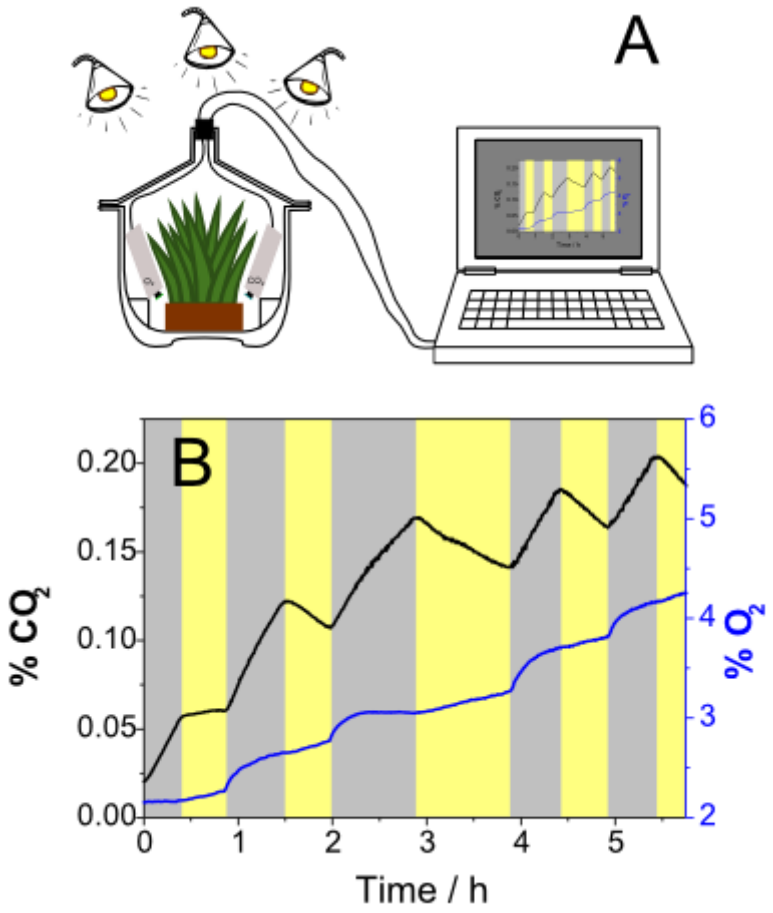

Fig 5 (A) Experimental set-up and (B) carbon dioxide and oxygen dynamics in a dessicator containing a Hebe plant during illumination (yellow zones) and in darkness (gray zones).

3.4 Conclusion

A new class of colorimetric pH-sensitive indicators for carbon dioxide sensors has been presented. The di-OH-aza-BODIPY dyes show characteristic CO_2-dependent absorption spectra in the near-infrared region. In addition to the remarkable photostability of the indicators and the high molar absorption coefficients, the dynamic ranges of the sensors can be tuned *via* electron-donating and electron-withdrawing substituents. This enables a broad range of applications from environmental monitoring to food packaging or capnography. The sensors based on di-CH_3-di-OH-aza-BODIPYs are the most sensitive sensors ever reported and resolve well below atmospheric CO_2 levels. The absorption-modulated inner-filter effect was used to enable

referenced luminescence-based ratiometric read-out. As an example the production/consumption of carbon dioxide of a Hebe plant was demonstrated.

3.5 References

1. D. Zhao, D. Miller, X. Xian, F. Tsow, E. S. Forzani, *Sens. Actuators B Chem.*, 2014, **195**, 171–176.

2. A. Mills, A. Lepre, L. Wild, *Sens. Actuators B-Chem.*, 1997, **39**, 419–425.

3. S. Trivedi, H. Mehta, R. Kashyap, *Indian J. Crit. Care Med.*, 2014, **18**, 348.

4. B. Rost, I. Zondervan, D. WolfGladrow, *Mar. Ecol. Prog. Ser.*, 2008, **373**, 227–237.

5. S. C. Doney, V. J. Fabry, R. A. Feely, J. A. Kleypas, In *Annual Review of Marine Science*; Annual Reviews: Palo Alto, 2009; Vol. 1, pp. 169–192.

6. A. E. Punt, D. Poljak, M. G. Dalton, R. Foy, J. *Ecol. Model.*, 2014, **285**, 39–53.

7. K. E. Fabricius, C. Langdon, S. Uthicke, C. Humphrey, S. Noonan, G. De'ath, R. Okazaki, N. Muehllehner, M. S. Glas, J. M. Lough, *Nat. Clim. Change*, 2011, **1**, 165–169.

8. P. Puligundla, J. Jung, S. Ko, *Food Control*, 2012, **25**, 328–333.

9. B. Weigl, A. Holobar, W. Trettnak, I. Klimant, H. Kraus, P. Oleary, O. Wolfbeis, *J. Biotechnol.*, 1994, **32**, 127–138.

10. T. Beuermann, D. Egly, D. Geoerg, K. I., Klug, W. Storhas, F.-J. Methner, *J. Biosci. Bioeng.*, 2012, **113**, 399–405.

11. A. G. Carroll, R. Przeslawski, L. C. Radke, J. R. Black, K. Picard, J. W. Moreau, R. R. Haese, S. Nichol, *Cont. Shelf Res.*, 2014, **83**, 116–128.

12. A. Mills, S. Hodgen, *Adv. Concepts Fluoresc. Spectrosc. Pt Small Mol. Sens.*, 2005, **9**, 119–161.

13. J. Zosel, W. Oelßner, M. Decker, G. Gerlach, U. Guth, *Meas. Sci. Technol.*, 2011, **22**, 072001.

14. M. Clegg, C. Sullivan, J. Eastin, J. *Plant Physiol.*, 1978, **62**, 924–926.

15. R. Arieli, O. Ertracht, Y. Daskalovic, *J. Appl. Physiol.* , 1999, **86**, 647–650.

16. D. García-Fresnadillo, M. D. Marazuela, M. C. Moreno-Bondi, G. Orellana, *.Langmuir* , 1999, **15**, 6451–6459.

17. Y. Liu, Y. Tang, N. N. Barashkov, I. S. Irgibaeva, J. W. Y. Lam, R. Hu, D. Birimzhanova, Y. Yu, B. Z. Tang, *J. Am. Chem. Soc.*, 2010, **132**, 13951–13953.

18. R. Ali, T. Lang, S. M. Saleh, R. J. Meier, O. S. Wolfbeis, *Anal. Chem.*, 2011, **83**, 2846–2851.

19. S. Pandey, S. N. Baker, S. Pandey, G. A. Baker, *Chem. Commun.*, 2012, **48**, 7043–7045.

20. W. Hong, Y. Chen, X. Feng, Y. Yan, X. Hu, B. Zhao, F. Zhang, D. Zhang, Z. Xu, Y. Lai, *Chem. Commun.*, 2013, **49**, 8229–8231.

21. X. Xie, M. Pawlak, M.-L. Tercier-Waeber and E. Bakker, *Anal. Chem*., 2010, **84**, 3163-3169.

22. L. Q. Xu, B. Zhang, M. Sun, L. Hong, K.-G. Neoh, E.-T. Kang and G. D. Fu, *J. Mater. Chem. A*, 2013, **1**, 1207-1212.

23. Q. Xu, S. Lee, Y. Cho, M. H. Kim, J. Bouffard and J. Yoon, *J. Am. Chem. Soc*., **2013**, 135, 17751-17754.

24. A. Mills, Q. Chang, N. Mcmurray, *.Anal. Chem.*, 1992, **64**, 1383–1389.

25. A. Mills, L. Monaf, *Analyst*, 1996, **121**, 535–540.

26. R. N. Dansby-Sparks, J. Jin, S.J. Mechery, U. Sampathkumaran, T. W. Owen, B. D. Yu, K. Goswami, K. Hong, J. Grant, Z.-L. Xue, *Anal. Chem.*, 2010, **82**, 593–600.

27. O. S. Wolfbeis, Kovács, B.; Goswami, K.; Klainer, S. M. *Microchim. Acta*, 1998, **129**, 181–188.

28. C. Von Bultzingslowen, A. K. McEvoy, C. McDonagh, B. D. MacCraith, I. Klimant, C. Krause, O. S. Wolfbeis, *Analyst*, 2002, **127**, 1478–1483.

29. O. Oter, K. Ertekin, S. Derinkuyu, *Talanta*, 2008, **76**, 557–563.

30. S. M. Borisov, C. Krause, S. Arain, O. S. Wolfbeis, *Adv. Mater* , 2006, **18**, 1511 – 1516.

31. N. B. Borchert, J. P. Kerry and D. B. Papkovsky, *Sens. Actuators, B*, **2013**, 176, 157-165.

32. S. Schutting, S. M. Borisov, I. Klimant, *Anal. Chem.*, 2013, **85**, 3271–3279.

33. S. Schutting, I. Klimant, D. de Beer, S. M. Borisov, *Methods Appl. Fluoresc.* , 2014, **2**, 024001.

34. Z. Xu, A. Rollins, R. Alcala, R. E. Marchant, *J. Biomed. Mater. Res.*, 1998, **39**, 9–15.

35. R. C. Hunter, T. J. Beveridge, *Appl. Environ. Microbiol* , 2005, **71**, 2501–2510.

36. K. W. Spitzer, R. L. Skolnick, B. E. Peercy, J. P. Keener, R. D. Vaughan-Jones, *J. Physiol.* , 2002, **541**, 159–167.

37. V.K. Ramshesh, J. J. Lemasters, In *Mitochondrial Bioenergetics: Methods and Protocols*; C. M. Palmeira, A. J. Moreno, Eds.; 2012; Vol. 810, pp. 243–248.

38. T. Jokic, S. M. Borisov, R. Saf, D. A. Nielsen, M. Kühl, I. Klimant, *Anal. Chem.*, 2012, **84**, 6723–6730.

39. S. M. Borisov, K. Gatterer, I. Klimant, *Analyst*, 2010, **135**, 1711–1717.

40. M. S. Briggs, D. D. Burns, M. E. Cooper, S. J. Gregory, *Chem. Commun.*, 2000, 2323–2324.

41.M. E. Cooper, S. Gregory, E. Adie, S. Kalinka, *J. Fluoresc.*, 2002, **12**, 425–429.

42. S. M. Borisov, I. Klimant, *Anal. Chim. Acta*, 2013, **787**, 219–225.

43. N. Nakamura, Y. Amao, *Anal. Bioanal. Chem.*, 2003, **376**, 642–646.

44. Y.Amao, N. Nakamura, *Sens. Actuators B Chem.*, 2004, **100**, 347–351.

45. I. M. Perez de Vargas-Sansalvador, M. A. Carvajal, O. M. Roldan-Munoz, J. Banqueri, M: D. Fernandez-Ramos, L. F. Capitan-Vallvey, *Anal. Chim. Acta*, 2009, **655**, 66–74.

46. S. M. Borisov, C. Wuerth, U. Resch-Genger and I. Klimant, *Anal. Chem.*, 2013, **85**, 9371-9377.

47. M. J. Hall, S. O. McDonnell, J. Killoran, D. F. O'Shea, *J. Org. Chem.*, 2005, **70**, 5571–5578.

48. A. Gorman, J. Killoran, C. O'Shea, T. Kenna, W. M. Gallagher, D. F. O'Shea, *J. Am. Chem. Soc.*, 2004, **126**, 10619–10631.

3.6 Supporting Information

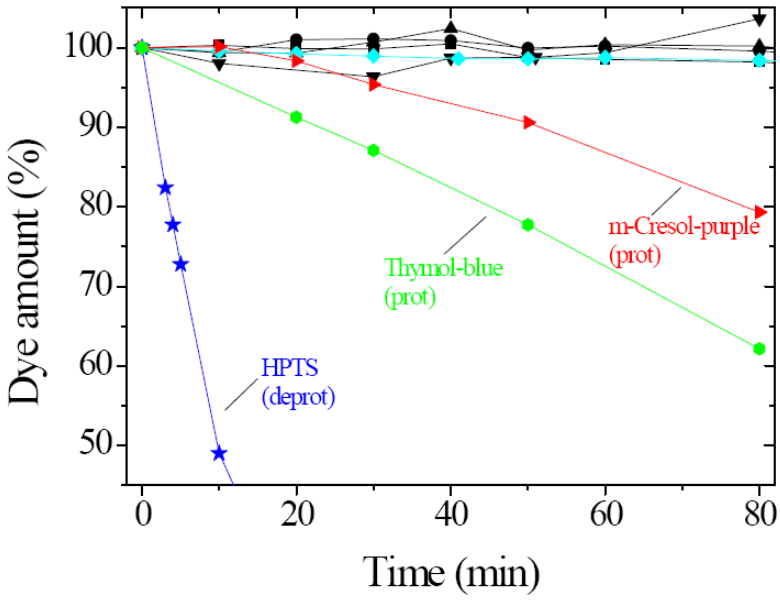

Figure S1. Photodegradation profiles for carbon dioxide sensors (EC49; base: TOAH; T=25 °C) based on the di-OH-aza-BODIPY dyes (black), m-cresol-purple (red triangles), thymol-blue (green dots) obtained from the absorption spectra of the respective neutral form and the absorption spectra of the deprotonated forms of the di-Cl-di-OH-complex (cyan) and HPTS(TOA)$_3$ (blue stars).

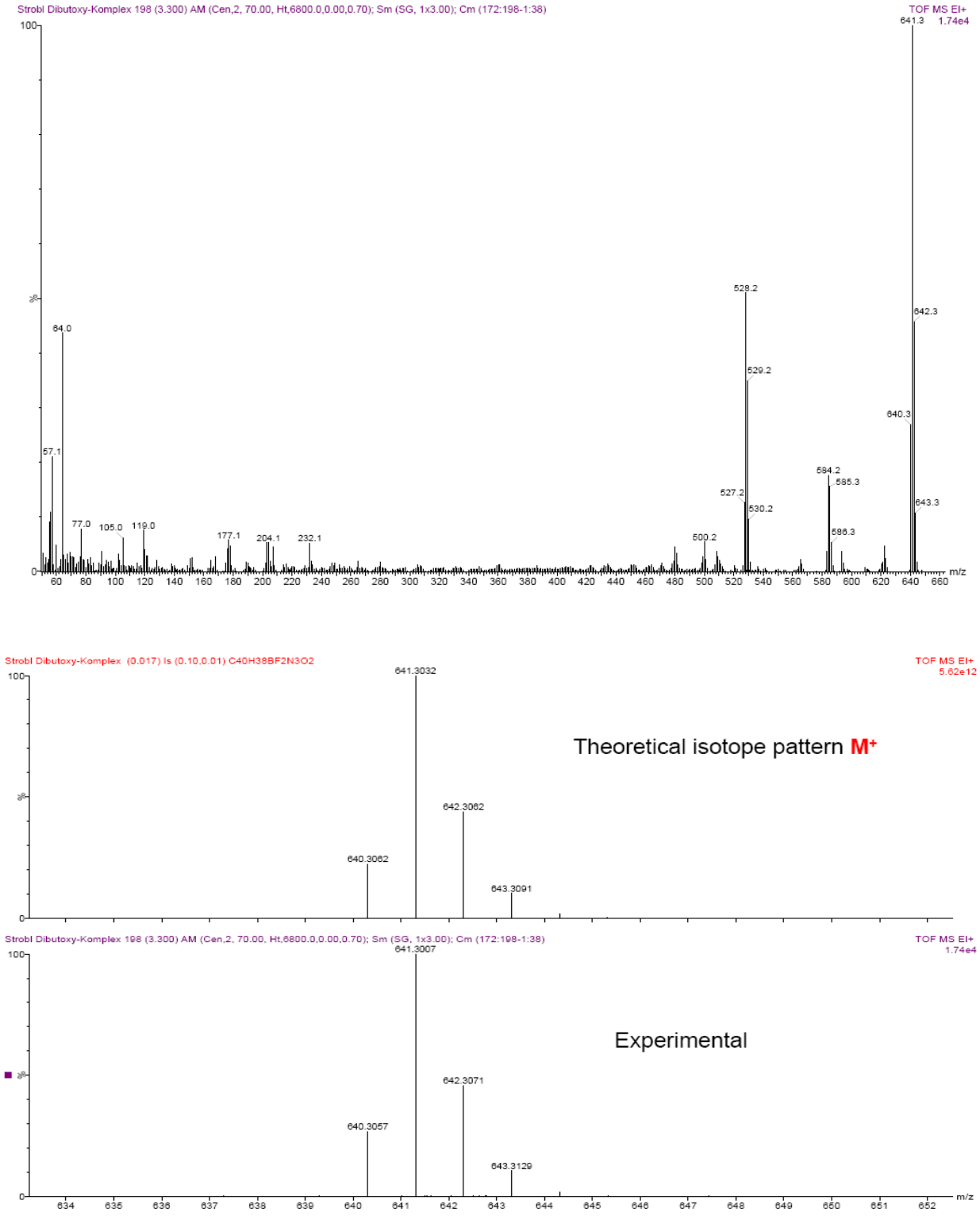

Figure S2. EI-DI Mass spectrum of 3,7-bis(4-butoxyphenyl)-5,5-difluoro-1,9-diphenyl-5H-4λ^4,5λ^4-dipyrrolo[1,2-c:2`,1`-*f*][1,3,5,2]triazaborinine (di-butoxy-complex).

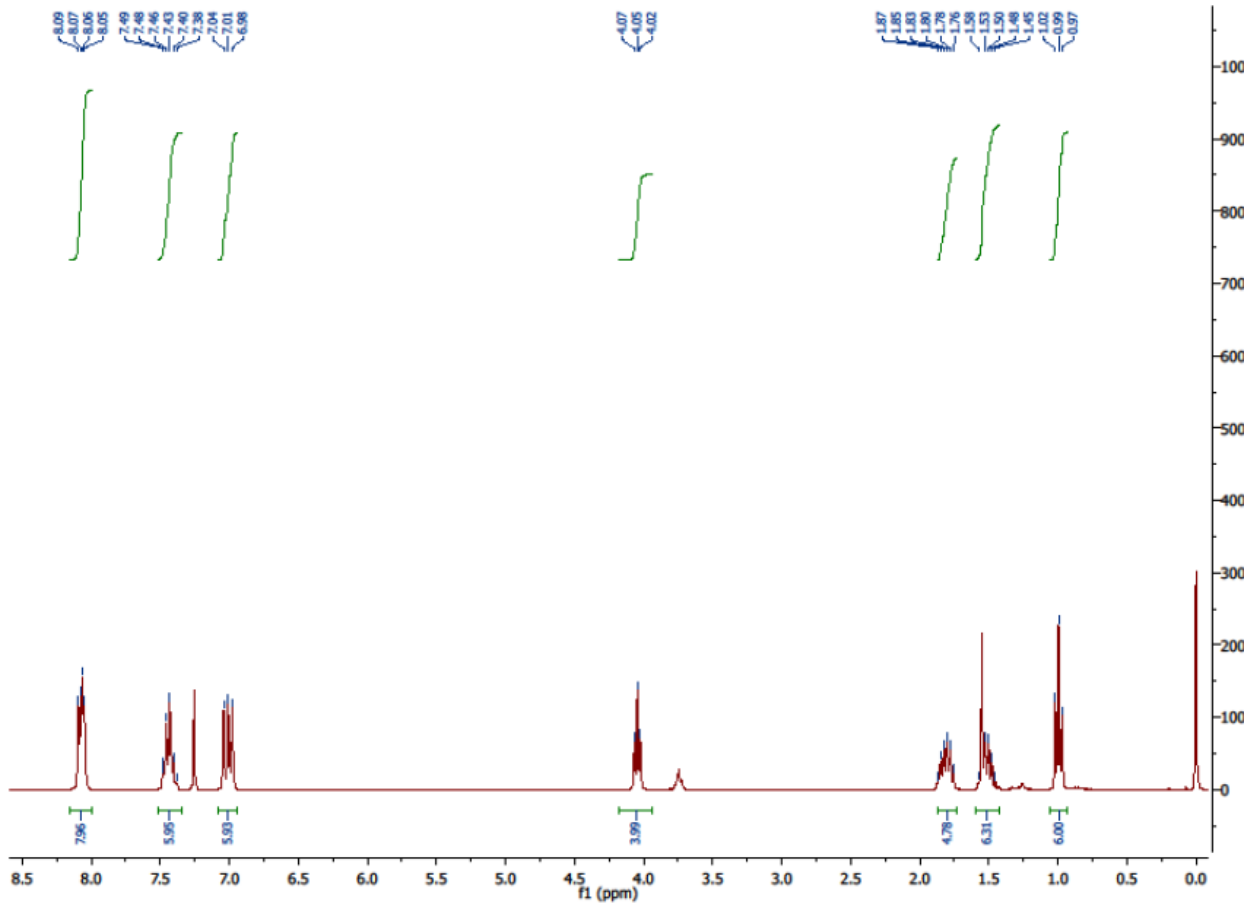

Figure S3. ^{1}H NMR of 3,7-bis(4-butoxyphenyl)-5,5-difluoro-1,9-diphenyl-5H-4λ^{4},5λ^{4}-dipyrrolo[1,2-c:2`,1`-*f*][1,3,5,2]triazaborinine (di-butoxy-complex).

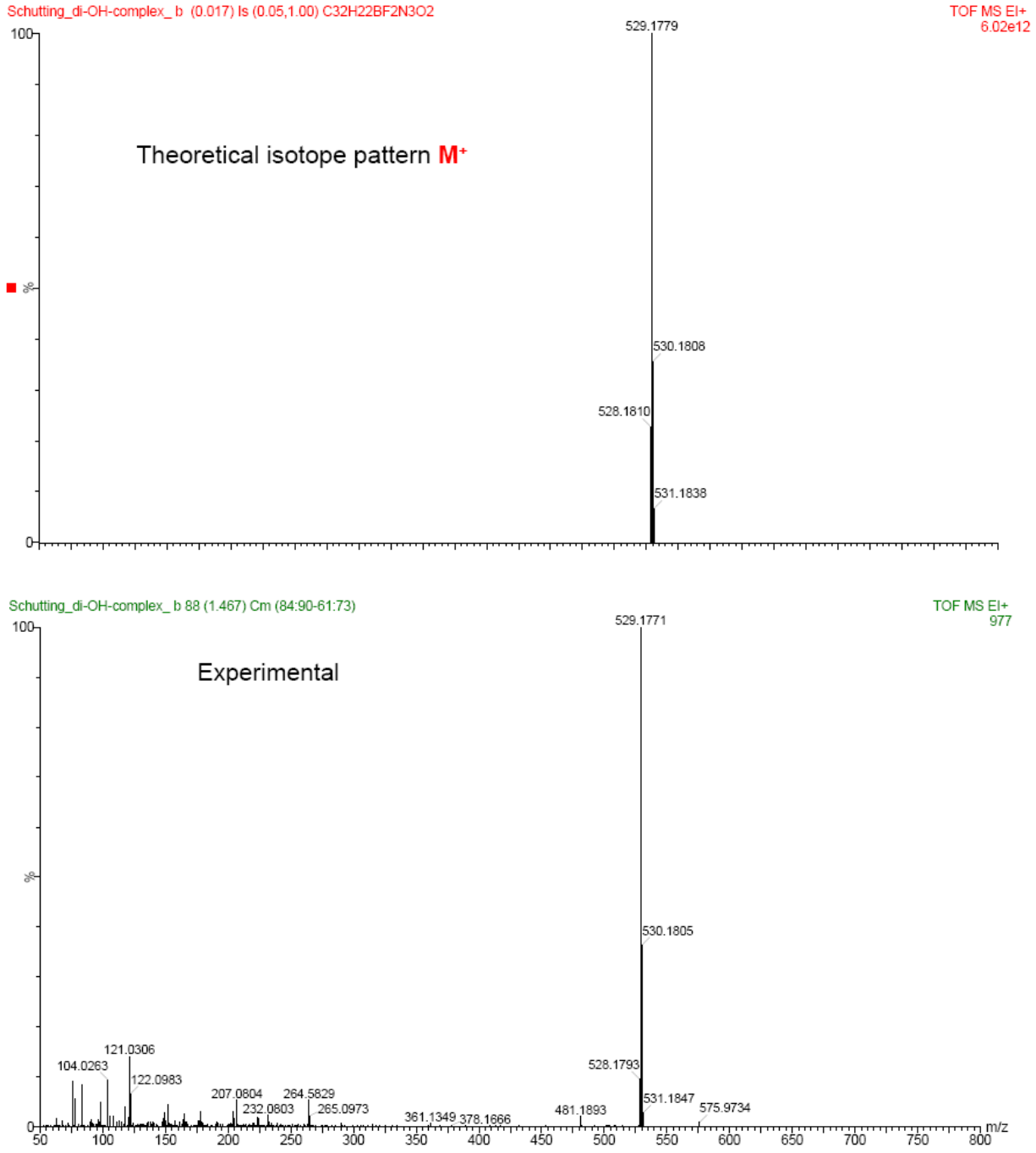

Figure S4. EI-DI Mass spectrum of 4,4`-(5,5-difluoro-1,9-diphenyl-5H-4λ$^4$,5λ$^4$-dipyrrolo[1,2-c:2`,1`-*f*][1,3,5,2]triazaborinine-3,7-diyl)diphenol (di-OH-complex).

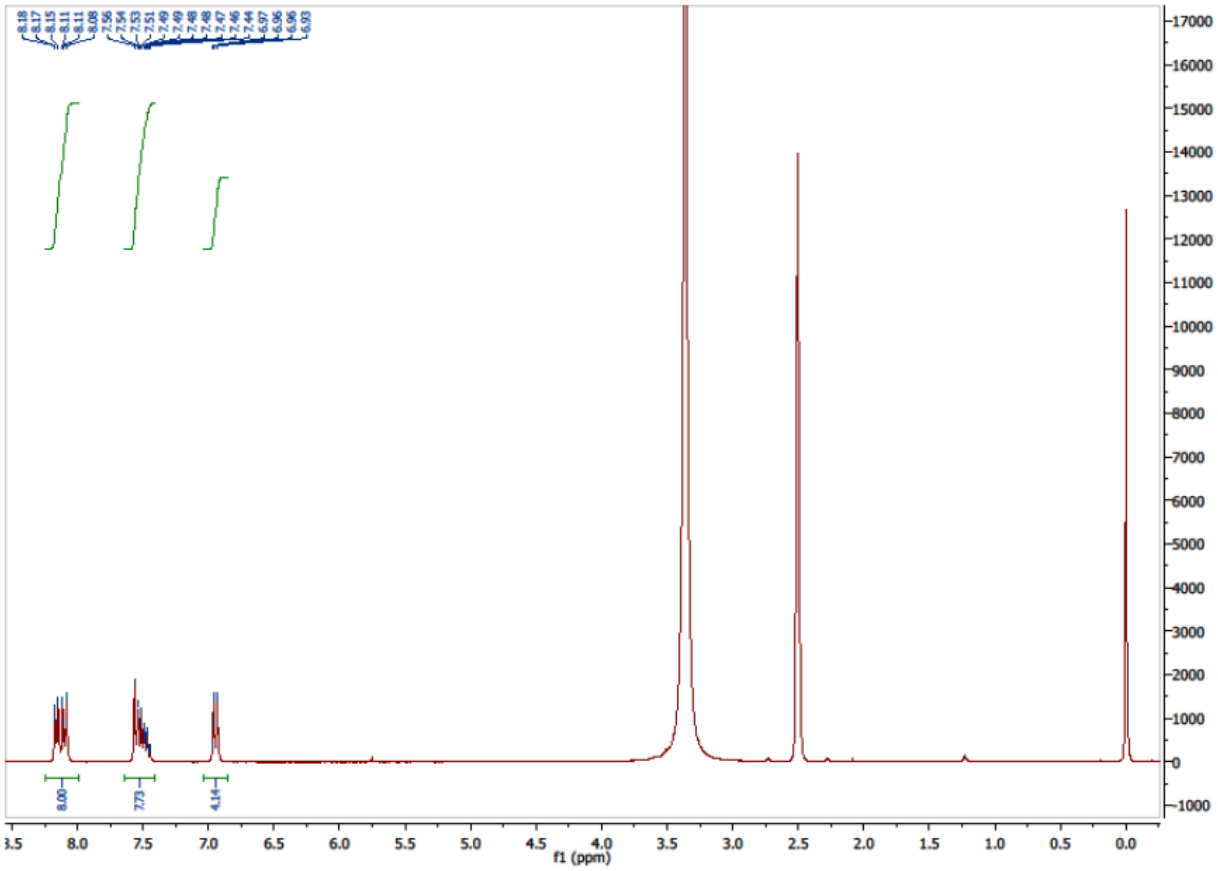

Figure S5. ^{1}H NMR of 4,4`-(5,5-difluoro-1,9-diphenyl-5H-4λ4,5λ4-dipyrrolo[1,2-c:2`,1`-*f*][1,3,5,2]triazaborinine-3,7-diyl)diphenol (di-OH-complex)

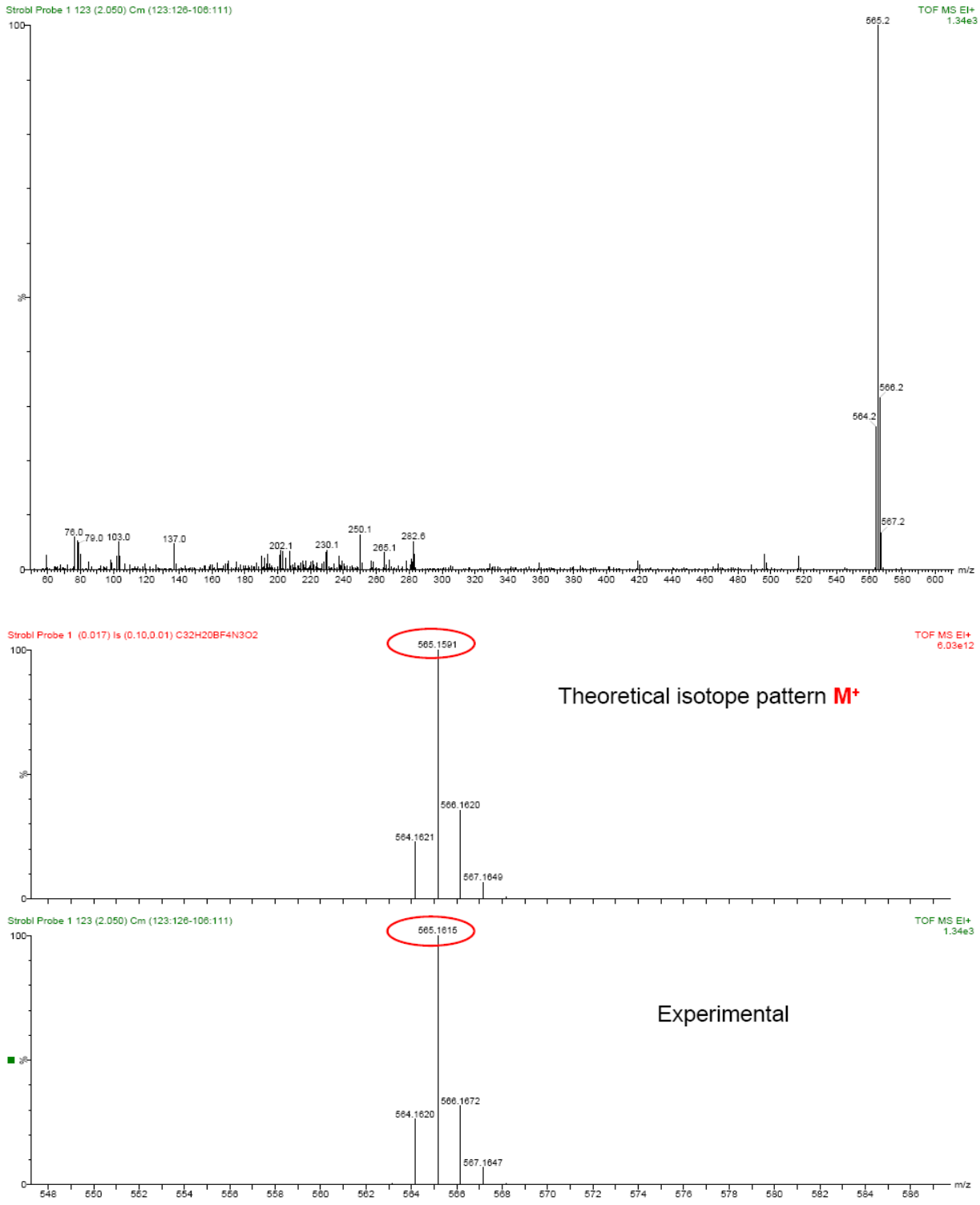

Figure S6. EI-DI Mass spectrum of 4,4`-(5,5-difluoro-1,9-diphenyl-5H-4λ$^4$,5λ$^4$-dipyrrolo[1,2-c:2`,1`-*f*][1,3,5,2]triazaborinine-3,7-diyl)bis(3-fluorophenol) (di-F-di-OH-complex).

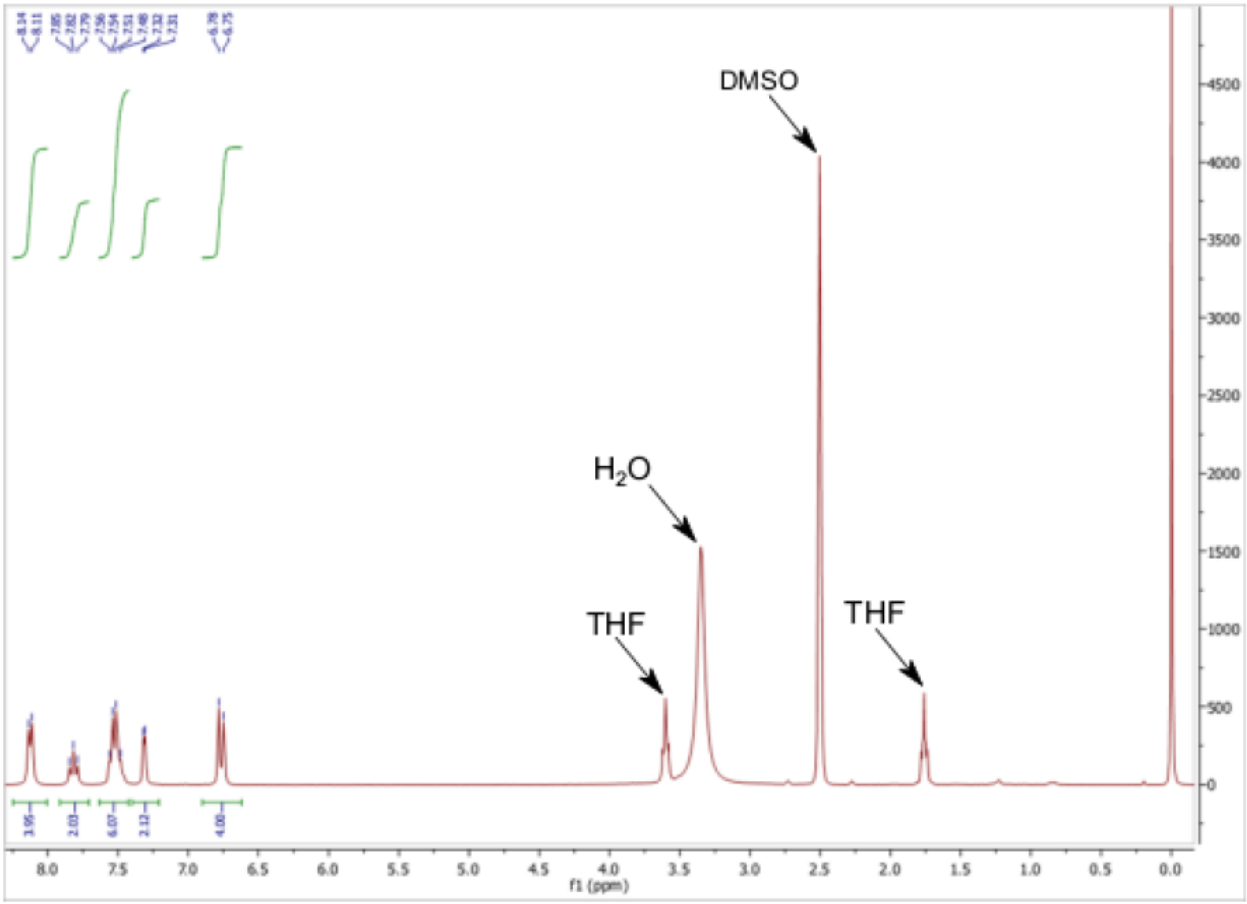

Figure S7. ^{1}H NMR of 4,4`-(5,5-difluoro-1,9-diphenyl-5H-4λ$^{4}$,5λ$^{4}$-dipyrrolo[1,2-c:2`,1`-*f*][1,3,5,2]triazaborinine-3,7-diyl)bis(3-fluorophenol) (di-F-di-OH-complex).

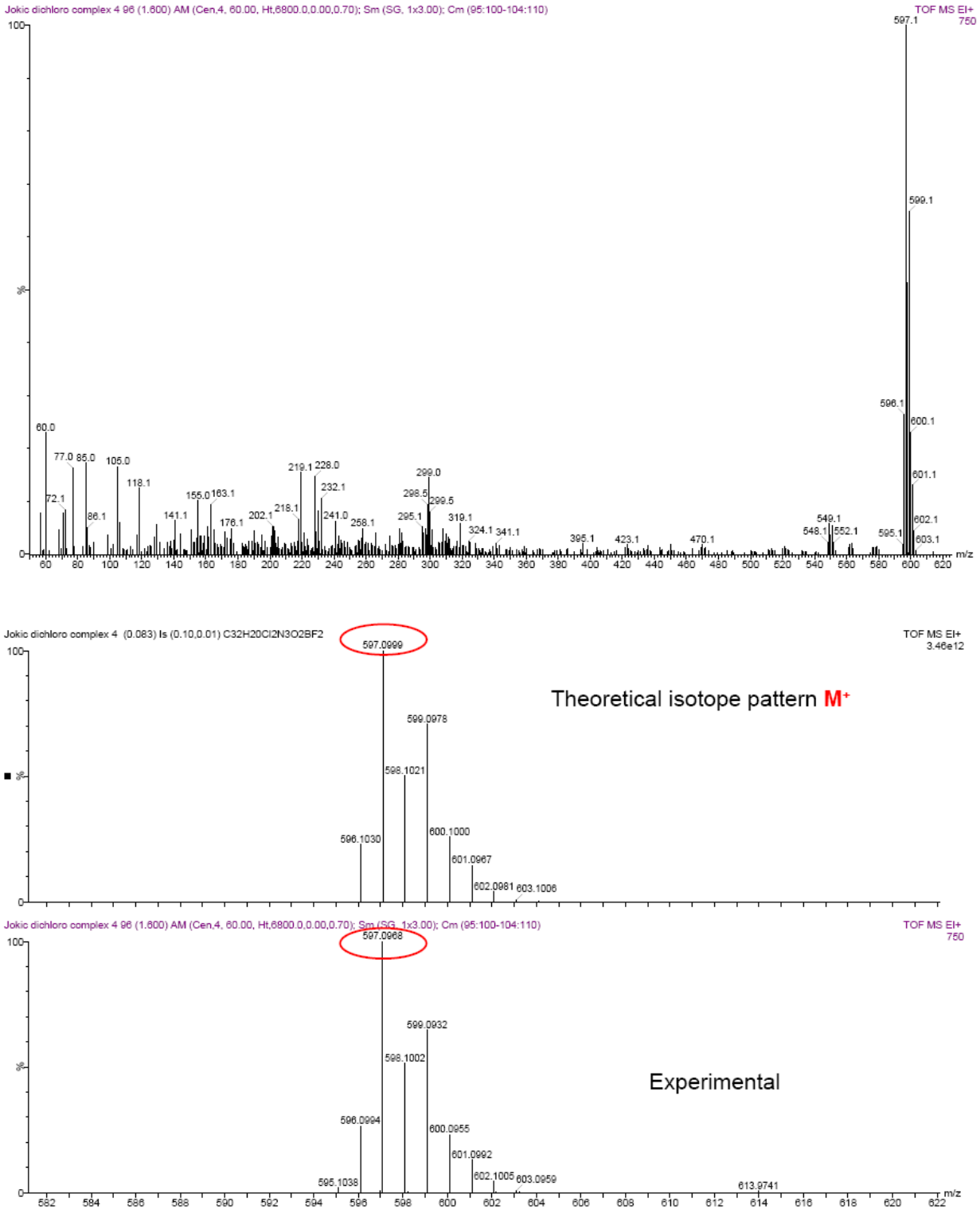

Figure S8. EI-DI Mass Spectrum of 4,4`-(5,5-difluoro-1,9-diphenyl-5*H*-4λ$^4$,5λ$^4$-dipyrrolo[1,2-c:2`,1`-*f*][1,3,5,2]triazaborinine-3,7-diyl)bis(2-chlorophenol) (di-Cl-di-OH-complex).

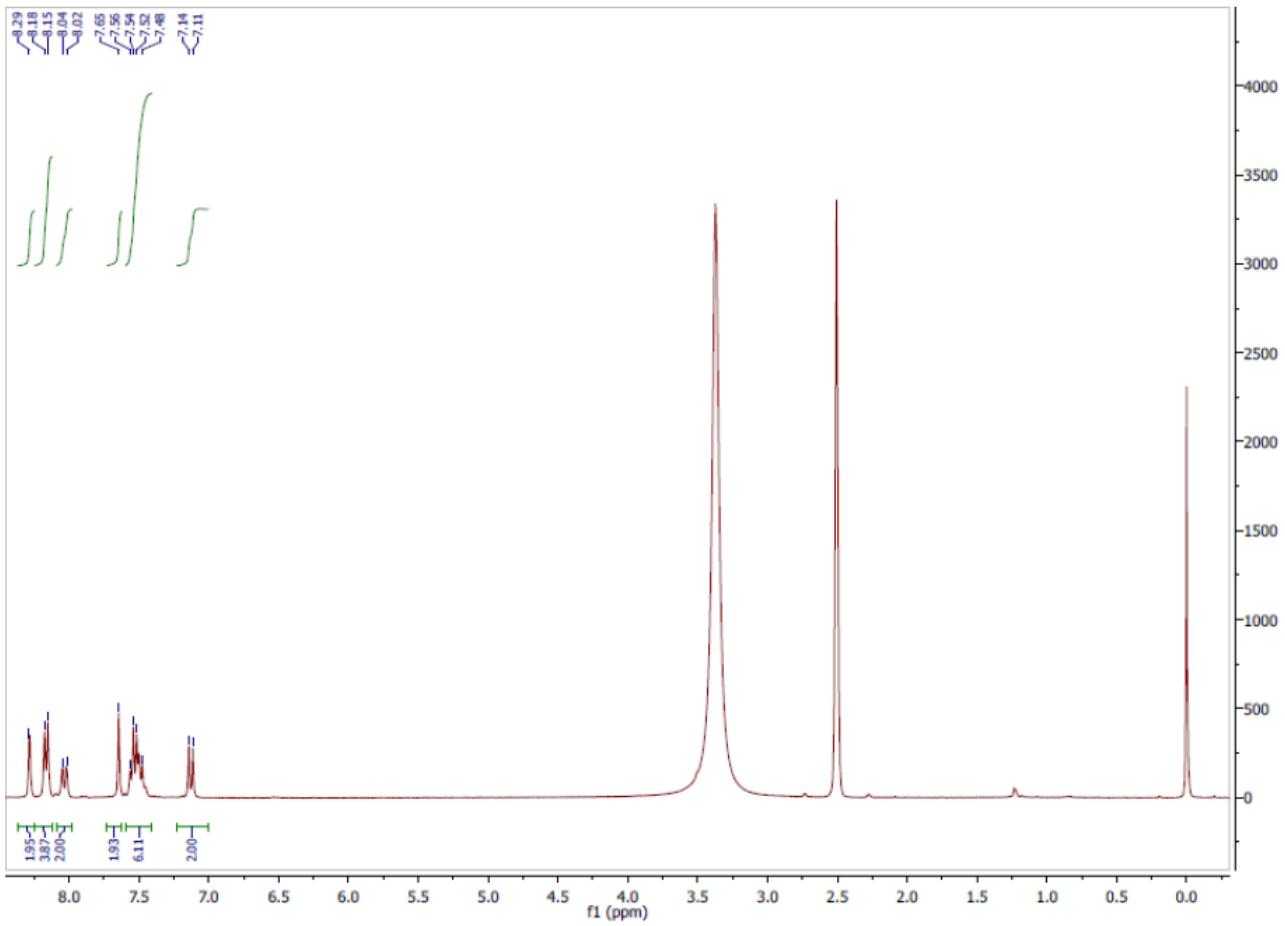

Figure S9. ^{1}H NMR of 4,4`-(5,5-difluoro-1,9-diphenyl-5*H*-4λ$^{4}$,5λ$^{4}$-dipyrrolo[1,2-c:2`,1`-*f*][1,3,5,2]triazaborinine-3,7-diyl)bis(2-chlorophenol) (di-Cl-di-OH-complex).

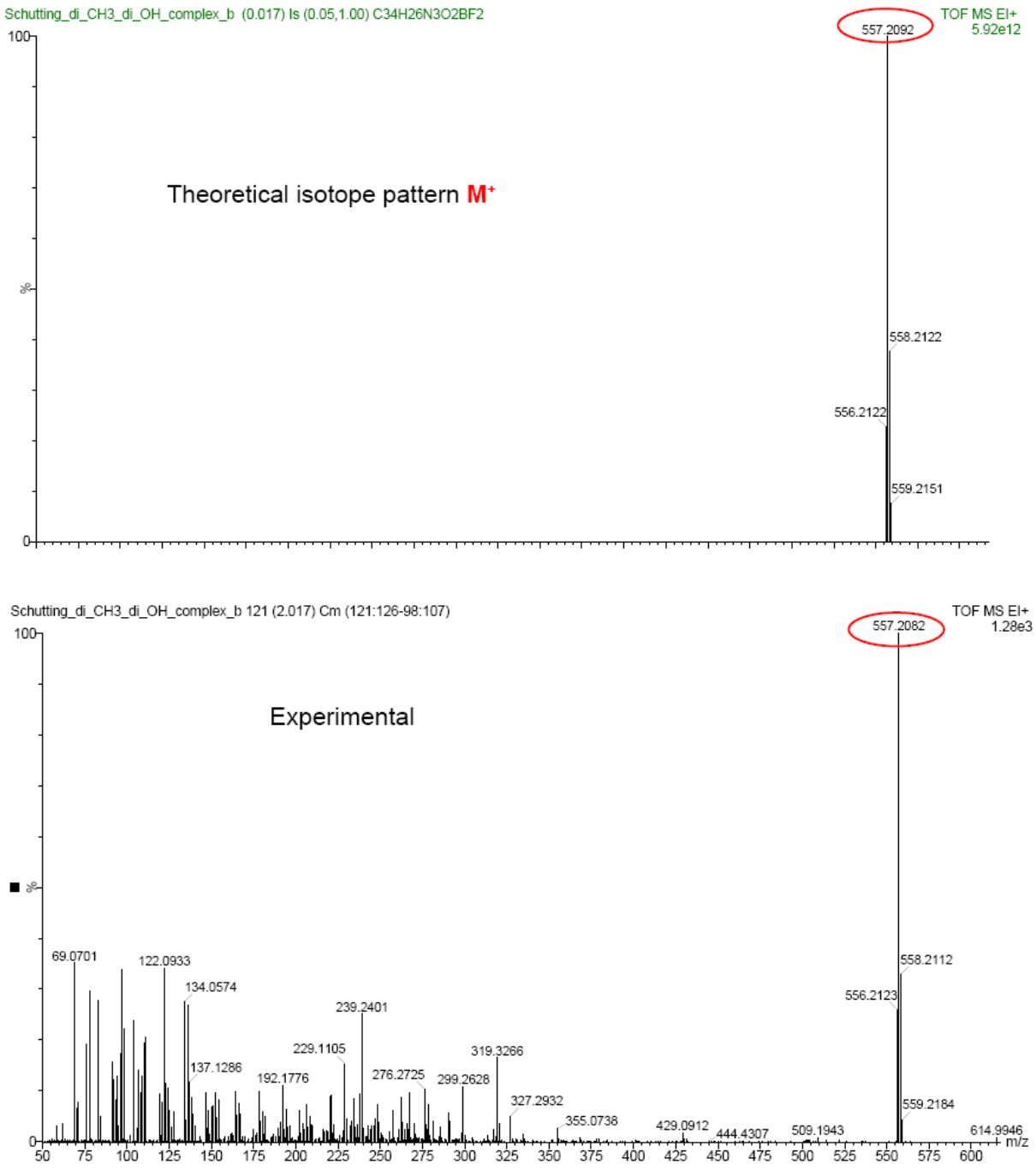

Figure S10. EI-DI Mass spectrum of 4,4`-(5,5-difluoro-1,9-diphenyl-5*H*-4λ$^4$,5λ$^4$-dipyrrolo[1,2-c:2`,1`-*f*][1,3,5,2]triazaborinine-3,7-diyl)bis(2-methylphenol) (di-CH_3-di-OH-complex).

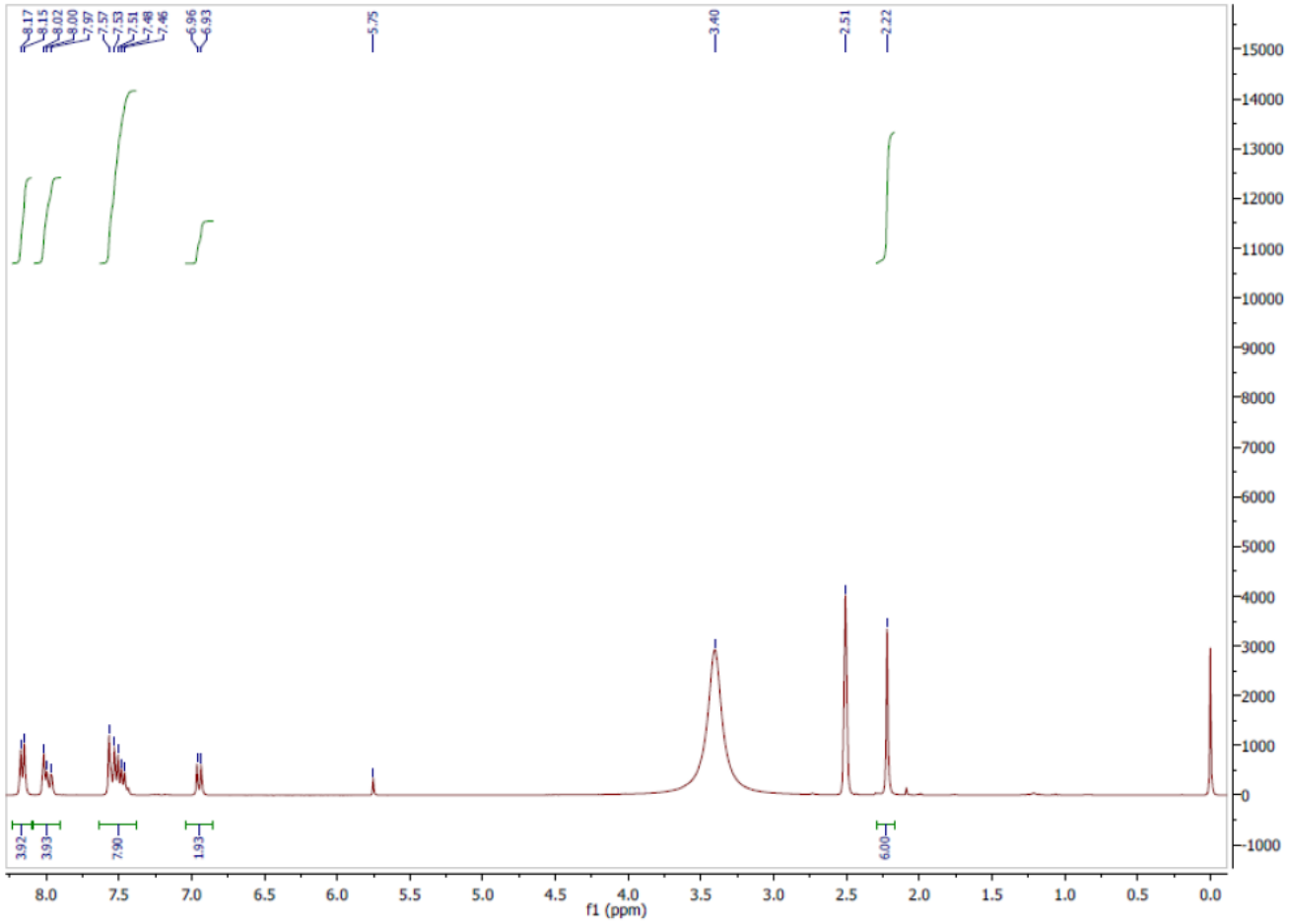

Figure S11. ^{1}H NMR of 4,4`-(5,5-difluoro-1,9-diphenyl-5*H*-4λ$^{4}$,5λ$^{4}$-dipyrrolo[1,2-c:2`,1`-*f*][1,3,5,2]triazaborinine-3,7-diyl)bis(2-methylphenol) (di-CH_3-di-OH-complex).

Chapter 4

pH-sensitive aza-BODIPY probe for fluorescence lifetime imaging in MEF cells

4.1 Introduction

Intracellular pH plays vital role in many metabolic functions of cells. Abnormal pH values are indicator of improper cell function and are associated with a number of diseases, such as renal acidosis, metabolic disorders, intoxication, diabetes, cancer[1] and Alzheimer's.[2]

Monitoring of intracellular pH can give critical information about physiological or pathogenic processes in living organisms and therefore provide essential information for disease identification and therapy.

In comparison to other methods used for pH measurements (electrochemical, NMR, absorption spectroscopy), fluorescence sensing has advantages in respect to dimensional and temporal monitoring of pH values. Fluorescence methods are more sensitive, more simple to use, and are nondestructive for in vivo measurements.

Fluorescence probes can detect pH changes by different mechanisms. Most common is using increase/decrease of fluorescence intensity or shifting of excitation and/or emission wavelength maximum that has highest response at the pH close to the pK_a of the indicator.

However, changes in optical properties of tissues and indicator concentration can influence measurement data. Fluorescence lifetime imaging microscopy (FLIM) overcomes the limitations of intensity-based measurements.[3,4] Fluorescence lifetime is not influenced by changes of indicator concentration and light source intensity and therefore the measurement data are more reliable.

Despite the significance of this topic, extensive research has not yet been done on FLIM pH imaging, most studies are still focused on ratiometric fluorescence measurements. Due to lack of probes with desirable lifetime sensitivities there is a growing demand for new probes with improved properties.

In our study of pH sensing properties of aza-BODIPY indicators we observed a decrease of 0.5 to 1 pH units in pK_a values in hydrogel D4 determined from fluorescence data in comparison to those in solution. This phenomenon is due to higher concentration of the indicator in the hydrogel than in the solution. In hydrogel the distance between indicator molecules is short enough for Förster resonance energy transfer (FRET) to take place from the protonated to the deprotonated form. In fact, pK_a values obtained from fluorescence data are decreasing with the increase of the indicator concentration in hydrogel D4.

When the energy is transferred from the donor molecule to the acceptor molecule, the lifetime of the donor molecule decreases. Therefore, it is expected that at concentration high enough to enable FRET, it is possible to measure lifetime of aza-BODIPY indicators. To demonstrate the feasibility of the approach the indicator was incorporated into RL 100 polymer, which was already used for similar dyes.

Hence, new intracellular probe (MRL) for lifetime imaging is presented based on a nanoparticles formulation of a RL-100[5] polymer and a fluorescent dye, methoxy – substituted azabodipy derivative[6]. (Fig.1)

4.2 Experimental

Materials and methods

Lysotracker Green, BCECF and Alexa Fluor 488-dextran 10000 were purchased from Invitrogen (Biosciences, Dublin, Ireland). PtTPTBPF-RL100 nanoparticles were prepared according to published procedure.[7] A CellTox Green Cytotoxicity assay kit was obtained from Promega (MyoBio, Ireland). Eudragit®RL100 was supplied by Evonik Industries (http://corporate.evonik.de). Other used chemicals were from Sigma Aldrich. Standard cell culture plastic plates were from Sarstedt (Wexford, Ireland) and Corning (VWR, Ireland), glass bottom culture dishes (diameter 35 mm) were from MatTek (Ashland, USA), and glass bottom 8-well slides from IBIDI (Martinsried, Germany). Absorption measurements were performed with Cary 50 UV-VIS spectrophotometer from Varian (www.varianinc.com). Fluorescence spectra were recorded with Hitachi F-7000 spectrofluorimeter (www.hitachi.com).

Preparation of polymer films and nanosensor particles

Particles were prepared according to a known procedure.[7] RL100 polymer (200 mg) and the indicator dye (0.5 mg) were dissolved in acetone (80 ml) and water (500 ml) was added. The suspension was evaporated under vacuum till concentration of 5 gl^{-1} was reached and the obtained particle solution was kept at 4°C.

Polymer films were prepared by dissolving indicator dye (0.5 mg) in 100 mg of RL100 in 2 ml of acetone. The "cocktail" was knife-coated on a plastic Mylar support to obtain ~ 7.5 thick sensing layer.

Cell culture

Mouse embrionic fibroblast (MEF) cells are obtained from ATCC (Manassas, VA, USA) and were cultured as described in literature.[14] For imaging experiments, cells were grown on $Cell^{+}$ dishes (confocal upright microscope) or glass bottom culture dishes coated with collagen-poly-D-lysine (inverted microscope). Cell staining was achieved by incubation of cells with pH probe in medium solution (1-24 h) and consequent washing with medium. Concentration/exposure time for probes was 2.5 µM/0.5 h (BCECF), 1 µM/0.5 h, 0.01% /10 min (CellTox Green), 25 µg ml^{-1} /0.5 h (Dextran 10000-Alexa Fluor 488), 1 µM/0.5 h Lysotracker Green and 10 µgml^{-1} /16 h (PtTPTBPF in RL100).

Microscopy

Investigation of staining kinetics, toxicity and photostability tests were carried out with a wide-field fluorescence microscope Axiovert (Zeiss). FLIM images were obtained with upright Axio Examiner Z1 (Zeiss) microscope with a 20x/1.0 W Apochromat objective, an integrated TCSPC scanning module DCS-120 (Becker & Hickl, Germany), R10467U-40, 50 photon counting detectors (Hamamatsu Photonics K.K.) and TCSPS hardwares (Becker & Hickl).[14] MRL probe was excited with a picoseconds super-continuum laser SC400-4 (Fianium, UK) at 632 nm (665 nm longpass filter, emission 750-810 nm), BCECF and Alexa Fluor 488-conjugates at 488 nm (495 nm longpass filter, emission 512-536 nm). PtTPTBPF in RL100 was excited at 614 nm (665 nm longpass filter, emission 750- 810 nm).

Buffers used for pH calibration contained 10 mM buffer salt (sodium acetate, MES, MOPS and HEPES), 135 mM KCl, 2mM $CaCl_2$, 1 mM $MgCl_2$ and 20 mM sacharose. Nigericin (10 µM) was added 15 min before the calibration.

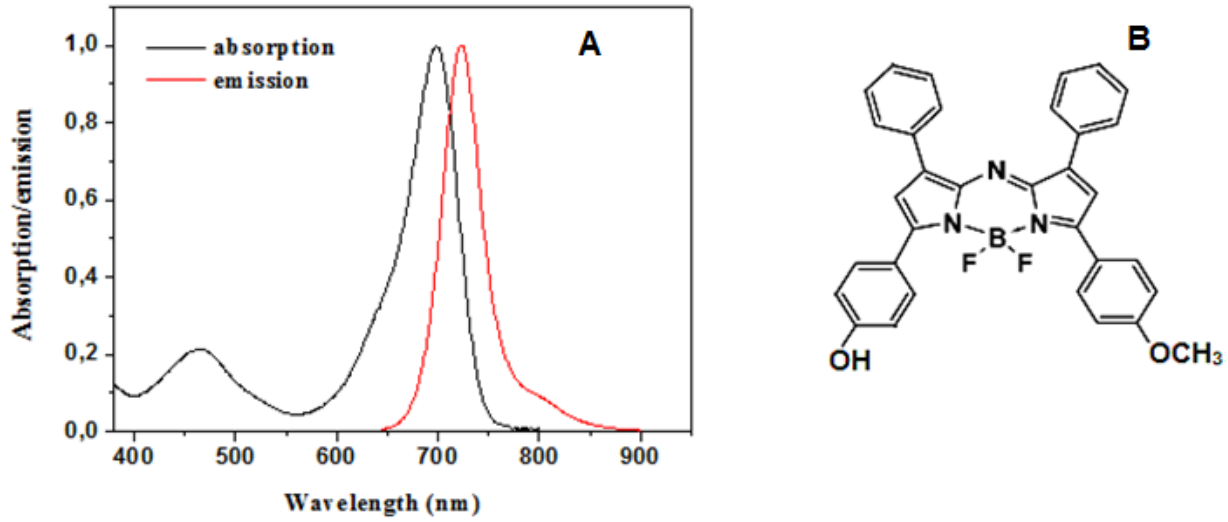

Figure 1. A. Absorption and fluorescence emission (λ_{exc} = 680 nm) spectra of MRL in THF/aqueous buffer. B. Structure of the indicator.

4.3 Results and Discussion

Cell penetration properties

The cell staining with MRL was investigated with mouse embryonic fibroblast (MEF) cells at concentrations of 20 $\mu g l^{-1}$ (indicator concentration of 0.05 µM). The highest signals for cell staining were achieved after 24 h with already observed staining after 6 h (Fig. 2).

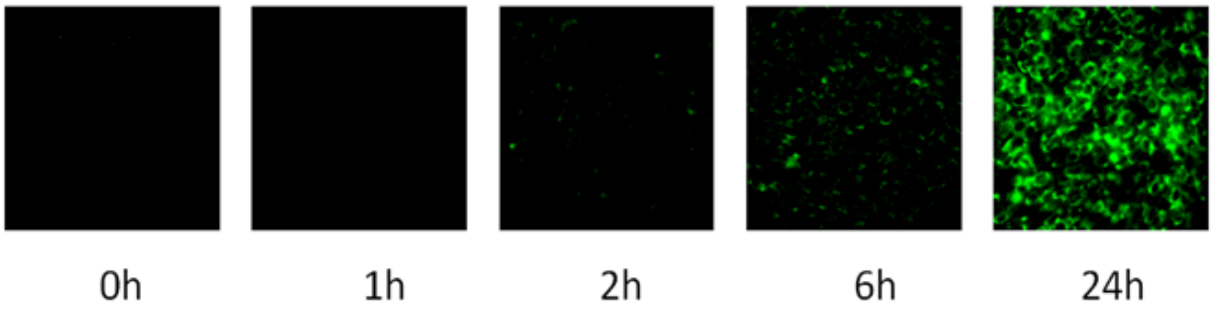

Figure 2. Staining kinetics in MEF cells (0-24 h).

MRL localization pattern overlapped partly with Alexa Fluor 488-d10 (marker of macropinosomes) and Lysotracker green (Fig. 3).

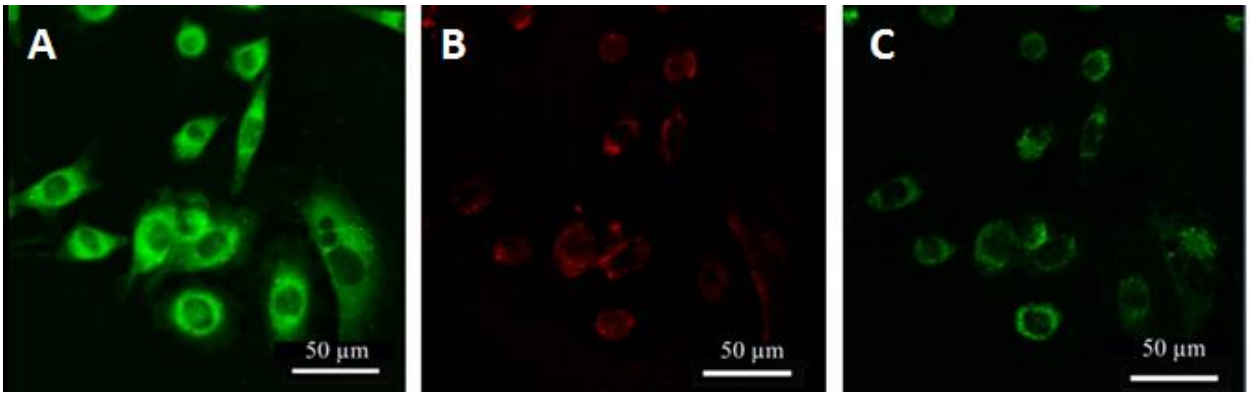

Figure 3. A: FLIM images displaying the localization of MRL in the cells; B: Co-localization of MRL with markers of d10; C: Co-localization of MRL with Lysotracker green.

Citotoxicity of NPs was assessed with CellTox Green Assay. As shown in Figure 4, no significant change in cell viability was observed after 24 h with 10-50 µg/ml of probe. Minimal staining was observed at highest concentration and cell viability was at 98-99%.

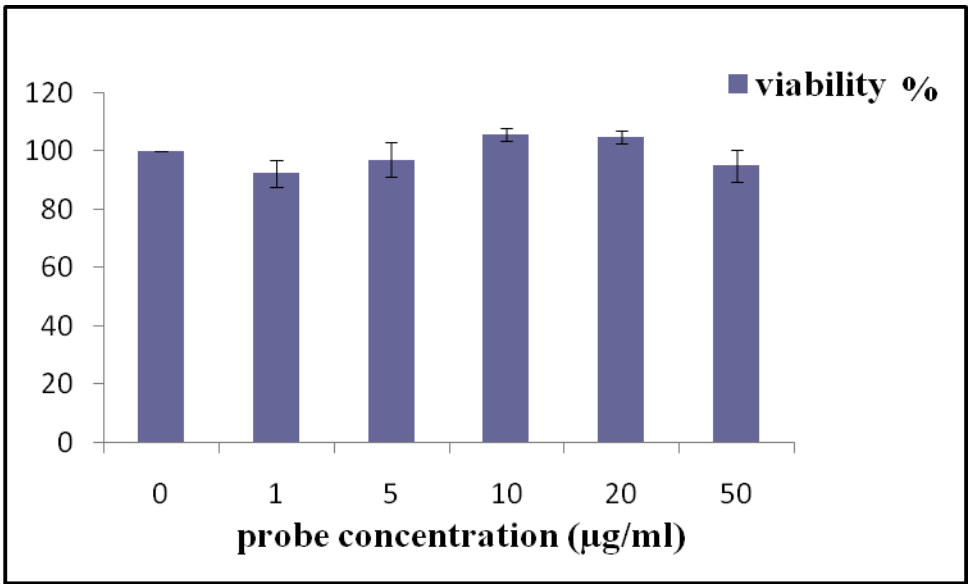

Figure 4. Cell viability determined by CellTox Green assay kit for MEF cells exposed to different concentrations of MRL after 24 h.

The photostability of MRL was investigated and compared with probes BCECF and PtTPTBPF (Fig. 5). Probes were continuously illuminated for 2 min and no change in fluorescence intensity

was observed, while for BCECF the intensity decreased by 30 % in the first 10 s. The PtTPTBPF signal decreased by ~20% during illumination while MRL signal stayed unchanged.

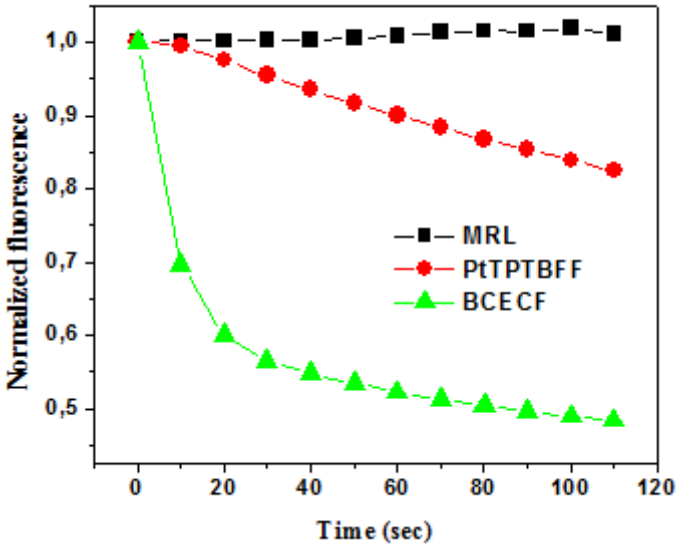

Figure 5. Photostability comparison for MRL probe (λ_{exc}=590 nm), PtTPTBFF (λ_{exc}=390 nm) and BCECF (λ_{exc}=470 nm) in MEF cells determined from the fluorescence measurements.

pH sensing and imaging with cultures of adherent cells

pH-dependent lifetime changes of MRL were investigated with fluorescence lifetime microscopy and compared with standard probe BCECF. Calibration was performed across the physiological range (4-8) after the cells were incubated with nigericin in order to equalize intracellular pH with the pH of extracellular buffers. (Fig. 6)

Smaller dynamic range was observed for MRL ($\Delta\tau$ = 0.3 ns) than for BCECF ($\Delta\tau$ = 1.5 ns). According to literature data $\Delta\tau$ for BCECF is between 0.5 and 1 ns, still absolute values for the protonated and deprotonated form differ considerably.[8-11] In our experiment BCECF emission intensity changed with pH (decreased at acidic pH, Fig.7), and the lifetime response was similar to literature data ($\Delta\tau$ ~ 1.5 ns). However, we observed much higher standard deviation for BCECF (17-30%), therefore our probe is much more reliable for intracellular pH measurements (standard deviation below 2%). pH calibrations for MRL in nanoparticles and polymer films in FLIM mode showed quite different dynamics ($\Delta\tau$ = 0.3 ns for nanoparticles and $\Delta\tau$ = 1.3 ns for

films). (Fig. 6) These data show that the environment has the effect on lifetime response and therefore there is place for optimization and improvement of probe performance.

The lifetime measured with MRL in resting cells showed low pH value (4.1 in MEF at 37°C), what indicated that the probe is localized in endosomes and lysosomes.[12,13] Therefore, this probe can be used for investigation of lysosomal or endosomal response on drug stimulation. In our experiment treatment of MEF cells with bafilomicin A1 (inhibitor of vacuolar type H^+-ATPase), caused decrease in the MRL lifetime in the area of interest. Lifetime was decreased for 0.1 ns (increase in pH by 2 pH units), in comparison to the initial value (pH=4.1). (Fig. 10)

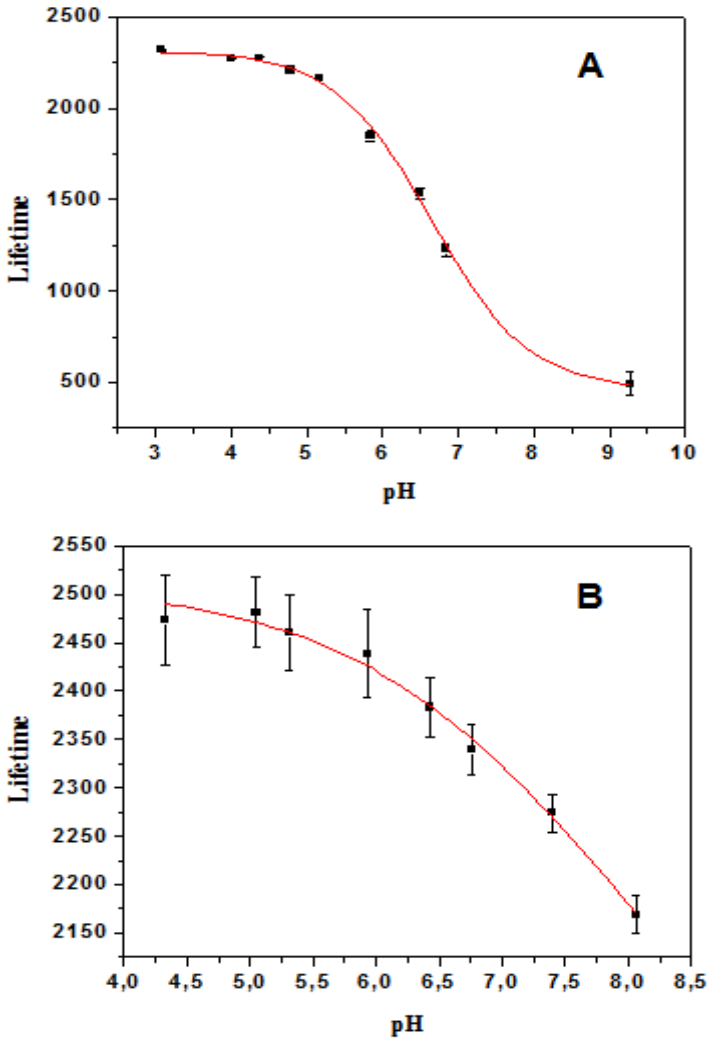

Figure 6. A: pH calibration curve of MRL (polymer films). B: pH calibration curve of MRL (nanoparticles).

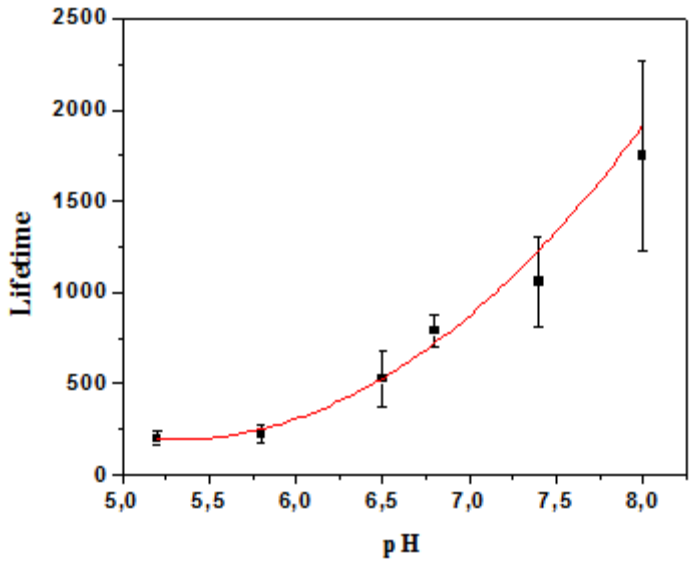

Figure 7. pH calibration plot obtained by confocal TCSPC-FLIM for cells stained with BCECF.

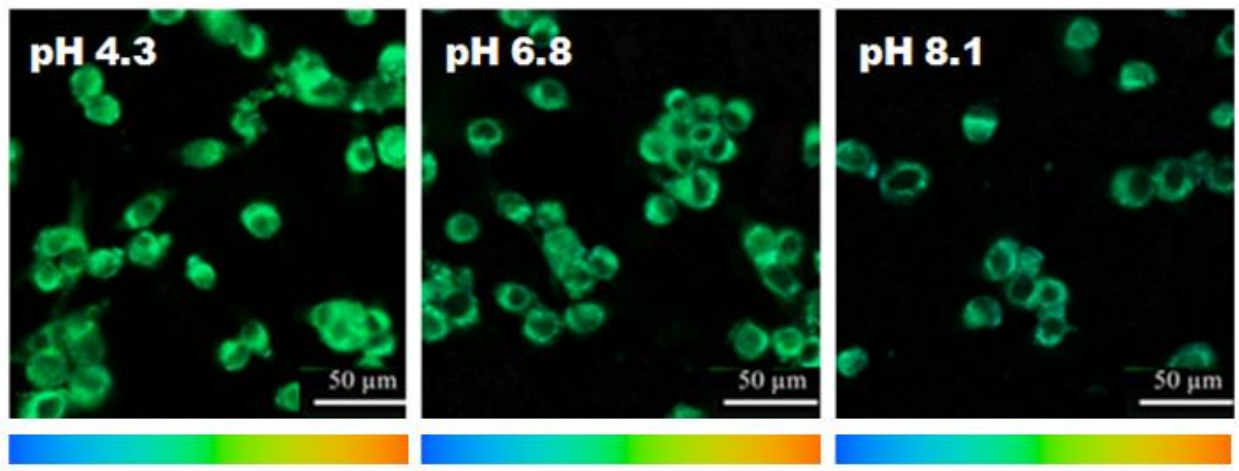

Figure 8. Confocal TCSPC-FLIM images of MEF cells stained with MRL at different pH values at 37 °C.

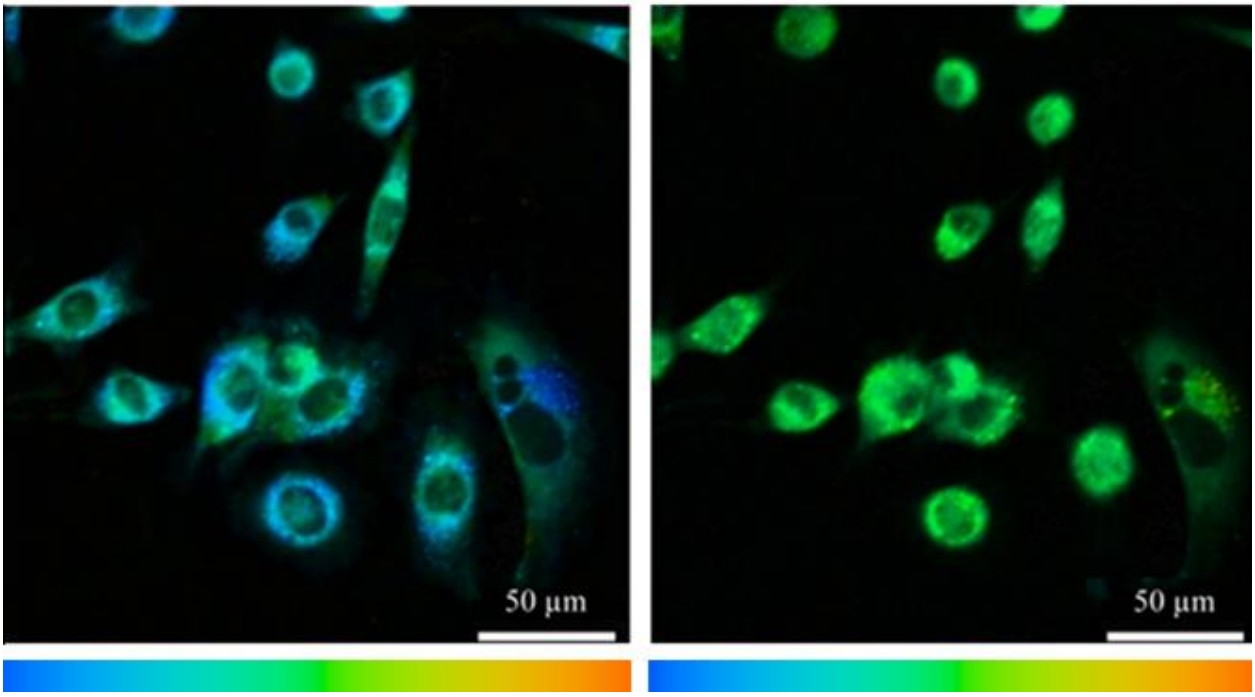

Figure 9. False-color images before (left) and after (right) cell exposure to bafilomycin A1.

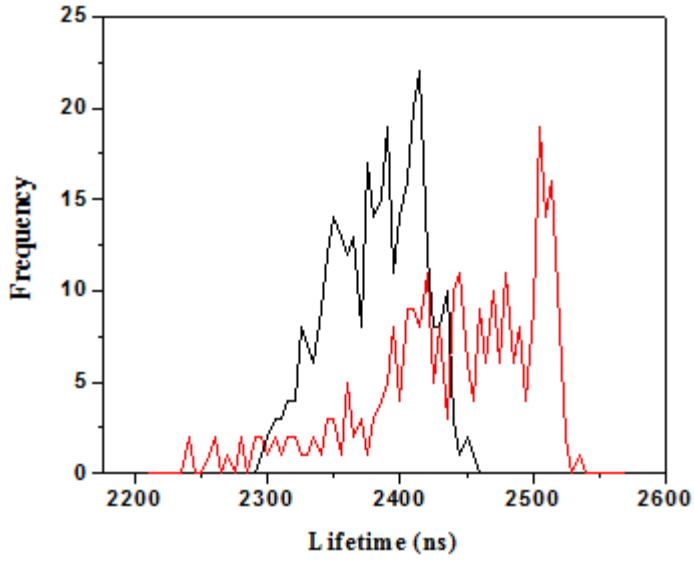

Figure 10. Distribution of lifetimes before (black line) and after (red line) cell exposure to bafilomicin A1.

4.4 Conclusion

In summary, new intracellular FLIM probes based on aza-BODIPY dye is presented, immobilized in cationic polymer particles. The probe showed mainly lysosomal staining, similar to previously reported RL-based probes and high photostability in contrast to standard probes such as BCECF.

Probe uptake and localization pattern in MEF cells were investigated in detail. Within the optimized concentration range, toxicity of the probe is negligible. Lifetime-based pH measurements showed that FLIM can measure the intracellular pH of the resting cells and determine the pH variations in cells after external stimulation.

Although the design of the probes can be further optimized to increase the dynamic range of sensing particles, the feasibility of the approach for intracellular pH measurements was demonstrated.

4.5 References

1. Izumi, H., Torigoe, T., Ishiguchi, H., Uramoto, H., Yoshida, Y., Nomoto, M., Kohno, K., *Cancer Treatment Rev*. **2003**, 29, 541-549.

2. Davies, T.A., Fine, R.E., Johnson, R.J., Levesque, C.A., Rathbun, W.H., Seetoo, K.F., Smith, S.J., Strohmeier, G., Volicer, L. et al., *Biochem. Biophys. Res. Commun*. **1993**, 194, 537-543.

3. Tadrous, P. J., *J. Pathol*. **2000**, 191, 229-234.

4. Suhling, K., French, P. M. W., Phillips, D., *Photochem. Photobiol. Sci*. **2005**, 4, 13-22.

5. Tsytsarev, V., Arakawa, H., Borisov, S., Pumbo, E., Erzurmlu, R. S., Papkovsky, D. B., *J. Neurosci. Methods* **2013**, 216, 146-151.

6. Jokic, T., Borisov, S., Saf, R., Nielsen, D. A., Kühl, M., Klimant, I., *Anal. Chem*. **2012**, 84, 6723-6730.

7. Kondrashina, A. V., Dmitriev, R. I., Borisov, S. M., Klimant, I., O'Brien, I., Nolan, Y. M., Zhdanov, A. V., Papkovsky, D. B., *Adv. Func. Mater*. **2012**, 22, 4931-4939.

8. Niesner, B., Peker, B., Schlüsche, P., Gericke, K.-H., Hoffmann, C., Hahne, D., Müller-Goymann, *Pharm. Res*. **2005**, 22, 1079-1087.

9. Hille, C., Berg, M., Bressel, L., Munzke, D., Primus, P., Löhmannsröben, H.-G., Dosche, C., *Anal. Bioanal. Chem*. **2008**, 391, 1871-1879.

10. Wang, H.-P., Nakabayashi, T., Tsujimoto, K., Miyauchi, S., Kamo, N., Ohta, N., *Chem. Phys*. *Lett*. **2007**, 442, 441-444.

11. Hanson, K. M., Behne, M. J., Barry, N. P., Mauro, T. M., Gratton, E., Clegg, R. M., *Biophys*. *J*. **2002**, 83, 1682-1690.

12. Dmitriev, R. I., Zhdanov, A. V., Jasionek, G., Papkovsky, D. B., *Anal. Chem*. **2012**, 84, 2930-2938.

13. Canton, I., Battaglia, G., *Chem. Soc. Rev*. **2012**, 41, 2718-2739.

14. Dmitriev, R. I., Kondrashina, A. V., Koren, K., Klimant, I., Zhadanov, A. V., Pakan, J. M., McDermott, K. W., Papkovsky, D. B., *Biomater. Sci*. **2014**, 2, 853-866.

15. Dmitriev, R. I., Zhadanov, A. V., Nolan, Y. M., Papkovsky, D. B. *Biomaterials* **2013**, 34, 9307-9317.

Chapter 5

CO_2 sensor based on rigid aza-BODIPY probe

5.1 Introduction

The advantages of fluorescence sensing in the NIR region (700-1100 nm) are many and have been extensively described. Compared to chromophores absorbing in the visible region, problems have been encountered in the design and synthesis of the red-shifted NIR counterparts, such as aggregation, photobleaching, and low fluorescence quantum yields. Therefore, there is a pressing demand for the development of new, more effective probes that emit in the NIR region.

We have chosen structurally rigidified aza-dipyrromethene dye as our target for synthesis.[1,2] We speculated that the rigidification of the aza-bodipy core would bring many advantages like simple synthesis and bathochromic shift in the absorption maxima in comparison to the non-rigid analogue. The probe shows intense, sharp absorption (full width at half maximum height, fwhm=30.4 nm; ε=145000 $M^{-1}cm^{-1}$) in the NIR region (λ_{max}=740 nm). Thus, the rigidification of the azaBODIPY core results in a 52-nm bathochromic shift and 2-fold decrease of the fwhm. Herein we present detailed characterization of the dye and its application as a carbon dioxide-sensitive material.

5.2 Experimental

Materials

Vinyldimethylsiloxy terminated polydimethylsiloxane (viscosity 1000 cSt), methylhydrosiloxane/dimethylsiloxane copolymer (viscosity 25-35 cSt), tetravinyltetramethylcyclotetrasiloxane, platinum divinyltetramethylsiloxane complex, imidazole, *tert*-butyl dimethyl chlorosilane, sodium nitrite and triethylamine were obtained from ABCR (www.abcr.de). Boron trifluoride diethyl etherate, MOPS buffer salt, sodium sulfate (anhydrous), acetic acid and acetic anhydride from Sigma Aldrich (www.sigmaaldrich.com), ethanol, tetrahydrofuran, hydrochloric acid (37%), dichloromethane and cyclohexane from VWR (www.vwr.com), 6-hydroxy-1-tetralone, 6-methoxy-1-tetralone and LDA (Lithium Diisopropylamide 20%) from TCI Europe (www.tcichemicals.com), potassium chloride, potassium carbonate, potassium hydroxide, sodium phosphate and sodium hydrogen phosphate

from Merck (www.merck.at), sodium hydroxide, the buffer salts CHES, MES and CAPS and ethyl acetate from Roth (www.carlroth.com) and Mylar support was received from Goodfellow.

Deuterated dimethyl sulfoxide (DMSO-*d6*) and Deuterated chloroform ($CDCl_3$) were obtained from Euriso-top (www.eurisotop.com). Nitrogen and carbon dioxide (all of 99.999 % purity) were obtained from Air Liquide (www.airliquide.at).

Methods. ^{1}H NMR spectra were recorded on a 300 MHz Bruker spectrometer in $CDCl_3$ or DMSO-d_6 with TMS as standard. Absorption spectra were recorded on a Cary 50 UV-vis Varian spectrophotometer. Fluorescence spectra were recorded on a Fluorolog fluorescence spectrometer (Horiba) with a NIR-sensitive photomultiplier R2658 from Hamamatsu (300-1050 nm). Gas calibration mixtures were obtained using a gas mixing device from MKS (www.mksinst.com). The gas mixture was humidified to about 85% relative humidity, using silica gel soaked with a saturated potassium chloride solution. Temperature was controlled with a cryostat ThermoHaake DC50.

Synthesis

6-(tert-Butyldimethylsilyloxy)-3,4-dihydronaphthalen-1(2H)-one (2). Compound 1 (3.0 g, 18.45 mmol) was reacted with imidazole (5.1 g, 75 mmol) and *tert*-butyl dimethyl chlorosilane (3.75 g, 24.75 mmol) in DMF (50 ml) and stirred for 24 h at room temperature. The product was extracted with ethylacetate (2x50 ml) and dried with anhydrous Na_2SO_4. Solvent was removed by evaporation and the crude product was separated with column chromatography (n-hexane:dichloromethane = 1:1) and the product 2 is obtained (1.94 g, 7.015 mmol, 24.4%).

7-(tert-Butyldimethylsilyloxy)-3-phenyl-4,5-dihydro-1H-benzo[g]indole (3).

Under nitrogen, LDA (3.56 ml, 14.22 mmol) in THF (42 ml) was reacted with 2 (1.94 g, 7.01 mmol) in THF (20 ml) at -78°C. 3-phenyl-2H-azirine (0.84 ml, 7.17 mmol) in THF (7 ml) was added and the stirring was continued for 2 h. The mixture is then slowly brought to room temperature. Reaction was stopped by addition of water and base was removed by addition of diluted HCl till pH~7 was achieved. The product was extracted with dichloromethane (2x50 ml), and the organic layer was dried with anhydrous Na_2SO_4. Solvent was removed by evaporation

and the crude product was separated with column chromatography on silica gel (n-hexane:dichloromethane=1:1) and product 3 was obtained (1.24 g, 3.3 mmol, 27.4 %).

Under nitrogen, LDA (4.57 ml, 18.26 mmol) in THF (54 ml) was reacted with 2 (5 g, 28.37 mmol) in THF (20 ml) at -78°C. 3-phenyl-2H-azirine[1] (2.17 ml, 18.53 mmol) in THF (18 ml) was added and the stirring was continued for 2 h. The mixture is then slowly brought to room temperature. Reaction was stopped by addition of water and base was removed by addition of diluted HCl till pH~7 was achieved. The product was extracted with dichloromethane (2x50 ml), and the organic layer was dried with anhydrous Na_2SO_4. Solvent was removed by evaporation and the crude product was separated with column chromatography on silica gel (n-hexane:dichloromethane=1:1) and product 4 was obtained (1.42 g, 5.16 mmol, 18.2 %).

Aza-BODIPY dye (5). Sodium nitrite (12.5 mg, 0.18 mmol) was reacted with 3 (50 mg, 0.18 mmol) in acetic acid (1.8 ml) at 0 °C for 10 min. The second pyrrole 4 (68 mg, 0.18 mmol) was added and acetic anhydride (0.72 ml). After 30 min, the mixture was reacted at 80 °C for 30 min. After that the reaction mixture is brought to room temperature and ice was added to the mixture. The product was filtered, washed with water and dissolved in dichloromethane. Solvent was removed by evaporation, the product was dissolved in dry 1,2-dichloromethane, triethylamine (0.43 ml) was added and $BF_3 \cdot Et_2O$ (0.43 ml). The mixture was stirred for 30 min, then heated at 80 °C for 30 min, and then cooled down. The reaction was stopped with ice, extracted with dichloromethane, purified by chromatography on silica gel and recrystalized from dichloromethane/n-hexane to afford 5 (65 mg, 0.102 mmol, 55.6%). ^{1}H NMR (300 MHz, $CDCl_3$): δ: 8.74-8.77 (d, 1H), 8.79-8.82 (d, 1H), 7.68-7.73 (t, 4H), 7.36-7.47 (m, 6H), 7.15-7.19 (dd, 1H), 7.07 (d, 1H), 7.02-7.06 (dd, 1H), 6.85-6.89 (d, 1H), 3.92 (s, 3H), 2.93 (s, 8H), 2.34 (s, 3H).

Aza-BODIPY dye (6): Compound 5 (32 mg, 0.05 mmol) was stirred overnight with K_2CO_3 (25.9 mg, 0.18 mmol) in a mixture of dichloromethane (10 ml), methanol (4 ml) and water (0.4 ml) at room temperature. Solvents are removed by evaporation, the product was dissolved in water (20 ml) and diluted NaH_2PO_4 was added till pH 5 was achieved. The precipitated product was filtered, washed and purified by chromatography on silica gel. Recrystallization was done from dichloromethane/n-hexane to yield 6 (8.7 mg, 0.146 mmol, 29.1%). ^{1}H NMR (300 MHz,

$CDCl_3$): δ: 8.56 (d, 1H), 8.49 (d, 1H), 7.71-7.76 (m, 4H), 7.47-7.53 (m, 4H), 7.37-7.44 (m, 2H), 7.09-7.13 (dd, 1H), 7.03-7.04 (d, 1H), 6.87-6.90 (dd, 1H), 6.83-6.84 (d, 1H), 3.89 (s, 3H), 2.87-2.91 (m, 8H).

Preparation of the CO_2 Sensing Material.

100 mg of hydrotane 25 was dissolved in 2 ml of THF and 200 µL of water. 60 µL of 0.2 M water solution of Na_3PO_4 was added and the indicator solution (0.5 mg dissolved in 500 µL of THF). The "cocktail" was knife-coated on a dust-free Mylar support to obtain a ~7.5 µm thick sensing layer after solvent evaporation.

The cocktail of silicon primers was obtained by mixing tetravinyltetramethylcyclotetrasiloxane (1.5 µL) with 500 mg of the vinyl-terminated PDMS in 1 ml of cyclohexan followed by addition of 15 µL of methylhyydrosiloxane-dimethylsiloxane copolymer and 2 µL of the platinum complex catalyst. The uncured silicone layer was coated onto sensing layer and cured for 10 min to obtain protection layer with the thickness of ~60 µm.

5.3 Results and Discussion

For the preparation of the pyrrole moieties 6-hydroxy-1-tetralone and 6-methoxy-1-tetralone were reacted with 3-phenyl-2H-azirine to give 3 in 27.4% yield and 4 in 18.2% yield in the presence of LDA, respectively[2,3] (Scheme 1). Aza-BODIPY 5 was successfully synthesized in 55.6 % yield by condensation of pyrrole with a nitrosopyrrole, which was prepared in a separate step. The complexation of dipyrromethane was achieved with $BF_3{\cdot}Et_2O$ in the presence of triethylamine in dichloromethane. After hydrolysis of acetate aza-BODIPY 6 was obtained in 29.1 % yield.

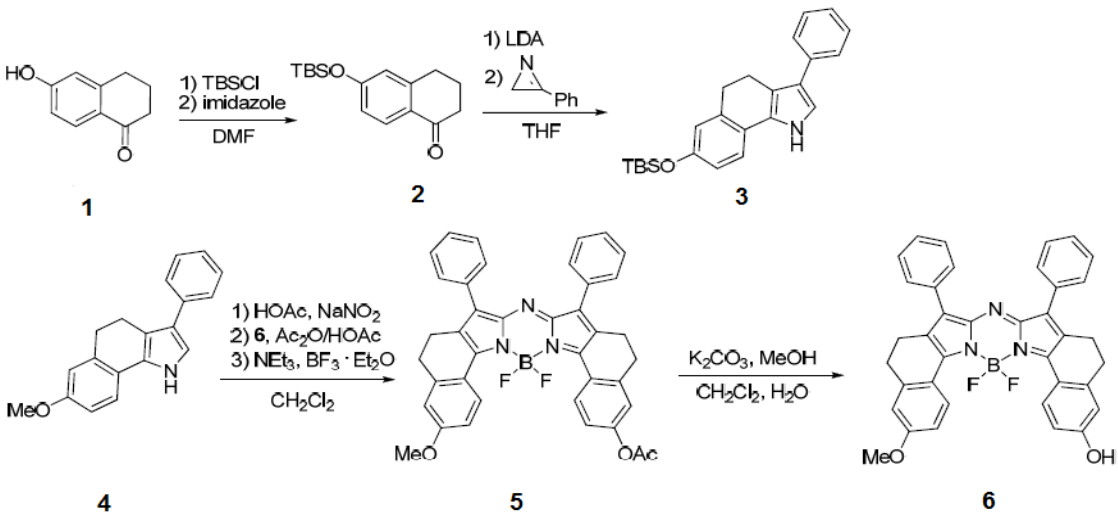

Scheme 1. Synthetic route for synthesis of aza-BODIPY probe 6.

Photophysical properties.

Rigidification of the dye resulted in its NIR absorption and emission. The absorption and emission spectra of the probe in THF/aqueous buffer (λ_{abs}=740 nm; λ_{em}=755 nm) are presented in Fig. 2. The probe exhibited high molar coefficient (145000 $M^{-1}cm^{-1}$) and a narrow full width at half maximum (30.4 nm). In comparison with the absorption maximum of non-rigid analog (λ_{abs}=670 nm), rigidification leads to 70 nm bathochromic shift. Stokes shift is 15 nm which is shorter than non-rigid dye (32 nm). As would be expected, the UV-visible spectrum was strongly influenced by pH. The absorption band at 740 nm was progressively reduced in intensity with increasing pH and a new band appeared at 778 nm with an isobestic point at 757 nm. (Fig. 1) The spectral shift upon deprotonation ($\Delta\lambda$=38 nm) is reduced in comparison to nonrigidified analog ($\Delta\lambda$=56 nm).

pK_a value of probe was determined both in solution and in a hydrogel D4 film from the fluorescence measurements. A sigmoidal plot of pH vs. fluorescence intensity predicted an apparent pK_a of 9.01 for indicator in solution (Fig. 3) and pK_a of 8.2 in hydrogel D4. (Fig. 4)

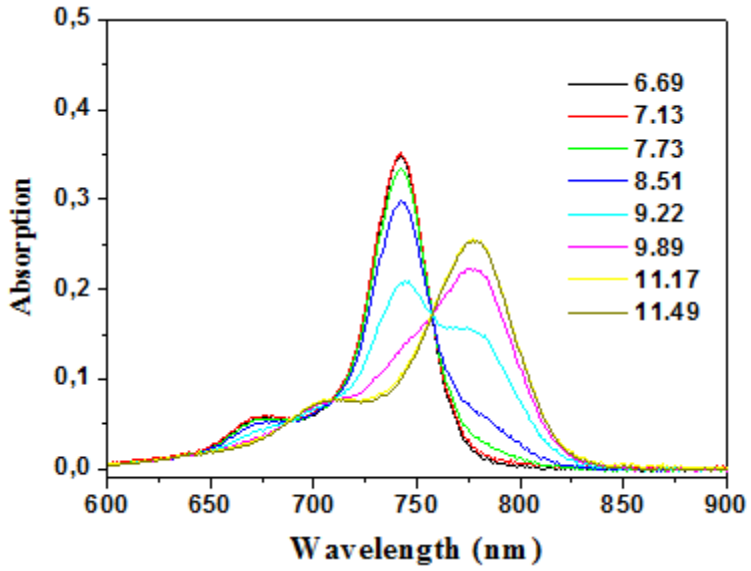

Figure 1. pH dependence of absorbance for indicator (5.6×10^{-6} M) in THF/aqueous buffer solution (1:1, IS 0.15 M).

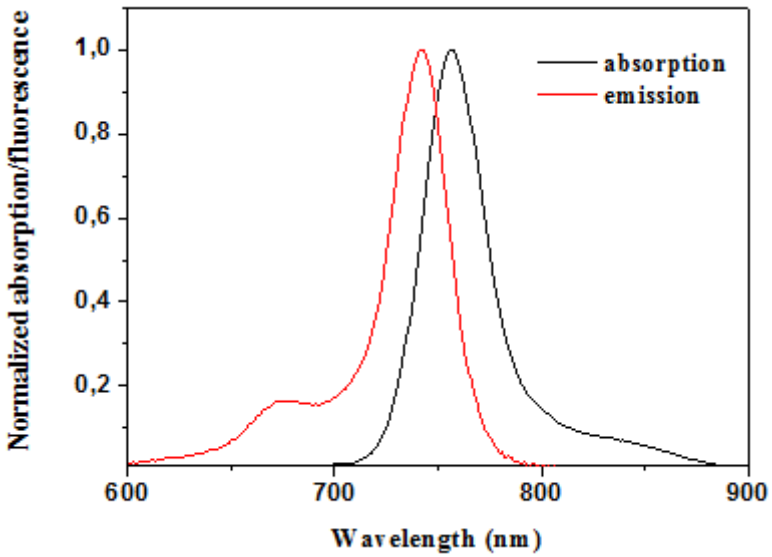

Figure 2. Normalized absorption/emission spectra of indicator in THF/buffer solution.

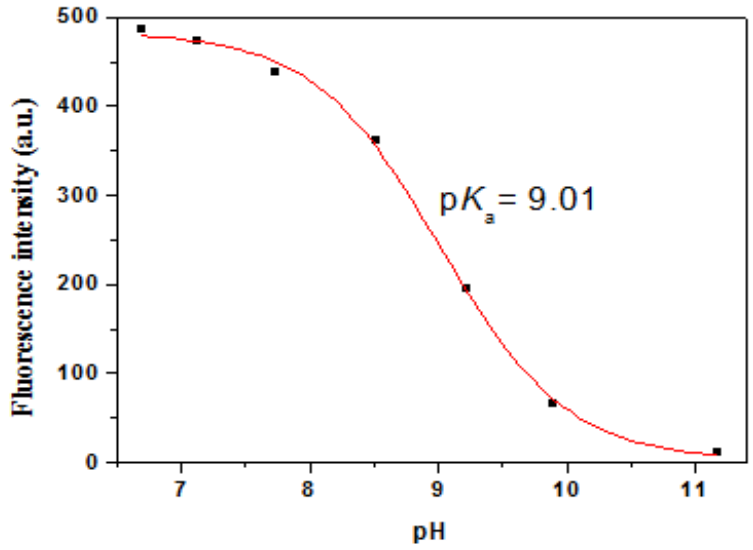

Figure 3. Calibration plot for pH indicator (1.4×10^{-6} M) in THF/aqueous buffer solution (1:1, IS 0.15 M).

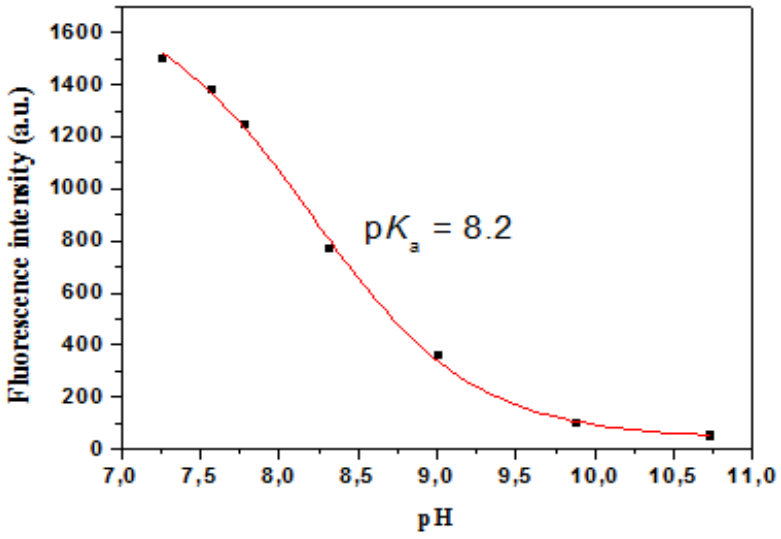

Figure 4. Calibration plot for the pH sensor containing pH indicator (0.25 %) in hydrogel D4 (IS 0.15 M).

Composition of the Sensors.

CO_2 sensing material presented here operates by Severinghaus type sensor[4] and was prepared by non-covalent entrapment of the indicator in hydrotane 25 matrix, which is a gas permeable, uncharged polymer with a water uptake capacity of about 25%. Apart from the dissolved indicator the system also includes water and inorganic base (sodium phosphate). To avoid poisoning of the sensor, polydimethylsiloxane-based silicone protection layer is used because it possesses excellent permeability for carbon dioxide and water vapour.

The sensing mechanism is straightforward. Carbon dioxide diffuses into the polymer matrix, where it dissolves and reacts with the base. With the increase of CO_2 concentration acidity is increased and therefore indicator is protonated, what is monitored via fluorescence or absorption measurements.

As illustrated in Fig. 5 and 6, the sensor shows distinct spectral changes in the near infrared (NIR) region. Although, the deprotonated form of the indicator wasn't fluorescent in solution, after incorporation in the sensor matrix, both protonated and deprotonated form were fluorescent. Compared to the measurements in solution the CO_2 sensor showed bathochromically shifted absorption spectra with maximum at 750 nm for protonated form and maximum at 786 nm for deprotonated form. Fluorescence maximum for the protonated form was 769 nm and for deprotonated 807 nm. As showed in Fig. 7 the dynamic range of the sensor enables measurements from 0 to 100% CO_2. However, fluorescence quantum yield drastically decreased in sensor film ($\Phi = 0.0027$) in comparison to solution ($\Phi = 0.22$).

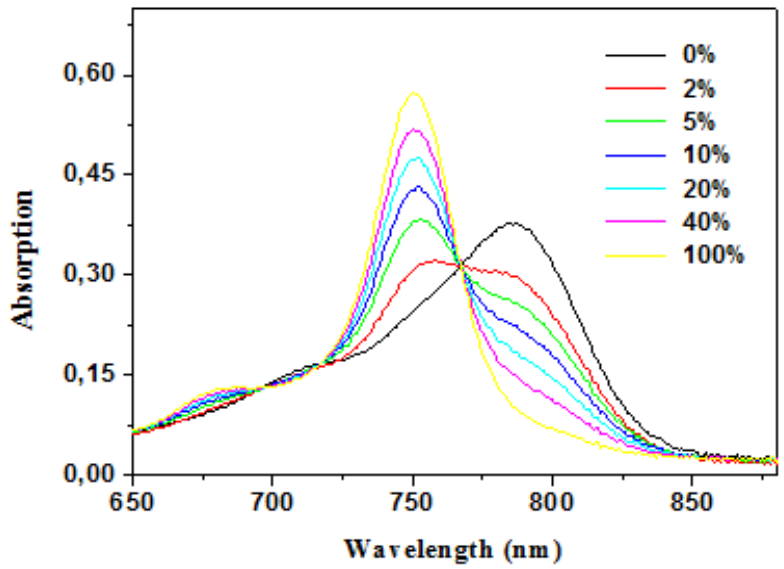

Figure 5. Absorption spectra of optical carbon dioxide sensor at 25 °C at various CO_2 concentrations.

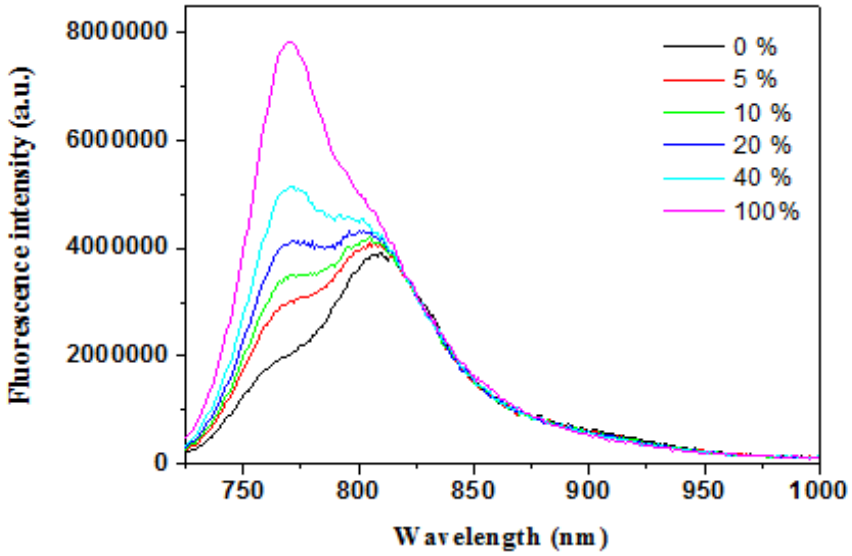

Figure 6. Response of the fluorescent sensing material to carbon dioxide at 25 °C.

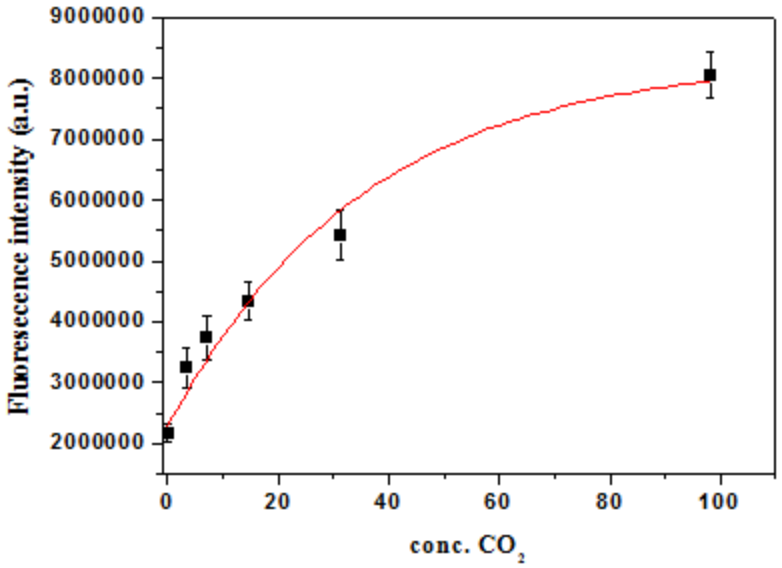

Figure 7. Calibration plot for the fluorescent sensing material to carbon dioxide at 25 °C.

Temperature dependence.

Sensitivity of optical CO_2 sensors depends to great extent on temperature.[5,6,7] Therefore, the temperature dependence of CO_2-sensitive material was studied.

Reproducible behavior was observed at temperatures from 15 to 35 °C, (Fig. 8) while the sensitivity decreased with the increase of temperature. Clearly, if the measurements aren't performed at constant temperature, temperature dependence should be determined to compensate for temperature changes.

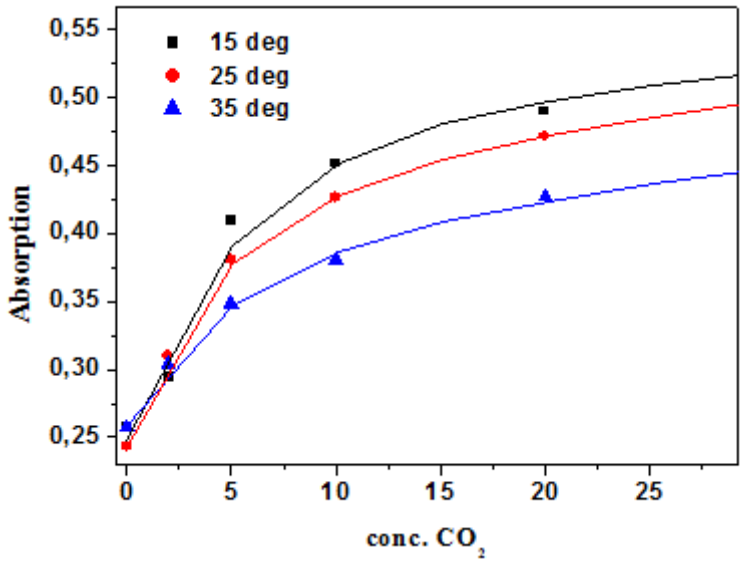

Figure 8. Temperature dependence of the response of sensor to carbon dioxide.

Reproducibility and Response Times. As can be seen from Figure 9, the sensor material responds fully reproducible to carbon dioxide. The response time t_{95} was estimated to be 145 s on going from 5 to 100% and 140 s in the reverse direction.

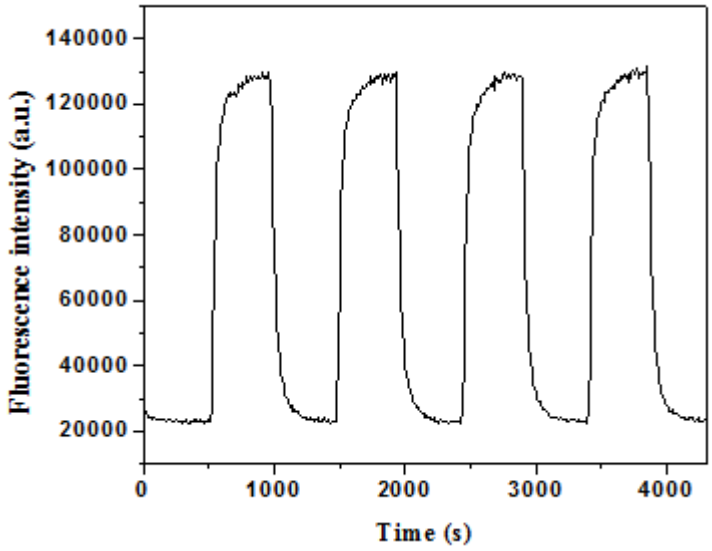

Figure 9. Response of the sensor material to altering concentrations of carbon dioxide at room temperature.

Long-term stability. Acidic gases such as HCl, H_2S or SO_2 can irreversibly poison optical CO_2 sensors, therefore careful storing and handling of the sensors is necessary. Figure 10 shows signal stability of the sensor monitored within 8 days under lab conditions at room temperature. The results show that the sensor material can be kept at room temperature for a period of 1 week without alteration of sensor properties.

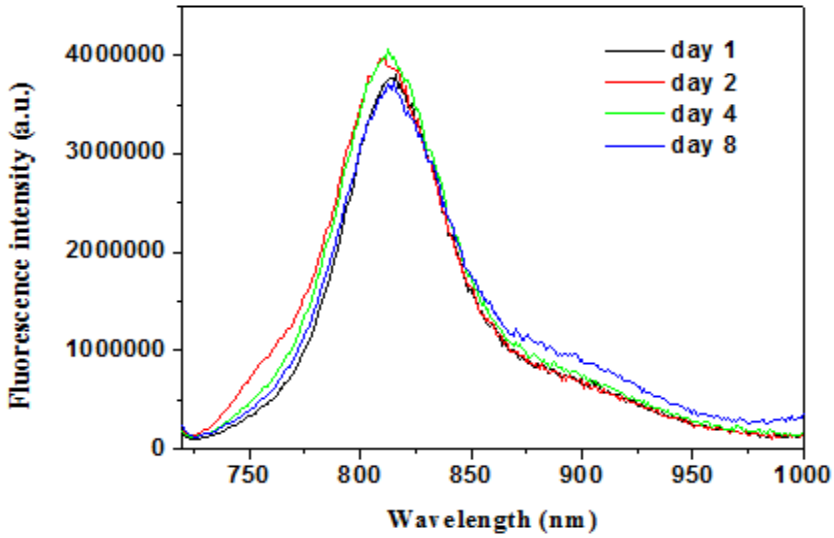

Figure 10. Stability of fluorescence signal within several days of observation.

5.4 Conclusion

In conclusion, a fluorescent turn-on NIR probe for application in pH and CO_2 monitoring is described. The dye shows excellent properties of a NIR fluorophore and can be prepared in a simple way in good yields. Novel material for carbon dioxide sensing makes use of the entrapped indicator in hydrotane 25 matrix with silicone protection based on Severinghaus type sensor. The sensor shows absorption/emission spectral changes in the near-infrared region according to varying CO_2 concentrations. The presented material can be potentially used in food-packaging applications.

5.5 References

1. Hortmann, A. G., Robertson, D. A., Gillard, B. K., *J. Org. Chem*. **1972**, 37, 322-324.

2. Jiang, X., Zhang, J., Shao, X., Zhao, W., *Org. Biomol. Chem***. 2012**, 10, 1966-1968.

3. Carreira, E. M., Zhao, W., *Angew. Chem*. **2005**, 117, 1705-1707.

4. Severinghaus, J. W., Bradley, A. F. *J. Appl. Physiol*. **1985**, 13, 515-520.

5. Mills, A., Chang, Q., McMurray, N., *Anal. Chem*. **1992**, 64, 1383-1389.

6. Borisov, S. M., Neurauter, G., Schroeder, C., Klimant, I., Wolfbeis, O. S. *Appl. Spectrosc*. **2006**, 60, 1167-1173.

7. Mills, A., Lepre, A., *Analyst* **1999**, 124, 685-689.

4. Tabacco, M. B., Uttamlal, M., McAllister, M., Walt, D. R., *Anal. Chem*. **1999**, 71, 154-161.

20. Zhujun, Z., Seitz, W. R., *Anal. Chim. Acta* **1984**, 160, 305-309.

21. He, X., Rechnitz, G. A., *Anal. Chem*. **1995**, 67, 2264-2268.

5.6 Spectra

1) Aza-BODIPY dye 5

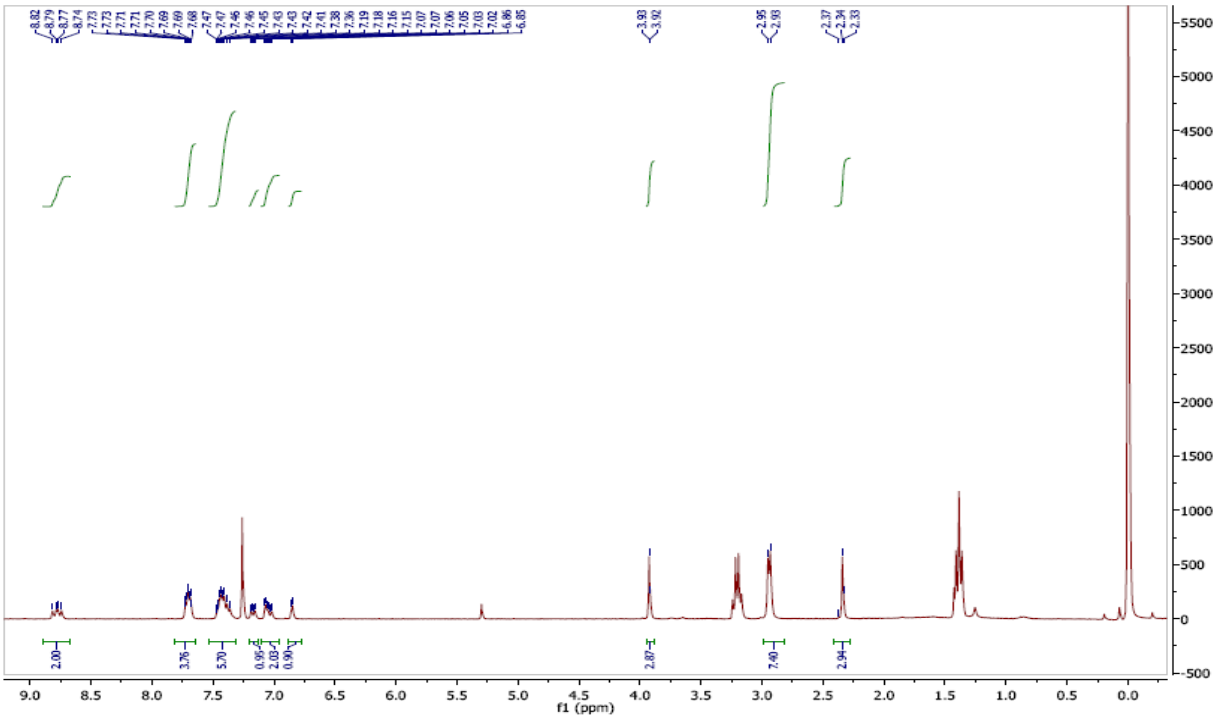

2) Aza-BODIPY dye 6